ABSTRACT

ROSSNER CAMPOS, ALFRED ARMIN. Removal of Polar and Emerging Organic Contaminants by Alternative Adsorbents. (Under the direction of Detlef Knappe).

The removal of polar and ionizable organic contaminants such as the fuel additive methyl tertiary butyl ether (MTBE) and pharmaceutically active compounds from drinking water sources is a challenge for many utilities. Effective treatment technologies are required to effectively remove these contaminants from drinking water. In this study the effectiveness of alternative adsorbents for the removal of MTBE and a mixture of 28 emerging contaminants was evaluated. Furthermore, adsorbent, adsorbate, and background water matrix characteristics that affect the adsorption of the antimicrobial compounds sulfamethoxazole (SMX) and trimethoprim (TMP) were identified.

In the first phase of this research, the MTBE removal effectiveness of activated carbon, a carbonaceous resin, and a silicalite zeolite was compared. Results showed that GAC was the most cost-competitive adsorbent when considering adsorbent usage rate only; however, the useful life of an adsorber containing silicalite zeolite was predicted to be ~5-6 times longer than that of an equally sized adsorber containing GAC. Pilot column results also showed that natural organic matter (NOM) preloading did not impair the MTBE removal efficiency of the silicalite zeolite. Thus, it may be possible to regenerate spent silicalite with less energy-intensive methods than those required to regenerate GAC.

One activated carbon, one carbonaceous resin, and two high-silica zeolites were studied to evaluate their effectiveness for the removal of a mixture of emerging pollutants of concern (EPOCs) from lake water. Adsorption isotherm experiments were performed with environmentally relevant concentrations of the 28 targeted EPOCs (~200-900 ng/L). Among the tested adsorbents, activated carbon was the most effective, and activated carbon doses typically used for taste and odor control in drinking water (1-10 mg/L) were sufficient to achieve a 2-log removal for most of the tested EPOCs. The results of this study demonstrate that heterogeneity in pore size and shape along with a large pore volume in the 6-9 Å size range are important adsorbent characteristics when an effective barrier against a broad spectrum of EPOCs is desired.

Five carbonaceous adsorbents were evaluated to evaluate the pH-dependent adsorption uptake of sulfamethoxazole (SMX) and trimethoprim (TMP). Results indicated that a coconut shell-based activated carbon more effectively removed both antimicrobial compounds from ultra-pure water, Tar River water, and Lake Mead water than coal- and wood-based activated carbons and a carbonaceous resin. TMP and SMX were more effectively removed at solution pHs at which the antimicrobial compounds were primarily present in the neutral form. SMX and TMP adsorption isotherm data at different solution pHs could be effectively normalized by dividing the equilibrium liquid-phase concentration of SMX and TMP by the pH-dependent aqueous solubility provided that the solution pH was within about 2 pH units of the pK_a. When the difference between the pK_a and pH was larger, where repulsive electrostatic interactions proved to be important, the normalization

procedure did not entirely account for the pH-dependence of the adsorption capacity of the ionizable organic compounds.

Removal of Polar and Emerging Organic Contaminants by Alternative Adsorbents

by

Alfred Armin Rossner Campos

A dissertation submitted to the Graduate Faculty of
North Carolina State University
in partial fulfillment of the
requirements for the Degree of
Doctor of Philosophy

Civil Engineering

Raleigh, North Carolina

2008

APPROVED BY:

_____	_____
Detlef Knappe (Chair of Advisory Committee)	Joel Ducoste (Advisory Committee)
_____	_____
Dean L. Hesterberg (Advisory Committee)	George W. Roberts (Advisory Committee)

BIOGRAPHY

Alfred Armin Rossner Campos was born on December 8, 1973 in Concepción, Chile. He is the son of Roberto Rossner and Carmen Campos. He has 5 siblings: 4 brothers and 1 sister. He graduated from the German school of Concepción-Chile in 1991. He received his Degree of Licentiate of Engineering Sciences in 1996 and graduated in July 1999 with a B.S. in Chemical Engineering from the University of Concepción-Chile. After graduating, Alfred worked as a research assistant in the Laboratory of Renewable Resources, University of Concepción, Chile.

In August 2002, Alfred came to the United States and began his Master of Science studies in the Department of Civil, Construction, and Environmental Engineering at North Carolina State University. In 2004, he graduated with a Master of Science and started the Ph.D. program in the same department. Over the last six years, he has been working as a Research and Teaching Assistant. Upon graduation, Alfred will join the Environmental Science Center EULA at the University of Concepción, Chile.

ACKNOWLEDGEMENTS

First, I want to specially tank my wife Carolina and my parents whose unconditional love and support helped me during these years to pursue my goals. I would also thank my advisor, Dr. Detlef R. U. Knappe, and the committee members Joel Ducoste, Dean Hesterberg, and George Roberts for their constant support and guidance throughout this research. A special thank you goes to all my friends that became my family during my stay in Raleigh, NC.

I would also like to thank the American Water Works Association Research Foundation (AwwaRF) for financial support through project #2905, the Greenville Utilities Commission (GUC) in Greenville, NC for support with the operation of the pilot plant, and the Southern Nevada Water Authority (SNWA) in Henderson, NV for LC-MS/MS analyses. I also want to extend my gratitude to the Inter-American Development Bank for the fellowship granted. In addition, I would like to thank US Filter and Calgon Carbon Corporation for their donations of activated carbons. Finally, I would also like to acknowledge David Black, who conducted the GC analyses in the Environmental Engineering Research Lab at NC State University.

TABLE OF CONTENTS

LIST OF TABLES

LIST OF FIGURES

CHAPTER 1

INTRODUCTION

The removal of polar and ionizable organic contaminants from drinking water sources is a challenge for many water utilities. Among the polar organic contaminants (POCs), the fuel additive methyl tertiary butyl ether (MTBE) has been of concern for the water treatment industry because it can adversely affect the taste and odor quality of water. MTBE is also difficult to remove from water because of its high solubility and low volatility. Furthermore, many emerging and non-regulated organic contaminants are ionizable at typical pH values encountered in drinking water treatment. For example, antimicrobial compounds are one class of ionizable organic compounds that have received increased attention in drinking water treatment because their presence may lead to the evolution of antibiotic-resistant bacteria in water distribution systems. In addition, many pesticides and pesticides degradates are ionizable.

Effective removal of POCs and ionizable organic contaminants from water can be achieved with adsorption as well as conventional and advanced oxidation processes. Conventional and advanced oxidation processes may lead to the formation of undesirable oxidation intermediates, which in some cases are more toxic and difficult to remove than the parent compounds. In addition, chlorine and ozone oxidation processes can form oxidation byproducts, such as halogenated organics and bromate. In contrast, adsorption processes do

not add undesirable byproducts to drinking water. However, high adsorbent usage rates can be expected for the removal of POCs such as MTBE when activated carbon is used.

In this research, MTBE and the ionizable antimicrobial compounds sulfamethoxazole (SMX) and trimethoprim (TMP) served as model POCs. In addition, the adsorption behavior of an emerging contaminat mixture containing 28 pharmaceuticals and endocrine disrupting chemicals was evaluated. The adsorptive removal of MTBE and the emerging contaminants was studied with a suite of commercially available activated carbons and high-silica zeolites as well as with a carbonaceous resin.

The overall objective of this research was to evaluate the effectiveness of alternative adsorbents for the removal of POCs from drinking water and to identify activated carbon, contaminant, and background water characteristics that affect the pH-dependent adsorption capacity of ionizable organic contaminants. Specific objectives were to (1) determine equilibrium and kinetic parameters that describe the adsorption of MTBE from both ultrapure water and natural water on alternative adsorbents, (2) predict and verify MTBE breakthrough curves in pilot-scale GAC and zeolite adsorbers, (3) compare costs associated with adsorbent usage rates for MTBE removal among adsorbents, (4) determine the importance of pH-mediated changes in contaminant solubility on the adsorption of ionizable organic contaminants, (5) determine how natural organic matter (NOM) preloading time affects the adsorption of SMX and TMP, and (6) evaluate the effects of solution pH on the adsorption capacity of SMX and TMP on preloaded activated carbons.

CHAPTER 2

MTBE Adsorption on Alternative Adsorbents and Packed Bed Adsorber Performance

Alfred Rossner and Detlef R.U. Knappe

Department of Civil, Construction, and Environmental Engineering,
North Carolina State University,
Campus Box 7908,
Raleigh, NC 27695-7908

* Corresponding author phone (919) 515-8791; fax (919) 515-7908;
e-mail knappe@ncsu.edu

Manuscript published in *Water Research*
April 2008

ABSTRACT

Widespread MTBE use of the fuel additive methyl *tertiary*-butyl ether (MTBE) has led to frequent MTBE detections in North American and European drinking water sources. The overall objective of this research was to evaluate the effectiveness of a silicalite zeolite, a carbonaceous resin, and a coconut-shell-based granular activated carbon (GAC) for the removal of MTBE from water. Isotherm and short bed adsorber tests were conducted in ultrapure water and river water to obtain parameters describing MTBE adsorption equilibria and kinetics and to quantify the effect of natural organic matter (NOM) on MTBE adsorption. Both the silicalite zeolite and the carbonaceous resin exhibited larger MTBE adsorption uptakes than the tested GAC. Surface diffusion coefficients describing intraparticle MTBE mass transfer rates were largest for the GAC and smallest for the carbonaceous resin. Pilot tests were conducted to verify MTBE breakthrough curve predictions obtained with the homogeneous surface diffusion model and to evaluate the effect of NOM preloading on packed bed adsorber performance. Results showed that GAC was the most cost-competitive adsorbent when considering adsorbent usage rate only; however, the useful life of an adsorber containing silicalite zeolite was predicted to be ~5-6 times longer than that of an equally sized adsorber containing GAC. Pilot column results also showed that NOM preloading did not impair the MTBE removal efficiency of the silicalite zeolite. Thus, it may be possible to regenerate spent silicalite with less energy-intensive methods than those required to regenerate GAC.

INTRODUCTION

The fuel additive methyl *tertiary*-butyl ether (MTBE) is frequently detected in surface and ground water. Sources of MTBE contamination include gasoline leaking from underground fuel-storage tanks, urban runoff, and water craft (Squillace et al. 1997, Deeb et al. 2003). In the U.S., more than 1,500 drinking water supply systems in 28 states have reported detectable levels of MTBE (Environmental Working Group 2003). MTBE concentrations in almost half of these systems reached or exceeded 2 μg/L, a concentration at which MTBE odor can be detected by some consumers (Stocking et al. 2001). MTBE has received attention in the drinking water industry because (1) MTBE is a potential human carcinogen, (2) MTBE can adversely affect the taste and odor quality of water, and (3) MTBE is difficult to remove from water because of its high water solubility and low volatility. In addition, MTBE is fairly resistant to biodegradation and chemical oxidation, and these processes may lead to the formation of undesirable metabolites or oxidation intermediates such as tertiary-butyl alcohol (Leitner et al. 1994, Mormile et al. 1994, Liang et al. 1999); in addition, oxidation processes can lead to the formation of background water-related oxidation byproducts such as bromate (e.g. Acero et al. 2001).

Adsorption processes do not add undesirable byproducts to drinking water, but high adsorbent usage rates can be expected if activated carbon is employed to adsorb MTBE (Knappe et al. 2003, Shih et al. 2003, 2005, Sutherland et al. 2004, Quinlivan et al. 2005). Recently published data show that some high-silica zeolites and carbonaceous resins exhibit

considerably larger single-solute MTBE adsorption uptakes than activated carbon (Melin 1999, Anderson 2000, Li et al. 2003a, Erdem-Senatalar et al. 2004; Bi et al. 2005; Hung et al. 2005; Knappe and Rossner Campos 2005; Hung and Lin 2006, Knappe et al. 2007). Few studies have quantified MTBE adsorption kinetics on activated carbon and alternative adsorbents, and little information exists about the effects of natural organic matter (NOM) on MTBE adsorption uptake and kinetics. Hung et al. (2005) showed that MTBE adsorption kinetics on a mordenite zeolite were considerably slower than on a coal-based activated carbon, especially in the presence of NOM. The practical implications of the trade-off between a high MTBE adsorption uptake and slow MTBE adsorption kinetics on such factors as adsorber life and zeolite usage rate have not been thoroughly investigated, however. The overall objective of this research was to evaluate the effectiveness of alternative adsorbents for the removal of MTBE from drinking water. Specific objectives were to (1) determine equilibrium and kinetic parameters that describe the adsorption of MTBE from both ultrapure water and natural water on one high-silica zeolite, one carbonaceous resin, and one activated carbon, (2) predict and verify MTBE breakthrough curves in pilot-scale GAC adsorbers, and (3) compare costs associated with adsorbent usage among the three tested adsorbents.

MATERIALS AND METHODS

Adsorbents

In this study, a silicalite zeolite (HiSiv 3000 in both powdered and extruded forms, UOP, Des Plaines, IL), a coconut-shell-based granular activated carbon (CC-602 GAC, Westates Carbon, Parker, AZ), and a spherical carbonaceous resin (Ambersorb 563, Supelco, Bellefonte, PA) were evaluated. These adsorbents were selected based on their comparatively high MTBE adsorption uptakes relative to other activated carbons and high-silica zeolites (Knappe and Rossner Campos 2005, Knappe et al. 2007). The scope of the carbonaceous resin evaluation was more limited because early results suggested that it would not be cost-competitive (unit cost of the carbonaceous resin is $35/lb). Silicalite is a hydrophobic zeolite, in which channels of uniform size reside within a crystalline structure. Intersecting at right angles are straight and sinusoidal channels with elliptical cross-sections; the minor and major axis dimensions are, respectively, 5.1 × 5.5 Å for the sinusoidal channels and 5.3 × 5.6 Å for the straight channels (Szostak 1998). Physical properties of the granular adsorbents were derived from N_2 adsorption isotherm data collected at 77 K (Knappe et al. 2007) and are summarized in Table 1. The surface morphology and shape of each adsorbent was evaluated by scanning electron microscopy (SEM, Hitachi S-3200 operating at an accelerating voltage of 5 kV, Analytical Instrumentation Facility, NC State University). Prior to SEM analysis, adsorbent samples were coated with Au/Pd layers of approximately 100 Å thickness using a K-550X sputter coater.

Waters

Single-solute adsorption experiments were conducted in ultrapure laboratory water (UPW), which was produced by treating Raleigh, NC, tap water by reverse osmosis, ion exchange, and granular activated carbon adsorption. UPW was amended with a 1 mM phosphate buffer (0.5 mM $Na_2HPO_4 \bullet 2H_2O$ and 0.5 mM $NaH_2PO_4 \bullet 7H_2O$) to maintain a pH of 7.2.

The effect of NOM on MTBE adsorption uptake and kinetics was evaluated with Tar River water (TRW). Raw TRW was collected at a North Carolina drinking water treatment plant (Greenville, NC). Prior to use in experiments, TRW was vacuum-filtered through a 0.45-μm nylon membrane filter (Magna-R, MSI, Westboro, MA). The TOC of filtered TRW, measured by the combustion infrared method (TOC-5000A, Shimadzu, Columbia, MD), was 6.1 mg/L, the UV absorbance at 254 nm was 0.264 cm^{-1}, and the specific UV absorbance (SUVA) was 4.3 L/mg-m. The pH of filtered TRW was 7.8 and the total alkalinity was 25 mg/L as $CaCO_3$.

MTBE (HPLC grade; Fisher Scientific) stock solutions were prepared in UPW without organic solvent carrier. MTBE stock solutions were used to spike UPW and TRW with targeted MTBE concentrations (typically 1000 μg/L in single-solute isotherm experiments and 100 μg/L in all other experiments).

Isotherm experiments

Adsorption isotherm experiments (T = 25°C) were performed with pulverized adsorbents using a bottle-point technique (Knappe et al. 2003, 2007). For single-solute adsorption isotherm experiments, weighed adsorbent aliquots were placed into brown glass bottles that were subsequently filled to the neck with buffered UPW. MTBE stock solution was added with a constant rate syringe (CR-700, Hamilton, Reno, NV) to yield an initial concentration of about 1000 μg/L. Upon MTBE addition, each bottle was topped off immediately with UPW to create headspace-free conditions and capped using PTFE-faced silicon septa and open-top closures. Samples were placed on a rotary tumbler for two weeks, a mixing time that was sufficient to reach adsorption equilibrium. No measurable MTBE losses occurred in triplicate blanks containing no adsorbent over that time period. Upon equilibration, adsorbents were separated from water by filtration through 0.22-μm membrane filters (MAGNA nylon, Osmonics/MSI, Westboro, MA). A similar approach was followed to determine MTBE adsorption isotherms in the presence of NOM. In these experiments, the MTBE concentration spiked into TRW was about 100 μg/L, and the equilibration time was extended to three weeks.

Short bed adsorber tests

To quantify MTBE adsorption kinetics, short bed adsorber (SBA) tests were conducted (Weber and Liu 1980, Knappe et al. 1999). With the GAC and the silicalite zeolite, SBA tests were conducted with both 12×40 (1.7×0.425 mm) and 30×40 (0.6×0.425

mm) U.S. mesh size fractions. The as-received CC-602 GAC particle size distribution was used to assemble a matching 12×40 U.S. mesh silicalite adsorbent after lightly crushing and sieving the as-received HiSiv 3000 extrudates. For the carbonaceous resin, only the 30×40 U.S. mesh size fraction was evaluated, which was the dominant particle size fraction in the commercially available 20×50 (0.85×0.3 mm) U.S. mesh product. Tables 2 and 3 show operating parameters for SBA tests conducted with 30×40 and 12×40 U.S. mesh adsorbents, respectively.

Prior to SBA tests, adsorbents were dried for 24 hours at 105°C. The weighed adsorbent was placed for two days in a desiccator without desiccant and with two beakers containing a supersaturated solution of calcium chloride (Erdem-Senatalar et al. 2004). Adsorbents were then washed with UPW until no fines were visible in the supernatant. Finally, adsorbents were soaked in UPW overnight. One hour prior to starting SBA tests, MTBE stock solution was spiked into the entire influent water volume to yield an MTBE concentration of ~100 μg/L. MTBE volatilization was minimized by containing the solution in a white LDPE bag that was placed in a stainless steel drum covered with a floating polypropylene lid. Influent MTBE samples were taken in triplicate at the start and at the completion of each SBA test. For the seven SBA tests shown here, MTBE losses in the column influent ranged from 3.6 to 9.0% during the 18-hour test, and the average influent MTBE concentrations shown in Tables 2 and 3 were used to describe the data with the homogeneous surface diffusion model (HSDM).

Adsorption kinetics model

The HSDM (Crittenden and Weber 1978) was used to determine film mass transfer (k_f) and surface diffusion (D_s) coefficients that best described the SBA data. Values of k_f and D_s were obtained by minimizing the root mean square difference between the HSDM output and the experimental data with a nonlinear least-squares optimization algorithm (Yuasa 1982, Knappe et al. 1999). Subsequently, equilibrium and kinetic parameters derived from isotherm and SBA experiments were used to predict MTBE breakthrough curves with the HSDM. Predicted MTBE breakthrough curves were used to compare adsorbent usage rates and associated costs.

Pilot-scale adsorbers

MTBE breakthrough curves predicted by the HSDM for the GAC and the silicalite were verified with pilot-scale adsorber data. To evaluate the effects of NOM preloading on MTBE removal, each adsorbent was tested in fresh form and after an NOM preloading period of two months. Selection of empty bed contact times (EBCTs) for the pilot-scale adsorbers (9.6 minutes for GAC, 2.2 minutes for silicalite) was based on HSDM predictions and a design target of reaching at least 50% MTBE breakthrough after two months of operation with an influent MTBE concentration of 100 μg/L. A schematic of the pilot-scale adsorber setup is shown in Figure 1. The pilot plant was operated at the Greenville, NC, drinking water treatment plant and consisted of two parallel trains, one containing two GAC

columns (fresh and preloaded) and the other two zeolite columns (fresh and preloaded). Table 4 shows key operating parameters for the pilot-scale adsorbers.

Prior to pilot testing, adsorbents were prepared in the manner described for SBA tests. Upon placement of the adsorbents into the glass columns and backwashing the bed, the adsorbent bed depth was measured to calculate the stratified bed density. One zeolite column and one activated carbon column were preloaded for two months with pre-settled TRW before MTBE spiking was initiated. During the preloading period, the influent TOC concentration ranged from 5.4-6.6 mg/L and the turbidity from 1.8-17 NTU. Following preloading, the influent to the columns was switched to settled water (TOC range was 1.7-3.4 mg/L, turbidity range was 0.28-0.71 NTU) that was spiked with MTBE using a syringe pump. Adsorbers were backwashed daily during both the preloading and MTBE-spiking phases. Duplicate influent and effluent samples were taken in 40-mL EPA vials three times per week and stored headspace-free at 4°C for up to 5 days prior to analysis.

MTBE analysis

Aqueous samples were analyzed for MTBE using a purge-and-trap concentrator (Tekmar 3100, Cincinnati, OH) that was connected to a gas chromatograph (Shimadzu 14a, Columbia, MD) equipped with a 30-m column (J&W Scientific DB-VRX, I.D. 0.45 mm, liner thickness 2.55 mm, Folsom, CA) and a flame ionization detector. (Knappe et al. 2003, 2007).

RESULTS AND DISCUSSION

MTBE adsorption isotherms

Comparing single-solute MTBE adsorption isotherm data for the three tested adsorbents, Figure 2 illustrates that the carbonaceous resin (Ambersorb 563) exhibited the largest MTBE adsorption uptake when the equilibrium liquid-phase MTBE concentration was less than ~25 μg/L. In contrast, the silicalite zeolite (HiSiv 3000) exhibited the largest MTBE adsorption uptake at higher liquid-phase MTBE concentrations. Compared to the carbonaceous resin and the silicalite zeolite, the MTBE adsorption uptake of the tested activated carbon was considerably smaller (Figure 2); i.e., relative to the MTBE adsorption uptakes of the carbonaceous resin and the silicalite, the MTBE adsorption uptake of the activated carbon was, respectively, 26% and 34% at an equilibrium liquid-phase MTBE concentration of 10 μg/L. Single-solute MTBE adsorption isotherms obtained with the silicalite zeolite and the carbonaceous resin agreed well with previously published data (e.g. Erdem-Senatalar et al. 2004, Bi et al. 2005).

To evaluate the effect of NOM on MTBE adsorption uptakes of alternative adsorbents, MTBE adsorption isotherm experiments were conducted in TRW. For the silicalite (HiSiv3000, Figure 2), a comparison of MTBE adsorption isotherms in UPW and TRW shows that the MTBE adsorption uptake in TRW was similar to that in UPW, especially at high adsorbent doses (low equilibrium liquid phase MTBE concentrations). In contrast, Figure 2 shows that the presence of NOM decreased the MTBE adsorption uptake

of the CC-602 GAC over the entire range of tested liquid-phase MTBE concentrations; the average MTBE adsorption uptake in TRW ($C_{0,MTBE}$ = 100 μg/L) was 62% of that measured in UPW. This results suggests that NOM had access to the internal pore structure of the GAC, where it competed with MTBE for adsorption sites and/or blocked MTBE access to micropores. As discussed by Knappe and Rossner Campos (2005), the presence of NOM decreased the MTBE adsorption uptake of the carbonaceous resin more dramatically than that of the CC-602 GAC.

MTBE adsorption kinetics

Short bed adsorber (SBA) tests were conducted with MTBE-spiked UPW to quantify single-solute MTBE adsorption kinetics on the activated carbon (CC-602), the carbonaceous resin (Ambersorb 563), and the silicalite zeolite (HiSiv 3000). Figure 3 depicts SBA test data describing MTBE adsorption rates from UPW on the 30×40 U.S. mesh size fraction of the three adsorbents. Using the HSDM with the Freundlich parameters describing the single-solute MTBE isotherms shown in Figure 2 as inputs, kinetic parameters (k_f and D_s) were determined from best fits of the HSDM to SBA test data (Table 5). As shown in Figure 3, good agreement between the HSDM fits and the experimental data suggests that the HSDM is an effective model for describing the adsorption of MTBE on a wide range of microporous adsorbents. Recent results by Hung et al. (2005) and Hung and Lin (2006) showed that the HSDM effectively described MTBE adsorption kinetics on a powdered mordenite zeolite. While Hung and Lin (2006) chose a pore diffusion model to describe the adsorption of

MTBE on two carbonaceous resins, Hand et al. (1994) showed that the HSDM effectively described the rate of TCE adsorption on the carbonaceous resin Ambersorb 563.

For the 30×40 U.S. mesh adsorbents evaluated here, k_f values in the range of 0.85×10^{-3} to 3.51×10^{-3} cm/s were obtained (Table 5). The k_f values for the carbonaceous resin and the silicalite zeolite were, respectively, ~45% and ~24% of that obtained for the activated carbon. Differences in k_f values for different adsorbents of similar size have been attributed to differences in particle shape and surface topography (van Vliet and Weber 1981). Figure 4 depicts scanning electron micrographs of the studied adsorbents. Both the GAC and the silicalite zeolite particles were angular and exhibited a rough surface. In contrast, the carbonaceous resin was approximately spherical and exhibited a relatively smooth surface. Consistent with van Vliet and Weber (1981), the k_f value obtained with activated carbon was larger than that obtained with a carbonaceous resin (Table 5), and these results may be partially explained by the greater angularity and roughness of the GAC. However, the k_f value of the silicalite was smaller than that of the carbonaceous resin, suggesting that adsorbent characteristics other than angularity and roughness influence the magnitude of k_f. It should be noted that *a priori* estimates of k_f (Gnielinski relationship, Sontheimer et al. 1988) yielded values in the range of $4.5\text{-}4.7\times10^{-3}$ cm/s.

Surface diffusion coefficients (D_s) describing intraparticle MTBE mass transfer for the three adsorbents differed by a factor of almost 30. The smallest D_s value was obtained for the carbonaceous resin and the largest for the GAC (Table 5). The D_s value describing

MTBE adsorption on the 30×40 U.S. mesh size fraction of the GAC (1.97×10^{-10} cm^2/s) obtained here is similar to recently published D_s values describing MTBE adsorption on the 40×50 U.S. mesh size fraction of coal-based F400 GAC (4.0×10^{-10} cm^2/s, Hung et al. 2005). Also, the surface diffusion coefficient describing MTBE adsorption on the 30×40 U.S. mesh size fraction of the carbonaceous resin (7.21×10^{-12} cm^2/s) is similar to D_s values describing TCE adsorption on the same resin (1.37×10^{-11} cm^2/s for the 20x50 U.S. mesh size fraction and 4.74×10^{-12} cm^2/s for the 60×80 U.S. mesh size fraction, Hand et al. 1994). For the silicalite (HiSiv 3000), no directly comparable data exist; however, Hung et al. (2005) reported a D_s value of 2×10^{-13} cm^2/s for MTBE adsorption from UPW on a powdered mordenite zeolite (d_p = 0.76 μm), a value that is more than two orders of magnitude smaller than the one obtained here for silicalite. The differences in MTBE diffusivities between the two zeolite types may be related to structural differences between mordenite and silicalite; the mordenite framework is essentially one-dimensional from a standpoint of MTBE accessibility while MTBE can be expected to diffuse in three dimensions within the silicalite framework (Olson et al. 1981).

To evaluate the effects of NOM on MTBE adsorption rates, SBA tests were conducted with the as-received 12×40 U.S. mesh size fraction of CC-602 GAC and a matching 12×40 U.S. mesh size fraction of HiSiv 3000 silicalite that was assembled in-house by lightly crushing as-received HiSiv 3000 extrudates. Figure 5 depicts MTBE adsorption rate data on the two adsorbents from UPW and TRW. Figure 5 clearly illustrates that the NOM in TRW negatively affected MTBE removal rates obtained with both the GAC and the

zeolite. While the NOM effect is in part embedded in the equilibrium parameters (see Freundlich isotherm parameters in Figure 2), it is also manifested in the kinetic parameters shown in Table 5. For example, k_f values obtained in TRW were ~70 and ~80% of the k_f values obtained in UPW for the silicalite and the GAC, respectively. Furthermore, D_s values obtained in TRW were ~35 and ~70% of those obtained in UPW for the silicalite and the GAC, respectively (Table 5). Thus, NOM more severely retarded MTBE adsorption kinetics on the silicalite zeolite than on the coconut-shell-based GAC. This result is supported by the work of Hung et al. (2005), who suggested that D_s values describing MTBE adsorption rates on coal-based F400 GAC were not affected by NOM; in contrast, the presence of NOM decreased the D_s value describing MTBE adsorption rates on pulverized mordenite by one order of magnitude from 2×10^{-13} to 2×10^{-14} cm^2/s. The NOM effects on D_s observed here and by Hung et al. (2005) support the hypothesis that a small portion of the NOM in TRW adsorbs near the pore entrances of high-silica zeolites and interferes with MTBE adsorption rates as manifested by decreases in both k_f and D_s.

A comparison of the kinetic parameters obtained for the 30×40 and 12×40 U.S. mesh size fractions (Table 5) permits the evaluation of adsorbent particle size effects on k_f and D_s values. For the 30×40 U.S. mesh size fraction (geometric mean diameter = 0.5 mm), k_f values were 7 and 20% larger than those obtained with the 12×40 U.S. mesh size fraction (d_{50} = 1.0 mm) for the silicalite and the GAC, respectively. This trend is reasonable given that the specific external surface area increases with decreasing particle size. For D_s, larger values were obtained with the 12×40 U.S. mesh size fraction than with the 30×40 U.S. mesh size

fraction for both the silicalite (~40% larger) and the GAC (~60% larger). Knowledge about the dependence of D_s values on adsorbent particle diameter (d_p) is important to properly scale such tests as the rapid small-scale column test (RSSCT). The results obtained here suggest that the constant diffusivity relationship (D_s is independent of d_p), which is frequently used to simulate trace organic contaminant removal in RSSCTs, would not be appropriate for simulating MTBE removal by the silicalite and the GAC used in this study. Additional SBA tests with different adsorbent particle diameters would be required to establish the proper dependence of D_s on d_p.

Verification of predicted MTBE breakthrough curves

Pilot tests were conducted with the GAC and the silicalite zeolite to verify MTBE breakthrough curves predicted with the HSDM. Equilibrium and kinetic parameters pertaining to TRW (Figure 2, Table 5) were used as inputs to the HSDM. Figure 6 compares predicted and experimentally determined MTBE breakthrough curves for the pilot-scale GAC and silicalite adsorbers. Comparing the predicted MTBE breakthrough curve for GAC and the data obtained with fresh GAC, Figure 6 shows that good agreement was obtained for the first 2,500 bed volumes, which included the onset of MTBE breakthrough. Beyond 2,500 bed volumes, the experimental data show MTBE breakthrough that proceeded more rapidly than that suggested by the model prediction. For example, the experimental data showed 50% MTBE breakthrough after approximately 3,700 bed volumes while the HSDM prediction suggested that 50% breakthrough would be reached after ~4,800 bed volumes. This result is

not surprising as it is well known that equilibrium and kinetic parameters change over time as activated carbon continues to be exposed to NOM (e.g., Carter and Weber 1994, Knappe et al. 1999, Li et al. 2003b). Thus, an HSDM, in which equilibrium and kinetic parameters are adjusted in a dynamic manner is required to properly describe the breakthrough of trace organic contaminants in the presence of NOM. Such a model was recently developed by Schideman et al. (2006a, b); however, the parameterization of this model would have required a number of additional experiments that were outside of the scope of this work.

Comparing the predicted MTBE breakthrough curve for silicalite and the data obtained with fresh silicalite, Figure 6 shows good agreement for the first 16,000 bed volumes. Because of the short EBCT of the zeolite adsorber, MTBE breakthrough occurred from the start, and 50% MTBE breakthrough was obtained after approximately 13,000 bed volumes, which closely matched the result of the HSDM prediction, that showed 50% MTBE breakthrough after ~14,000 bed volumes.

A comparison of the experimentally obtained MTBE breakthrough curves for fresh and preloaded GAC shows (1) that preloaded NOM caused MTBE to break through almost immediately and (2) 50% MTBE breakthrough was obtained after ~2,500 bed volumes with preloaded GAC rather than after ~3,700 bed volumes with fresh GAC. For the silicalite, a comparison of the MTBE breakthrough curves obtained with fresh and preloaded adsorbent shows that NOM preloading did not appear to affect the MTBE removal performance. Apart from one MTBE excursion after ~3,000 bed volumes, the preloaded zeolite performed

similarly or slightly better than the fresh zeolite (e.g., 50% breakthrough did not occur until ~19,000 bed volumes with the preloaded zeolite). The latter result suggests that the effect of NOM on equilibrium and kinetic parameters describing MTBE adsorption on silicalite could be quantified with simple isotherm and SBA tests that employed the fresh adsorbent and the natural water of interest. Longer-term NOM fouling effects that continuously degrade the effectiveness of GAC adsorbers did not appear to play a role in the silicalite-based adsorption system.

Estimates of adsorbent usage rates and associated costs

Using the HSDM, MTBE breakthrough curves were predicted to estimate adsorbent usage rates and associated costs. Equilibrium and kinetic parameters shown in Figure 2 and Table 5 served as inputs to the HSDM. One set of MTBE breakthrough curves was predicted for adsorbers containing the 30×40 U.S. mesh size fraction of (1) CC-602 GAC, (2) Ambersorb 563 carbonaceous resin, and (3) HiSiv 3000 silicalite. An EBCT of 15 minutes, an approach velocity of 6 m/h, and an influent MTBE concentration of 100 μg/L in UPW were assumed. Table 6 summarizes adsorber life predictions for an assumed termination criterion of 10% MTBE breakthrough. The longest adsorber life figures were obtained for the silicalite (568 d) and the shortest for the GAC (114 d). Table 6 also shows adsorbent usage rates (AURs) and associated costs, again assuming a termination criterion of 10% MTBE breakthrough. AURs were smallest for the silicalite (~12 mg/L) and largest for the GAC (~46 mg/L). Assuming adsorbent costs of ~$7/lb for HiSiv 3000 (Price and Schmidt 1998, Hajdu

2004), ~$35/lb for Ambersorb 563 (Melin 1999), and ~$1/lb for CC-602 (Melin 1999), costs associated with adsorbent usage ranged from $0.38/1000 gal for CC-602 to $6.47/1000 gal for Ambersorb 563 (Table 6). The cost associated with the silicalite usage rate was predicted to be $0.70/1000 gal; i.e. ~84% larger than that associated with the GAC usage rate.

To evaluate the effect of NOM on MTBE breakthrough curve predictions, equilibrium and kinetic parameters for the 12×40 U.S. mesh size fractions of the GAC and the silicalite were used as input to the HSDM (Figure 2, Table 5). Adsorber life predictions at a termination criterion of 10% MTBE breakthrough were considerably shorter with TRW than with UPW (12x40 mesh size fraction entries in Table 6). The predicted decreases in adsorber life were >50% for both the GAC and the silicalite. Effects of NOM on costs associated with adsorbent usage were also compared at 10% MTBE breakthrough. As shown in Table 6, costs associated with CC-602 usage were predicted to increase from $0.46/1000 gal in UPW to $0.98/1000 gal in TRW while those associated with HiSiv 3000 usage were predicted to increase from $0.90/1000 gal in UPW to $2.22/1000 gal in TRW. For the 10% MTBE breakthrough criterion, costs associated with CC-602 usage are expected to remain at $0.98/1000 gal for other influent MTBE concentrations in TRW (Matsui et al. 2002). In contrast, HSDM predictions suggest that costs associated with HiSiv 3000 usage decrease to $1.83/1000 gal and $1.52/1000 gal for influent MTBE concentrations of 50 and 25 μg/L in TRW, respectively.

While the predicted cost associated with the silicalite usage rate is larger than that associated with the GAC usage rate, factors such as adsorbent change-out and adsorbent regeneration need to be considered to obtain true treatment costs. For example, adsorbent change-out for the single-column operation scenario, for which predictions were made, would have to occur ~11 times per year for an adsorber filled with CC-602 GAC but only ~twice per year for an adsorber filled with HiSiv 3000 silicalite. Furthermore, the pilot column results suggest that NOM preloading does not impair the MTBE removal efficiency of silicalite. Thus, it may be possible to regenerate spent HiSiv 3000 silicalite with steam or microwave methods rather than with more energy-intensive thermal methods that are required to regenerate GAC. This opportunity may further lower the life-cycle cost of a silicalite-based adsorption system for MTBE removal from water.

Finally, adsorbent usage rates can be decreased by operating adsorbers in parallel (where a second adsorber is brought on-line after the first adsorber has reached the termination criterion and the effluents of the two adsorbers are blended once the second adsorber is put into service) or in series (where one column is operated until the termination criterion is reached, at which point the second column is added in series behind the first column; once the termination criterion for the column-in-series operation is reached, adsorbent is replaced in the lead column, and the column order is switched). To illustrate the advantages of operating columns in parallel, Figure 7 compares MTBE breakthrough curves predicted for single adsorbers and blended MTBE effluent concentrations predicted for adsorption systems, in which two and four columns are operated in parallel (see Snoeyink

and Summers 1999 for relevant calculations). At a termination criterion of 10% MTBE breakthrough, Table 7 summarizes bed volumes that can be treated with individual CC-602 and HiSiv 3000 adsorbers for the single-column, the two-columns-in-parallel, and the four-columns-in-parallel scenarios. The effects of operating columns in parallel on adsorber life, AURs, and associated costs are shown in Table 7. For HiSiv 3000, operating four columns in parallel decreased costs associated with adsorbent usage by ~32% compared to the single-column operation. Similarly, operating four CC-602 GAC columns in parallel decreased costs associated with adsorbent usage by ~23% compared to the single-column operation. Comparing treatment costs between the GAC and the silicalite, the predicted costs associated with the silicalite usage rate were double those predicted for the GAC usage rate when four columns in parallel are used. Adsorbent replacement would have to occur 8.4 times per year for the GAC and 1.4 times per year for the silicalite.

CONCLUSIONS

The MTBE removal effectiveness of a silicalite zeolite and a carbonaceous resin was compared to that of a coconut-shell-based GAC. Adsorption isotherm and short bed adsorber tests were completed in UPW and river water to determine equilibrium and kinetic parameters describing the adsorption of MTBE. The HSDM was used to describe adsorption kinetic data and to predict MTBE breakthrough curves for packed bed adsorbers. The results of this research showed that:

- MTBE adsorption uptakes of the silicalite zeolite and the carbonaceous resin were larger than that of the tested GAC
- For the silicalite, co-adsorbing NOM had a small effect on the MTBE adsorption uptake but a more pronounced effect on MTBE adsorption kinetics. For the GAC, co-adsorbing NOM had a more pronounced effect on MTBE adsorption uptake but a smaller effect on MTBE adsorption kinetics.
- For equally sized adsorbers with an empty-bed contact time of 15 minutes, an influent MTBE concentration of 100 μg/L in river water, and a termination criterion of 10% MTBE breakthrough (i.e., effluent MTBE concentration of 10 μg/L), an adsorber containing coconut-shell-based GAC was predicted to have a useful life of 33 days while an adsorber containing silicalite was predicted to have a useful life of 175 days.
- While costs associated with silicalite usage (cost: ~$7/lb) were approximately double those associated with GAC usage (cost: ~$1/lb), other factors such as costs associated with adsorbent replacement and regeneration/disposal need to be included to obtain an improved estimate of overall treatment cost.
- While the tested carbonaceous resin exhibited an MTBE adsorption uptake similar to that of silicalite, its unit cost was too high to make the carbonaceous resin cost-competitive.

Overall, the results of this research showed that silicalite is an alternative adsorbent that should be considered for full-scale applications that specifically target MTBE removal.

ACKNOWLEDGMENTS

The authors would like to thank the American Water Works Association Research Foundation for funding this research. In addition, we would like to thank Cliff Strickland and other staff members at the Greenville Utilities Commission for pilot plant maintenance and sample collection, Carl Saquing for SEM images, Nneka Ubaka-Adams for sieve analyses and adsorbent preparation, and David Black for GC analyses.

REFERENCES

Acero, J.L., Haderlein, S.B., Schmidt, T.C., Suter, M.J.F., von Gunten, U., 2001. MTBE oxidation by conventional ozonation and the combination ozone/hydrogen peroxide: Efficiency of the processes and bromate formation. Environ. Sci. Tech. 35(21), 4252-4259.

Anderson, M.A. 2000. Removal of MTBE and other organic contaminants from water by sorption to high silica zeolites. Environ. Sci. Tech. 34(4), 725-727.

Bi, E., Haderlein, S.B., Schmidt, T.C., 2005. Soprtion of methyl *tert*-butyl ether (MTBE) and *tert*-butyl alcohol (TBA) to synthetic resins. Wat. Res. 39, 4164-4176.

Carter, M.C., Weber, W.J. Jr., 1994. Modeling adsorption of TCE by activated carbon preloaded by background organic matter. Environ. Sci. Tech. 28(4), 614-623.

Crittenden, J.C., Weber, W.J. Jr., 1978. Predictive model for design of fixed-bed adsorbers: Parameter estimation and model development. J. Environ. Eng. 104, 185-197.

Deeb, R.A., Chu, K., Shih, T., Linder, S., Suffet, I., Kavanaugh, M.C., Alvarez-Cohen. L., 2003. MTBE and other oxygenates: Environmental sources, analysis, occurrence, and treatment. Environ. Eng. Sci. 20(5), 433-447.

Environmental Working Group., 2003. MTBE in drinking water." http://www.ewg.org/node/21314, accessed August 2007.

Erdem-Senatalar, A., Bergendahl, J.A., Giaya, A., Thompson, R.W., 2004. Adsorption of methyl tertiary butyl ether on hydrophobic molecular sieves. Environ. Eng. Sci. 21(6), 722-729.

Hajdu, D. 2004. Personal communication, UOP Molecular Sieves, Mt. Laurel, NJ.

Hand, D.W., Herlevich, J.A., Jr., Perram, D.L., Crittenden, J.C., 1994. Synthetic adsorbent versus GAC for TCE removal. J. Am. Water Works Assoc. 86(8), 64-72.

Hung, H.W., Lin, T.F., Baus, C., Sacher, F., Brauch, H.J., 2005. Competitive and hindering effects of natural organic matter on the adsorption of MTBE onto activated carbons and zeolites. Environ. Tech. 26, 1371-1382.

Hung, H.W., Lin, T.F., 2006. Adsorption of MTBE from contaminated water by carbonaceous resins and mordenite zeolite. J. Hazard. Mat. 135(1-3), 210-217.

Knappe, D.R.U., Snoeyink, V.L., Roche, P., Prados, M.J., Bourbigot, M.M., 1999. Atrazine removal by preloaded GAC. J. Am. Water Works Assoc. 91(10), 97-109.

Knappe, D.R.U., Li, L., Quinlivan, P.A., Wagner, T.B., 2003. Effects of activated carbon surface chemistry and pore structure on the adsorption of trichloroethene and methyl tertiary-butyl ether from natural water. American Water Works Association Research Foundation: Denver, Colorado.

Knappe, D.R.U., Rossner Campos, A.A., 2005. Effectiveness of high-silica zeolites for the adsorption of methyl tertiary-butyl ether from natural water." Water Sci. Tech. – Water Supply 5(5), 83-91.

Knappe, D.R.U., Rossner, A., Snyder, S.A., Strickland, C., 2007. Alternative adsorbents for the removal of polar organic contaminants. American Water Works Association Research Foundation: Denver, Colorado.

Leitner, N.K.V., Papailhou, A.L., Croue, J.P., Peyrot, J., Dore, M., 1994. Oxidation of methyl tert-butyl ether by ozone and combined ozone hydrogen-peroxide. Ozone Sci. Eng. 16(1), 41-54.

Li, S., Tuan, V.A., Noble, R.D., Falconer, J.L., 2003a. MTBE adsorption on all-silica ß zeolite. Environ. Sci. Tech. 37(17), 4007-4010.

Li, Q., Snoeyink, V.L., Mariñas, B.J., Campos, C. 2003b. Elucidating competitive adsorption mechanisms of atrazine and NOM using model compounds. Water Res. 37, 773-784.

Liang, S., Palencia, L.S., Yates, R.S., Davis, M.K., Bruno, J.M., Wolfe, R.L., 1999. Oxidation of MTBE by ozone and peroxone processes. J. Am. Water Works Assoc. 91(6), 104-114.

Matsui, Y., Knappe, D.R.U., R. Takagi, 2002. Pesticide adsorption by granular activated carbon adsorbers – 1. Effect of natural organic matter preloading on removal rates and model simplification. Environ. Sci. Tech. 36(15), 3426-3431.

Melin, G., 1999. Evaluation of the applicability of synthetic resin sorbents for MTBE removal from water. The California MTBE Research Partnership. National Water Research Institute, Fountain Valley, CA.

Mormile, M.R., Liu, S., Suflita, J.M., 1994. Anaerobic biodegradation of gasoline oxygenates: Extrapolation of information to multiple sites and redox conditions. Environ. Sci. Tech. 28(9), 1727-1732.

Olson, D.H., Kokotailo, G.T., Lawton, S.L., Meier, W.M., 1981. Crystal structure and structure-related poroperties of ZSM-5. J. Phys. Chem. 85, 2238-2243.

Price, D.W. and Schmidt, P.S., 1998. VOC recovery through microwave regeneration of adsorbents: Process design studies. J. Air & Waste Management Assoc. 48(12), 1135-1145.

Quinlivan, P.A., Li, L., Knappe, D.R.U., 2005. Effects of activated carbon characteristics on the simultaneous adsorption of aqueous organic micropollutants and natural organic matter. Water Res. 39(8), 1663-1673.

Schideman, L.C., Mariñas, B.J., Snoeyink, V.L., Campos, C., 2006a. Three-component competitive adsorption model for fixed-bed and moving-bed granular activated carbon adsorbers. Part I. Model development. Environ. Sci. Tech. 40, 6805-6811.

Schideman, L.C., Mariñas, B.J., Snoeyink, V.L., Campos, C., 2006a. Three-component competitive adsorption model for fixed-bed and moving-bed granular activated carbon adsorbers. Part II. Model parameterization and verification. Environ. Sci. Tech. 40, 6812-6817.

Shih, T.C., Wangpaichitr, M., Suffet, M., 2003. Evaluation of granular activated carbon technology for the removal of methyl tertiary butyl ether (MTBE) from drinking water. Water Res. 37, 375-385.

Shih, T., Wangpaichitr, M., Suffet, M., 2005. Performance and cost evaluations of synthetic resin technology for the removal of methyl tert-butyl ether from drinking water. J. Environ. Eng. 131, 450-460.

Snoeyink, V.L., Summers, R.S., 1999. Adsorption of organic compounds. In Water quality and treatment, 5th ed., Letterman, R.D. (ed.), McGraw-Hill, Inc., New York, NY, pp. 13.57-13.60.

Sontheimer, H., Crittenden, J.C., Summers, R.S., 1988. Activated carbon adsorption for water treatment. 2nd ed. DVGW Forschungsstelle, Karlsruhe, Germany.

Stocking, A.J., Suffet, I.H., McGuire, M.J., Kavanaugh, M.C., 2001. Implications of an MTBE odor study for setting drinking water standards. J. Am. Water Works Assoc. 93(3), 95-105.

Sutherland, J., Adams, C., Kekobad, J., 2004. Treatment of MTBE by air stripping, carbon adsorption, and advanced oxidation: technical and economic comparison for five groundwaters. Water Res. 38, 193-205.

Szostak, R., 1998. Molecular sieves: principles of synthesis and identification. 2nd ed. Blackie Academic & Professional: New York, NY.

Van Vliet, B.M., Weber, W.J., Jr., 1981. Comparative performance of synthetic adsorbents and activated carbon for specific compound removal from wastewaters. J. Water Poll. Control Fed. 53(11), 1585-1598.

Weber, W.J., Jr., Liu, K.T., 1980. Determination of mass transport parameters for fixed-bed adsorbers. Chem. Eng. Comm. 6, 49-60.

Yuasa, A. 1982. A kinetic study of activated carbon adsorption processes. Doctoral Dissertation, Hokkaido University, Sapporo, Japan.

Table 1. Physical characteristics of granular adsorbents

Adsorbent	BET Surface Area (m^2/g)	Micropore Volume [*] (cm^3/g)	DFT Mesopore Volume [+] (cm^3/g)	BJH Mesopore Volume [§] (cm^3/g)
HiSiv 3000	346			
CC-602	1270	4.77×10^{-1}	3.93×10^{-2}	7.00×10^{-2}
Ambersorb 563	566	2.04×10^{-1}	4.21×10^{-1}	4.43×10^{-1}

[*] Micropore volume calculated with density functional theory (DFT) for pores with widths less than 20 Å

[+] Mesopore volume calculated with DFT for pores in the 20 to 360 Å (upper limit for the employed DFT model) size range

[§] Mesopore volume calculated with Barrett, Joyner, and Halenda (BJH) method for pores in the 20 to 500 Å size range

Table 2. Short bed adsorber operating parameters (30×40 U.S. mesh size fraction)

	HiSiv 3000	CC-602	Ambersorb 563
Dry adsorbent mass (g)	2.42	1.06	1.10
Bed depth (cm)	2.1	1.2	1.1
Apparent (bed) density (g/cm^3)	0.65	0.50	0.57
Bed porosity (-)*	0.35	0.33	0.33
Grain diameter (mm)§	0.50	0.50	0.50
Initial MTBE Conc. (µg/L)	94.6±2.79	93.9±1.89	93.0±3.05
Approach velocity (cm/min)	10.5±0.05	10.7±0.11	10.7±0.06
EBCT (min)	0.20	0.11	0.10
Column diameter (cm)	1.5	1.5	1.5

* Estimated from apparent (bed) densities and the following particle densities: 1 g/cm^3 for HiSiv 3000, 0.75 g/cm^3 for CC-602, and 0.85 g/cm^3 for Ambersorb 563

§ Geometric mean diameter of 30×40 U.S. mesh size fraction

Table 3. Short bed adsorber test operating parameters (12×40 mesh size fraction)

	HiSiv 3000		CC-602	
	UPW	**TRW**	**UPW**	**TRW**
Dry adsorbent mass (g)	14.5	13.4	4.85	4.93
Bed depth (cm)	3.8	3.8	2.0	2.0
Apparent (bed) density (g/cm^3)	0.75	0.70	0.48	0.49
Bed porosity (-)*	0.25	0.30	0.36	0.35
Grain diameter (mm)§	1.02	1.02	1.02	1.02
Initial MTBE Conc. (µg/L)	97.7±2.42	102.2±2.36	99.2±1.34	94.7±2.28
Approach velocity (cm/min)	10.4±0.15	10.1±0.08	10.6±0.11	10.7±0.06
EBCT (min)	0.36	0.38	0.19	0.19
Column diameter (cm)	2.54	2.54	2.54	2.54

* Estimated from apparent (bed) densities and the following particle densities: 1 g/cm^3 for HiSiv 3000 and 0.75 g/cm^3 for CC-602

§ d_{50} from sieve analysis

Table 4. Pilot plant operating parameters (12×40 mesh size fraction)

Conditions	HiSiv 3000		CC-602	
	Preloaded TRW*	TRW	Preloaded TRW*	TRW
Dry adsorbent mass (g)	80.34+	73.71	193.4§	183.6
Bed depth (cm)	21.7±0.55	22.8±1.22	95.2±3.26	96.8±3.59
Apparent (bed) density (g/cm^3)⌂	0.69	0.64	0.38	0.37
Bed porosity (-)⌂	0.31	0.36	0.49	0.50
Initial MTBE Conc. (µg/L)	98.6±4.34	97.6±4.55	99.4±5.14	98.5±5.39
Approach velocity (cm/min)	10.3±0.46	10.4±0.49	10.2±0.53	10.3±0.54
EBCT (min)	2.19±0.10	2.27±0.13	9.62±0.37	9.65±0.47
Column diameter (cm)	2.54	2.54	2.54	2.54

* Except for adsorbent mass, all parameters apply to the period, during which MTBE was spiked

\+ Approximately 4.7 g of the stated zeolite mass was lost during the preloading period (backwashing error). Bed depth of non-preloaded TRW column matched that of the preloaded TRW column as measured at the end of the preloading period

§ Approximately 9.2 g of the stated GAC mass was lost during the preloading period (backwashing error). Bed depth of non-preloaded TRW column matched that of the preloaded TRW column as measured at the end of the preloading period

⌂ For stratified bed

Table 5. Kinetic parameters describing MTBE adsorption from ultrapure water and Tar River water on 12×40 and 30×40 mesh size adsorbents

Adsorbent	Water Type	30×40 Mesh Size Fraction		12×40 Mesh Size Fraction	
		k_f (cm/s)	D_s (cm^2/s)	k_f (cm/s)	D_s (cm^2/s)
HiSiv 3000	UPW	8.47×10^{-4}	3.34×10^{-11}	7.92×10^{-4}	4.66×10^{-11}
	TRW			5.71×10^{-4}	1.65×10^{-11}
CC-602	UPW	3.51×10^{-3}	1.97×10^{-10}	2.92×10^{-3}	3.16×10^{-10}
	TRW			2.38×10^{-3}	2.19×10^{-10}
Ambersorb 563	UPW	1.59×10^{-3}	7.20×10^{-12}		

Table 6. Adsorber life, adsorbent usage rates (AURs), and costs associated with adsorbent usage based on HSDM predictions[*]

Adsorbent	Mesh Size Fraction	Water Type	ρ_{bed} (g/cm^3)	BV to 10% break-through	Adsorber life to 10% break-through (d)	AUR (mg/L)	Adsorbent cost ($/1000 gal)
HiSiv 3000	30×40	UPW	0.65[+]	54,560	568	11.9	0.70
	12×40	UPW	0.64[§]	41,600	433	15.3	0.90
	12×40	TRW	0.64[§]	16,820	175	37.9	2.22
CC-602	30×40	UPW	0.50[+]	10,980	114	45.6	0.38
	12×40	UPW	0.37[§]	6,740	70.2	55.5	0.46
	12×40	TRW	0.37[§]	3,180	33.1	118	0.98
Ambersorb 563	30×40	UPW	0.56[+]	25,540	266	22.1	6.47

[*] $C_{0,MTBE}$ = 100 μg/L; EBCT = 15 minutes

[+] Measured in SBA tests conducted with the 30×40 U.S. mesh size fraction

[§] Measured for stratified bed in pilot tests conducted with the 12×40 U.S. mesh size fraction

Table 7. Adsorber life, adsorbent usage rates (AURs), and cost estimates associated with adsorbent usage based on columns in parallel operation (12×40 mesh size fraction)[*]

Adsorbent	Column Operation	ρ_{bed} (g/cm^3)[+]	BV to 10% break-through	Adsorber life to 10% break-through (d)	AUR (mg/L)	Adsorbent cost ($/1000 gal)
HiSiv 3000	single	0.64	16,820	175	37.9	2.22
	2 parallel	0.64	21,460	223	29.7	1.73
	4 parallel	0.64	24,810	258	25.7	1.50
CC-602	single	0.37	3,180	33.1	118	0.98
	2 parallel	0.37	3,656	38.1	102	0.85
	4 parallel	0.37	4,140	43.5	90.3	0.75

[*] $C_{0,MTBE}$ = 100 μg/L; EBCT = 15 minutes; TRW

[+] Measured for stratified bed in pilot tests conducted with the 12×40 U.S. mesh size fraction

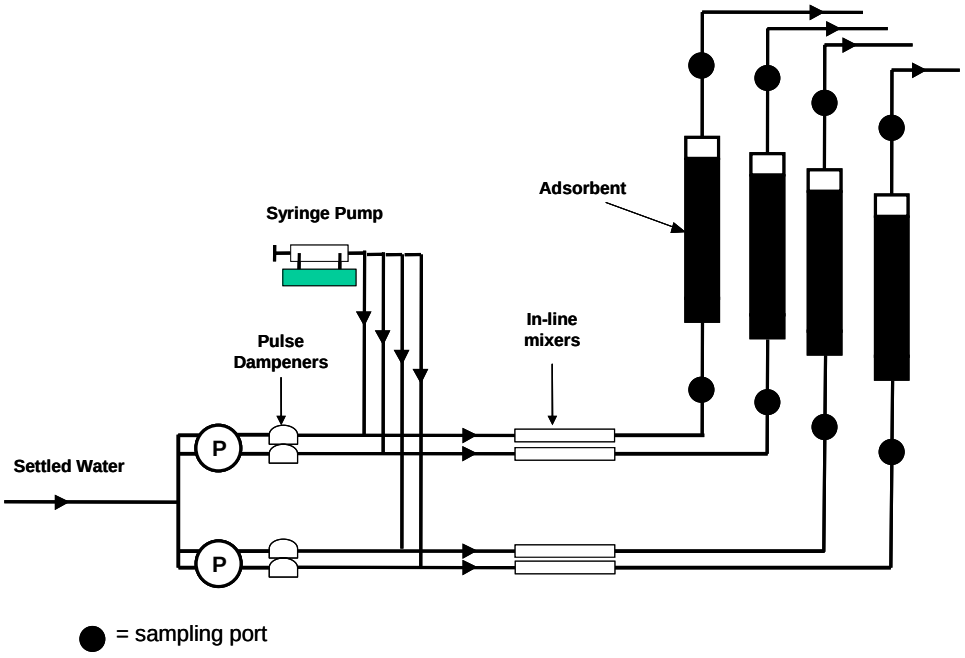

Figure 1. Pilot-scale adsorber setup

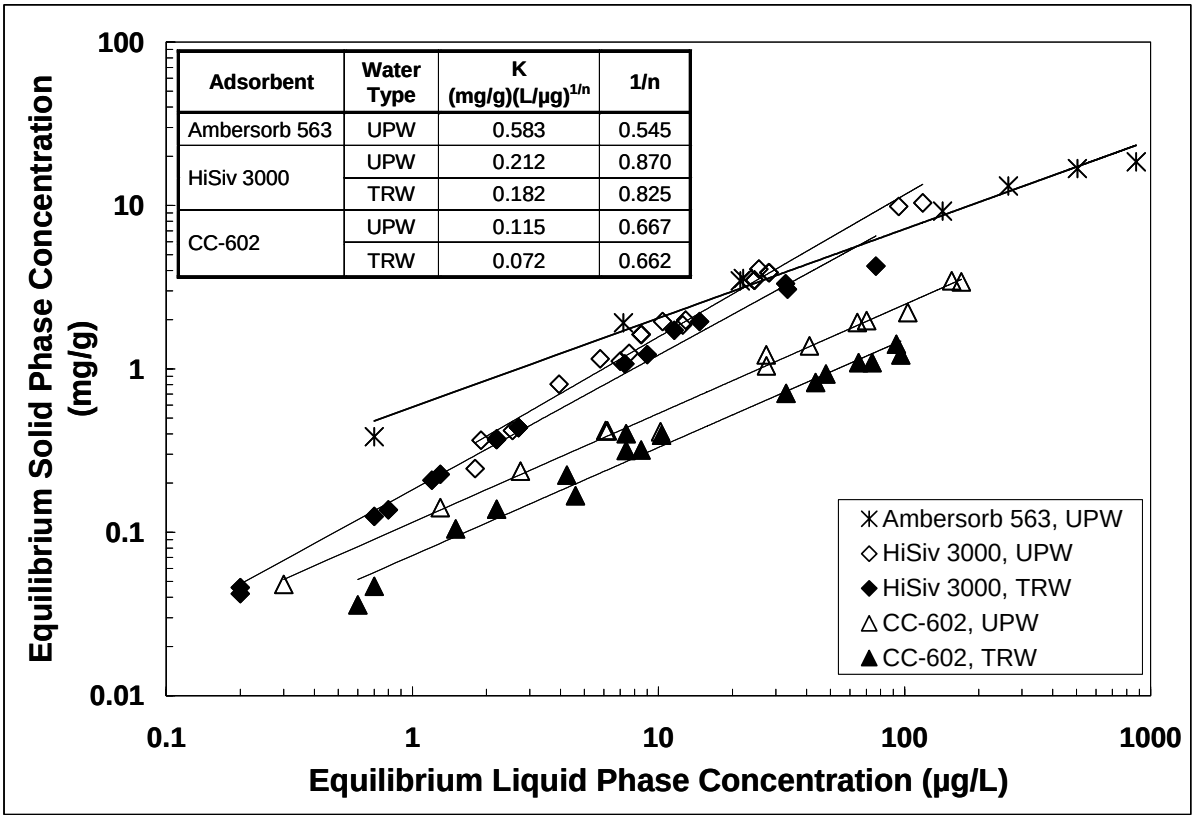

Figure 2. Effect of adsorbent type and natural organic matter on MTBE adsorption isotherms. Lines represent Freundlich isotherm model fits; Freundlich isotherm parameters are shown in the upper left hand corner.

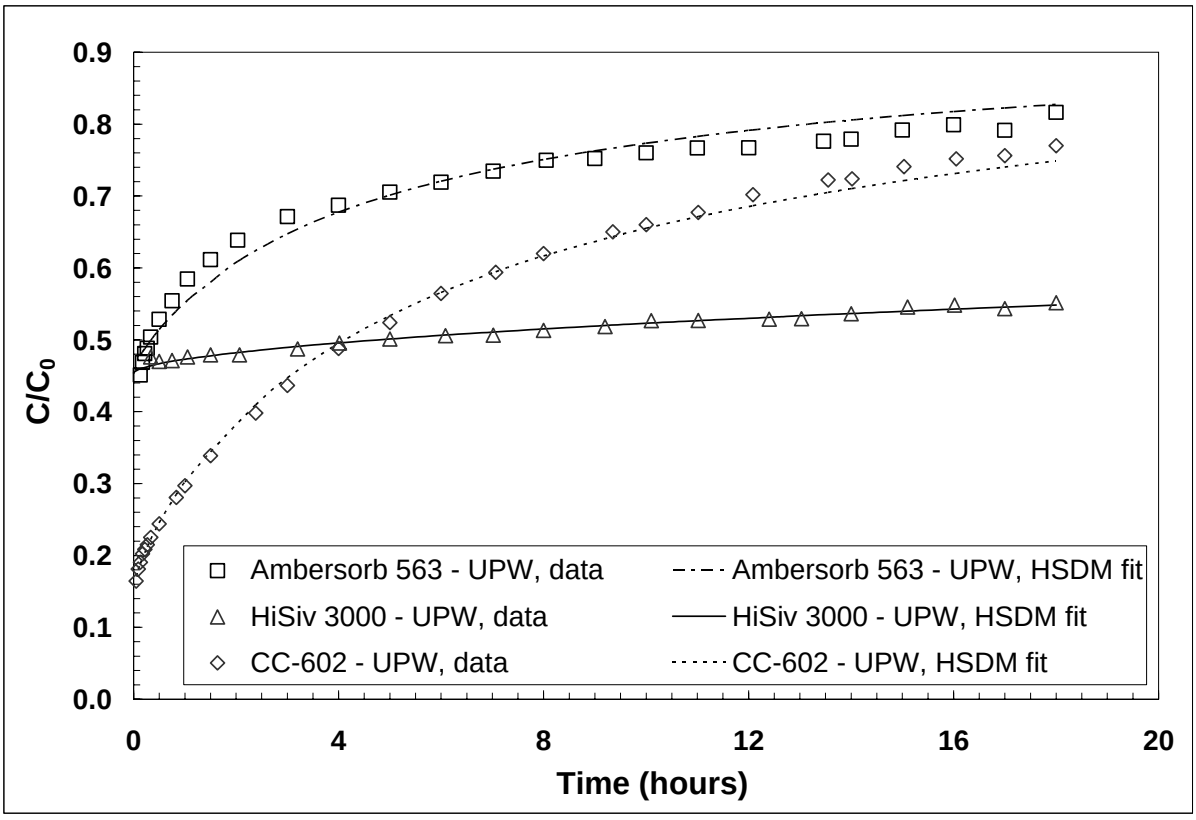

Figure 3. MTBE adsorption kinetics from UPW on 30×40 mesh adsorbents – short bed adsorber data and HSDM fits

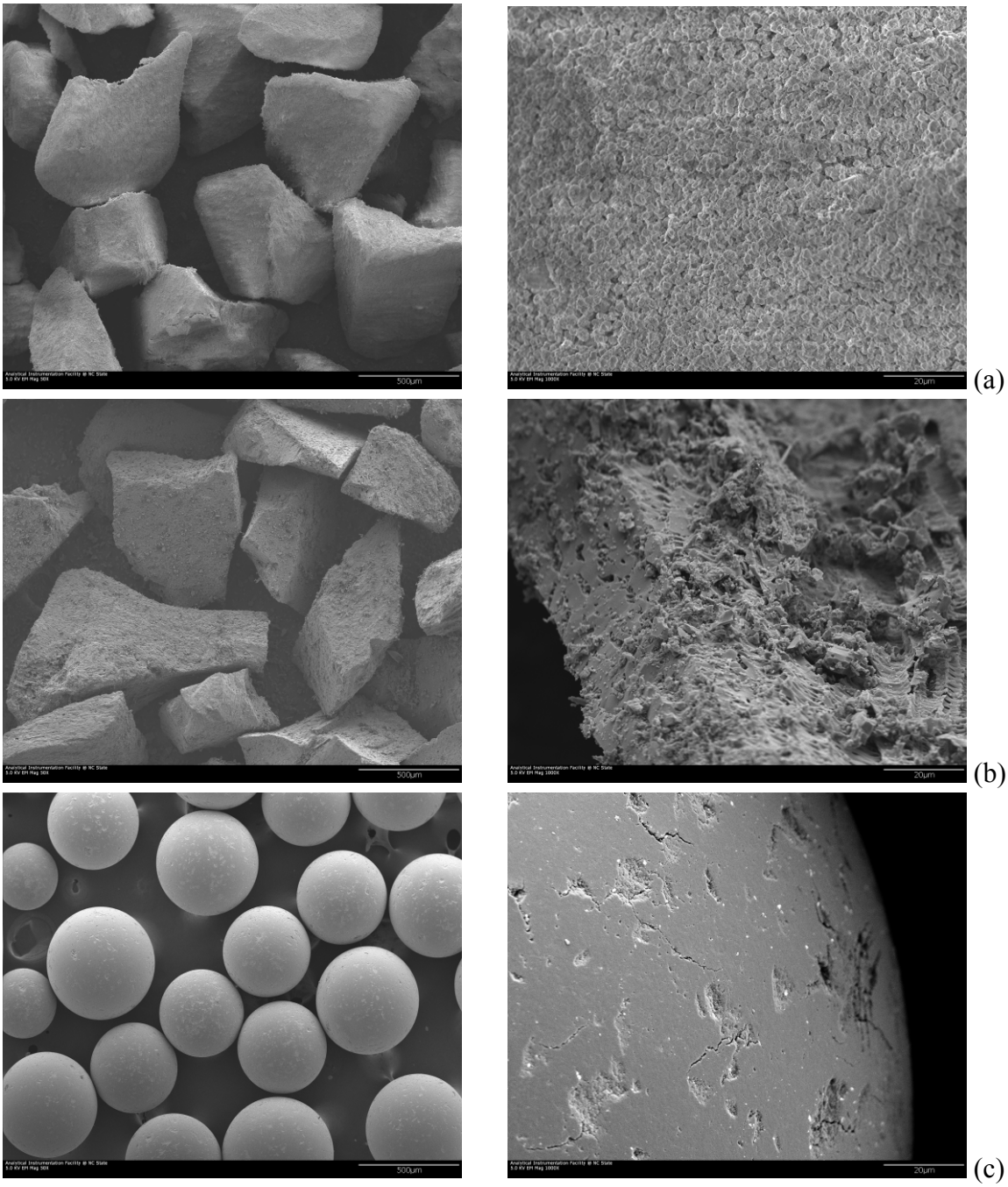

Figure 4. Scanning electron micrographs of the 30×40 U.S. mesh size fraction of (a) HiSiv3000 silicalite, (b) CC-602 GAC, and (c) Ambersorb 563 carbonaceous resin at two magnifications. Scale bar in images on the left indicates 500 µm; scale bar in images on the right indicates 20 µm.

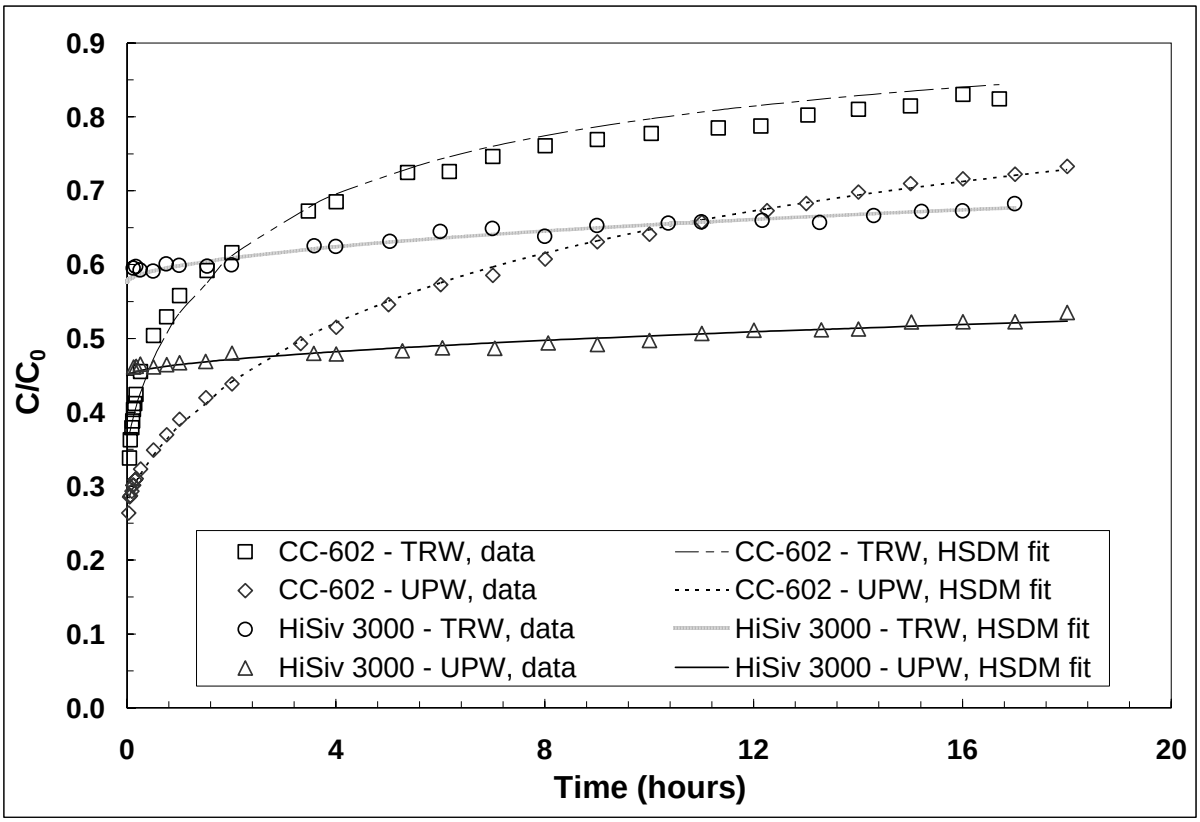

Figure 5. MTBE adsorption kinetics from UPW and TRW on 12×40 mesh adsorbents – short bed adsorber data and HSDM fits

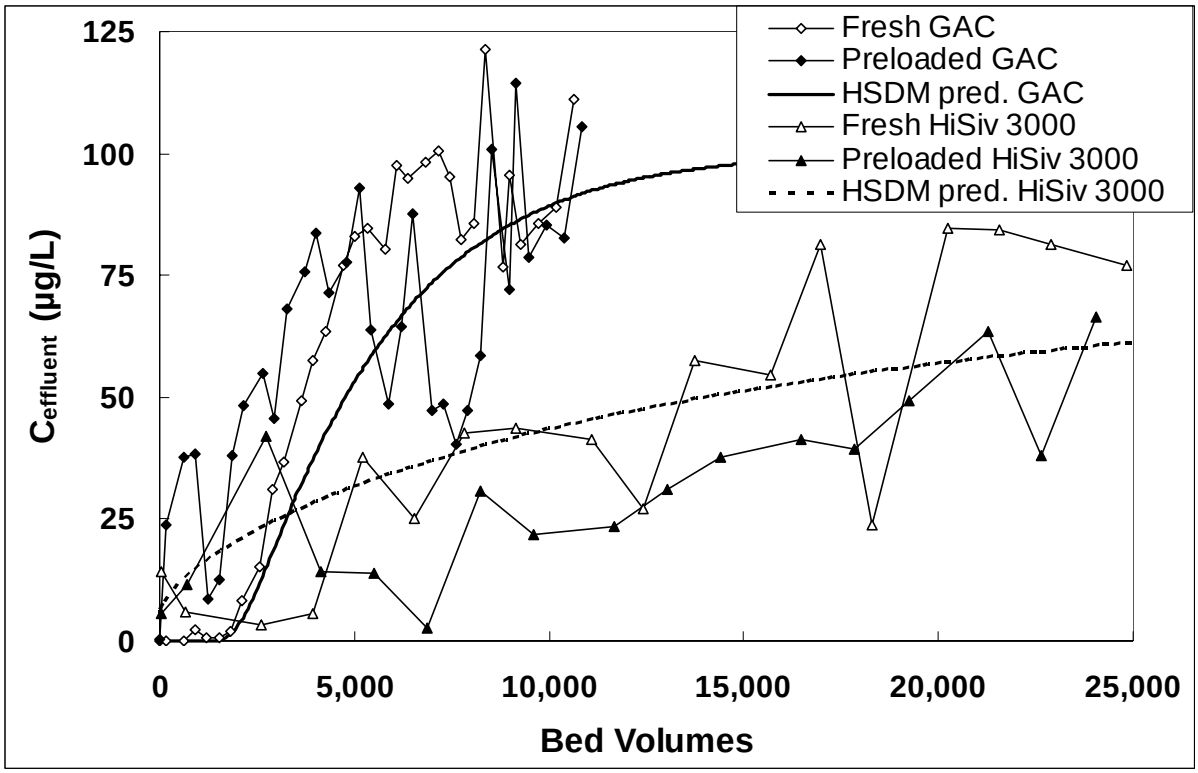

Figure 6. MTBE breakthrough curves obtained in TRW with fresh and preloaded GAC and silicalite zeolite

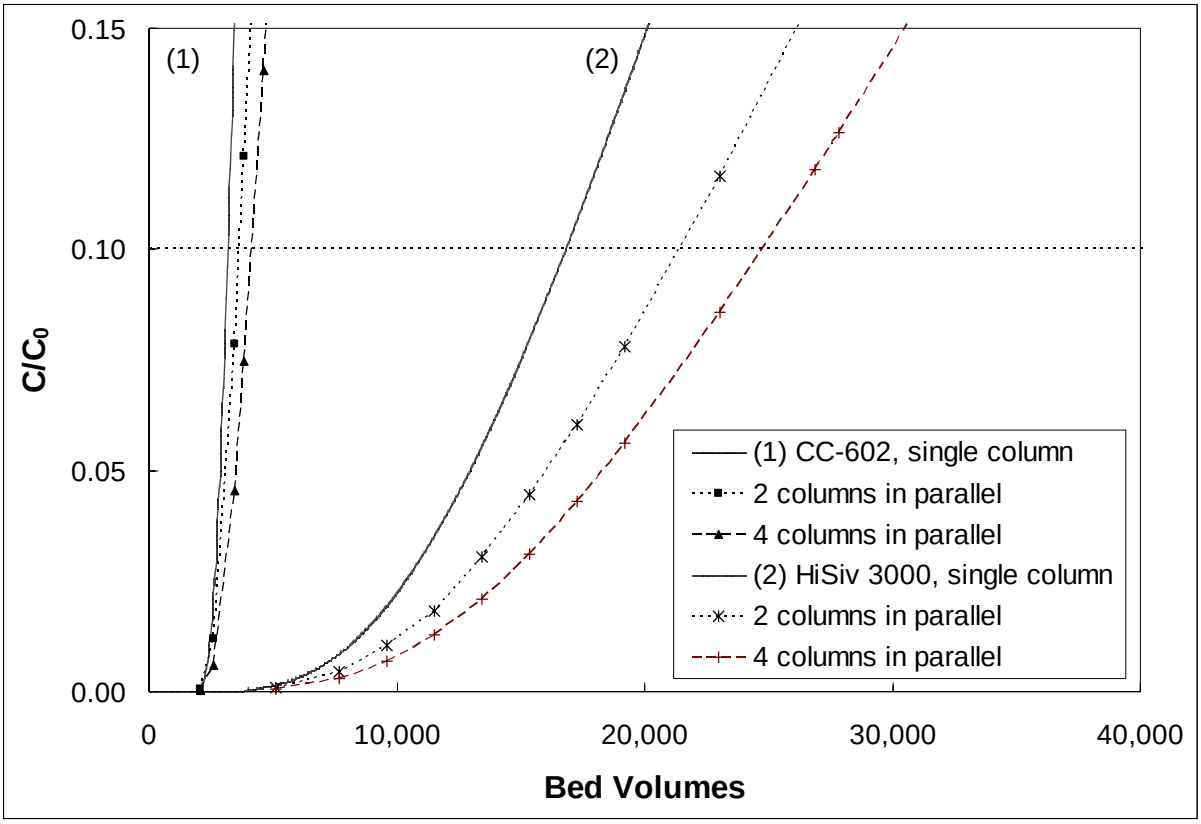

Figure 7. Effect of operating columns in parallel on blended effluent MTBE concentration predictions

CHAPTER 3

Removal of an Emerging Contaminant Mixture by Alternative Adsorbents

Alfred Rossner[1], Shane A. Snyder[2], and Detlef R.U. Knappe[1]

[1]Department of Civil, Construction, and Environmental Engineering, Campus Box 7908, North Carolina State University, Raleigh, North Carolina 27695-7908

[2]Department of Research and Development, Southern Nevada Water Authority, 1350 Richard Bunker Avenue, Henderson, Nevada 89015.

ABSTRACT

The effective removal of emerging pollutants of concern (EPOCs) such as endocrine-disrupting chemicals, pharmaceutically active compounds, personal care products, and flame retardants is a desirable water treatment goal. In this study, one activated carbon, one carbonaceous resin, and two high-silica zeolites were studied to evaluate their effectiveness for the removal of an EPOC mixture from lake water. Adsorption isotherm experiments were performed with environmentally relevant concentrations of the 28 targeted EPOCs (~200-900 ng/L). Among the tested adsorbents, activated carbon was the most effective, and activated carbon doses typically used for taste and odor control in drinking water (1-10 mg/L) were sufficient to achieve a 2-log removal for most of the tested EPOCs. The carbonaceous resin was less effective than the activated carbon because this adsorbent had a smaller volume of

pores in the size range required for the adsorption of many EPOCs (~ 6-9 Å). For the removal of the EPOC mixture, zeolites were less effective than the carbonaceous adsorbents. Because zeolites contain pores of uniform size and shape, a few of the tested EPOCs with matching pore size/shape requirements were well removed, but others barely adsorbed, even at zeolite doses of 100 mg/L. The results of this study demonstrate that heterogeneity in pore size and shape along with a large pore volume in the 6-9 Å size range are important adsorbent characteristics when an effective barrier against a broad spectrum of EPOCs is desired.

INTRODUCTION

The removal of emerging pollutants of concern (EPOCs) such as endocrine-disrupting chemicals, pharmaceutically active compounds, personal care products, and flame retardants is an important concern in the production of safe drinking water. Prescription and non-prescription drugs are present at detectable levels in many US surface waters (Kolpin et al. 2002), and conventional water treatment processes (coagulation/flocculation/sedimentation, filtration, and chlorination at levels required to achive 0.5-log Giardia inactivation) do not provide an effective barrier for many EPOCs (Adams et al. 2002). Therefore, effective treatment technologies are required to successfully remove this contaminant from drinking water.

Treatment options that are typically considered for the removal of EPOCs from drinking water include adsorption and (advanced) oxidation processes. While conventional and advanced oxidation processes can be effective for the removal of these compounds (e.g. Leitner et al. 1994, Liang et al. 1999, Adams et al. 2002, Westerhoff et al. 2005, Dodd et al. 2006), these processes lead to the formation of oxidation intermediates that are mostly unknown at this point. In addition, unwanted oxidation byproducts, such as halogenated organic compounds or bromate, form in oxidation processes involving chlorine and ozone. Adsorption processes do not add undesirable byproducts to drinking water, but high adsorbent usage rates can be expected if activated carbon is employed to adsorb polar organic contaminants (e.g., Knappe et al. 2003, Quinlivan et al. 2005).

While several studies have evaluated the adsorption of individual EPOCs on activated carbons in ultrapure water and in competition with natural organic matter (NOM) (Ternes et al. 2002, Adams et al. 2002, Yoon et al. 2003, Yoon et al. 2005, Choi et al. 2006), just one evaluated the removal of a mixture of contaminants by activated carbon adsorption (Westerhoff et al. 2005). No studies have investigated the effects of adsorbent pore size on EPOC removal, and no information is available on the effectiveness of high-silica zeolites and carbonaceous resins for the removal of EPOCs from drinking water sources. The objective of this study, therefore, was to compare the removal of an EPOC mixture spiked at environmentally relevant concentrations in lake water by four adsorbents (two high-silica zeolites, a carbonaceous resin and an activated carbon) with different pore sizes or pore size distributions.

Yoon et al. (2005) studied the removal of estradiol from ultrapure water and Colorado River water. In the presence of natural organic matter (NOM), lower estradiol removal was achieved compared to that obtained in ultrapure water. Furthermore, initial concentration effects on percent estradiol removal were negligible in the presence of NOM. A 1 mg/L carbon dose and a contact time of 4 hours yielded 70 to 85% estradiol removal from ultrapure water and 40 to 50% from CRW for initial estradiol concentrations ranging from 6.8 ng/L to 1362 ng/L (Yoon et al. 2005). Adsorption of estradiol and ethynyl estradiol on six activated carbons was reported by Yoon et al. (2003). For a contact time of 4 hours and a carbon dose of 5 mg/L, removal of estradiol and ethynyl estradiol from a model water exceeded 95% for all six activated carbons. Estradiol and ethynyl estradiol removal ranged from 87.4 to 98.6% in one natural water and from 50.4 to 96.4% in another when evaluating the six different carbons. Activated carbon adsorption was less effective for bisphenol A removal, ranging from 89.5 to 98.6% in a model water, from 47.2 to 87.6% in one natural water, and from 33.3 to 63.1% in another natural water (Yoon et al. 2003). Bisphenol A removal from natural water with powdered activated carbon (PAC) doses of 1-10 mg/L and 15 minutes of contact time, ranged from ~2 to 36% at an initial concentration of 497 ng/L and from 15 to 39% at an initial concentration of 1053 ng/L (Choi et al. 2005). Adsorption of seven antibiotics from distilled/deionized water (DD) and Missouri River water (MRW) was studied with Calgon WPH activated carbon using a contact time of 4 hours (Adams et al. 2002). Antibiotics removal ranged from 57 to 97% in DD water and from 49 to 73% in MRW at a 10 mg/L carbon dose. Ternes et al. (2002) reported high adsorption capacities of a coal based activated

carbon for four different pharmaceuticals (diclofenac, carbamazepine, clofibric acid and bezafibrate) in deionized water. Comparison of Freundlich adsorption parameter, K, showed lower adsorption capacities of the activated carbon in groundwater than in deionized water (Ternes et al. 2002). A recent study on adsorption of a mixture of EDC/PPCP in natural water by activated carbon reported removals in the range of 10 to more than 95% when using carbon doses of 5 mg/L at a contact time of 4 hours. Initial contaminant concentration did not affect percentage removal (Westerhoff et al. 2005).

MATERIALS AND METHODS

Materials.

Adsorption isotherm experiments were performed with Lake Mead water (LMW; Boulder City, NV) that was filtered through a 0.45-μm nylon membrane filter (Magna-R, MSI, Westboro, MA). The dissolved organic carbon (DOC) concentration of filtered LMW was 2.5 mg/L, the pH was 8.1, and the total alkalinity was approximately 140 mg/L as $CaCO_3$.

Four adsorbents were tested in this research: one coconut shell based GAC (CC-602, Westates Carbon, Siemens), one carbonaceous resin (Ambersorb 563, Rohm and Haas), one mordenite zeolite (HSZ-690HOA, Tosoh Corporation), and one Y zeolite (HSZ-390HUA, Tosoh Corporation). To enhance adsorption rates in isotherm experiments, all pelletized zeolites, the GACs, and the Ambersorb 563 resin were pulverized with a mortar and pestle

until >95% by mass passed a 74-µm sieve (200 U.S. mesh). Upon sieving, the portion remaining on the sieve was recombined with the portion that passed through the sieve to prevent bias as a result of any physical and/or chemical differences between the two fractions. Pulverized adsorbents were dried at 105°C for one day and stored in a desiccator.

Adsorption isotherm experiments were conducted with a mixture of 28 EPOCs. Table 1 lists the tested adsorbates and selected physicochemical properties. EPOCs were purchased in neat form and dissolved in methanol to yield a stock solution with EPOC concentrations of approximately 10 mg/L. All compounds were obtained from Sigma-Aldrich (St. Louis, MO) except atrazine and N,N-diethyl-m-toluamide (DEET), which were obtained from Accustandard (New Haven, CT), fluoxetine and iopromide, which were obtained from the United States Pharmacopeia (Rockville, MD), and hydrocodone, which was obtained from Cerilliant (Round Rock, TX).

Adsorbent characterization.

BET surface areas of the four adsorbents were determined from N_2 adsorption isotherm data collected at 77 K (Autosorb-1-MP, Quantachrome Corporation, Boynton Beach, FL). Prior to analysis, adsorbent samples were outgassed for 20 hours at 423 K. Micropore volume, mesopore volume and pore size distribution of carbonaceous adsorbents were computed from N_2 adsorption isotherm data using the Density Functional Theory (DFT) with the N2_carb1.gai kernel (PC software version 1.51, Quantachrome, Boynton Beach, FL). In addition, the mesopore volume was computed using the Barrett, Joyner, and Halenda

(BJH) method because this method captures the entire mesopore range (20 to 500 Å) while the DFT method was only able to calculate a mesopore volume for pores with widths in the range of 20 to 360 Å. A more detailed description of the procedures used for adsorbent characterization is given elsewhere (Knappe et al., 2007).

Isotherm experiments.

In adsorption isotherm experiments, adsorbent doses between 0.3 and 10 mg/L were used for carbonaceous adsorbents while adsorbent doses in the range of 10 to 300 mg/L were used for high-silica zeolites. The stock solution containing the EPOC mixture shown in Table 1 was added with a constant rate syringe (CR-700-200, Hamilton Co., Reno, NV) to yield an initial concentration of approximately 500 ng/L per compound. Sodium azide (100 mg/L) was added to all bottles to inhibit aerobic biological activity during equilibration. For zeolites, pre-weighed aliquots were added directly to 500 mL isotherm bottles while carbonaceous adsorbents were added using slurries of known adsorbent concentration. Adsorbents were added after the addition of EPOCs to simulate conditions that would be encountered when powdered adsorbents are added in drinking water treatment; i.e., NOM and all contaminants compete simultaneously for adsorption sites. A mixing time of 3 weeks in a rotary tumbler was used to reach adsorption equilibrium. Apart from bottles containing adsorbents, three types of adsorbent-free blanks were prepared in duplicate:

(1) Type 1 blanks were prepared to determine background levels of EPOCs and the effects of sample handling on EPOC concentrations in LMW used in isotherm experiments. These

blanks were prepared by filtering LMW through a 0.45-µm membrane filter and amending the filtrate with 100 mg/L sodium azide. This water was placed into isotherm bottles without spiking chemicals and sent immediately after preparation by overnight carrier for analysis.

(2) Type 2 blanks were prepared to verify spiked EPOC concentrations. These blanks were prepared by spiking 50 µL of the EPOC stock solution into LMW. Duplicate type 2 blanks were prepared with 0.45-µm membrane-filtered LMW, amended with 100 mg/L sodium azide and sent immediately after preparation by overnight carrier for analysis.

(3) Type 3 blanks were prepared to test emerging contaminant stability over the 3-week contact time that was used for adsorption isotherm experiments. Preparation of type 3 blanks was identical to type 2 blanks. Duplicate type 3 blanks were placed in a rotary tumbler for 3 weeks prior analysis.

Upon equilibration, samples containing adsorbent were filtered through 0.7-µm glass fiber filters. Prior to use, filters were baked for two hours at 400°C and cooled in a desiccator for one hour.

Analytical method for emerging organic contaminant concentrations.

EPOC analyses were completed at the laboratories of the Southern Nevada Water Authority (SNWA) using the analytical method of Vanderford et al. (2003). Prior to analysis, analytes in 1-L or 0.5-L samples were concentrated by solid-phase extraction. Compound separation and quantification was accomplished by liquid chromatography/tandem mass

spectrometry (LC/MS/MS), using electrospray ionization in both positive and negative modes and atmospheric pressure chemical ionization in positive mode. Method reporting limits for most compounds were 1.0 ng/L in water.

RESULTS AND DISCUSSION

Adsorbent properties.

Properties of the tested carbonaceous adsorbents and zeolites are summarized in Tables 2 and 3, respectively. The BET surface area and micropore volume of the carbonaceous resin Ambersorb 563 was approximately half that measured for the CC-602 GAC (Table 3). In contrast, the mesopore volume of the carbonaceous resin was larger than that of the activated carbon. Figure 1 depicts micropore size distributions of the carbonaceous adsorbents used in this study. The micropore size distribution of adsorbents is important because the pore volume in a size range similar to the molecular size of the targeted contaminant is one important factor that determines the adsorption capacity of a given adsorbent (e.g., Newcombe et al. 1997, Li et al. 2002, Karanfil and Dasthgeib 2004). It is important to note that assuming spherical molecules all the compounds listed in Table 1 exhibit diameters in the range of 6 to 10 Å. Therefore, the carbonaceous resin Ambersorb 563 may not be as effective for the removal of larger organic contaminants, such as most of the emerging contaminants listed in Table 2, because the micropore volume of Ambersorb 563 in the 6-9 Å range is considerably smaller than that of the CC-602 GAC (Figure 1).

Zeolites are crystalline, microporous materials with uniform pore dimensions. The primary zeolite building blocks are TO_4 tetrahedra, where T is either a $Si^{(IV)}$ or $Al^{(III)}$ atom located at the center of the tetrahedron. Tetrahedra are linked via their oxygen atoms to other tetrahedra to form structural subunits. The linking of recurring structural subunits produces the crystalline framework structure of a zeolite, within which exist voids and channels of discrete and regular size. The mordenite zeolite framework contains oval twelve- and eight-ring channels (i.e. the perimeter of the elliptical channel opening is formed by 12 and 8 T atoms, respectively). These channels are connected by eight-ring channels. The twelve- and eight-ring channels have dimensions of 6.5 × 7.0 Å and 2.6 × 5.7 Å, respectively. Because of the small size of the eight-ring channels, they are not accessible by organic contaminants (McCusker and Baerlocher 2001). The Y-zeolite has circular, 12-ring windows with a diameter of 7.4 Å (or 7.4 × 7.4 Å) and supercages with a diameter of about 13 Å (Rouquerol et al. 1999). BET surface areas of the zeolites were 505 and 810 m^2/g for the Mordenite and Y zeolites, respectively (Table 3).

Removal of an emerging contaminant mixture by alternative adsorbents.

The adsorption of a mixture of 28 emerging organic contaminants (Table 2) was compared for two high-silica zeolites (mordenite and Y), a carbonaceous resin (Ambersorb 563), and a coconut-shell-based GAC (CC-602). Adsorption isotherm experiments were conducted by spiking the emerging contaminants at environmentally relevant concentrations (~200-900 ng/L) into Lake Mead water (LMW).

To measure background levels of emerging contaminants in LMW and the effects of sample handling on background contaminant levels, "type 1 blanks" were prepared by filtering LMW through a 0.45-µm membrane filter and amending the filtrate with 100 mg/L sodium azide. Of the emerging contaminants shown in Table 2, type 1 blanks showed that the following compounds were present above the method reporting limit: oxybenzone (58 ng/L), caffeine (37 ng/L), triclosan (16 ng/L), meprobamate (13 ng/L), DEET (9.0 ng/L), sulfamethoxazole (8.2 ng/L), estriol (6.8 ng/L), carbamazepine (3.1 ng/L), dilantin (2.3 ng/L), atrazine (1.2 ng/L), and ibuprofen (1.2 ng/L). For a number of compounds, very similar levels were obtained by Vanderford et al. (2003) in their analysis of triplicate LMW samples as follows: meprobamate (14 ng/L), DEET (3.9 ng/L), sulfamethoxazole (5.4 ng/L), carbamazepine (3.9 ng/L), dilantin (2.6 ng/L), and atrazine (1.2 ng/L). Three compounds in particular were present at lower concentrations in the samples analyzed by Vanderford: oxybenzone (3.1 ng/L), caffeine (3.0 ng/L), and triclosan (<1 ng/L). The higher levels of these compounds in type 1 blanks suggest that they were introduced during sample handling. Because all samples in this study were prepared in an identical manner and because spiked concentration of these compounds were 1-2 orders of magnitude higher than the levels observed in type 1 blanks, the possible introduction of some compounds during sample handling did not affect the results and associated data interpretation.

To test the stability of the contaminants throughout the 3-week equilibration time, results for "type 2" and "type 3 blanks were compared. Figure 2 illustrates that most compounds were stable throughout the 3-week mixing period, and good agreement was

obtained between compound concentrations in type 2 and type 3 blanks. However, three compounds were not stable: androstenedione, progesterone, and testosterone, which were spiked at levels of ~550-600 ng/L according to type 2 blanks, were below the method reporting limit in type 3 blanks (Figure 2). As a result, no adsorption data are presented for these three EDCs. In addition, poor agreement between type 2 and type 3 blanks was obtained for estrone, estriol, and estradiol in the second batch of blanks that were prepared, suggesting that initial concentration values for these three compounds are more uncertain than those for the remaining compounds.

Figure 3 summarizes concentrations for each of the 25 stable emerging organic contaminants in type 3 blanks and in samples that were equilibrated with 1 mg/L Ambersorb 563 in LMW. The results in Figure 3 show that removal percentages between 20 and 50% were achieved for 19 of the 25 compounds at this adsorbent dose. Iopromide and estradiol were the two most poorly removed compounds, but the result for estradiol may have been influenced by uncertainty in the initial concentration (see large error bars in Figure 3). Removal percentages in excess of 50% were observed for the 4 compounds triclosan, oxybenzone, fluoxetine, and acetaminophen. Triclosan, oxybenzone, and fluoxetine were three of the more hydrophobic compounds in the contaminant mixture (log K_{ow} values >3.8, Table 2), and acetaminophen was the smallest (molecular diameter 6.5 Å) and thus may have benefited from the presence of a large volume of small pores in Ambersorb 563.

Figure 4 summarizes concentrations for each of the 25 stable emerging organic contaminants in type 3 blanks and in samples that were equilibrated with 1 mg/L CC-602 in LMW. The results in Figure 4 show that removal percentages exceeded 50% for 15 compounds at this adsorbent dose. For nine compounds, removal percentages between 20 and 50% were achieved, and for one compound, iopromide, removal was <20%. These results illustrate that the CC-602 GAC was more effective for the removal of emerging organic contaminants than Ambersorb 563, most likely because the GAC exhibited a larger volume of pores with widths in the 6-9 Å range. Figure 4 also illustrates that estradiol removal percentage was 79%, which is higher than for Yoon et al. (2005) (40 to 50% from CRW) with a 1 mg/L carbon dose. However contact time was 4 hours for that study, which is insufficient for equilibrium to be established. A higher carbon dose (5 mg/L) attained an estradiol removal of 90% with 4 hours contact time, which is more similar to the results of this study.

Figure 5 illustrates the comparison of the removal percentages of the 25 stable compounds in LMW obtained with a 1 mg/L activated carbon CC-602 dose and three weeks contact time (this study) with the average removal percentages of the 25 compounds in four different natural waters obtained with a 5 mg/L activated carbon WPM dose and 4 hours contact time (Westerhoff et al. 2005). Despite the differences in experimental conditions, Figure 5 shows that results are very comparable between the data. Linear regression analysis of the two data sets yielded a coefficient of determination (R^2) of 0.9, demonstrating the good agreement in the results.

Figure 6 summarizes concentrations for each of the 25 stable emerging organic contaminants in type 3 blanks and in samples that were equilibrated with 100 mg/L of mordenite (HSZ-690HOA) or Y (HSZ-390HUA) zeolite. The results in Figure 6 show that 15 compounds were either completely or partially removed with the mordenite zeolite; in contrast, only 3 compounds (fluoxetine, oxybenzone, and triclosan) were removed by the Y zeolite. Thus, mordenite was a more effective adsorbent than the Y zeolite for the removal of emerging organic contaminants that were spiked at levels between ~200 and 900 ng/L into LMW. It is interesting to note that seemingly small differences in pore size and shape had an important effect on removal efficiencies observed with the two high-silica zeolites. Mordenite has elliptical channels with minor and major axis dimensions of 6.5 and 7 Å, respectively, while Y zeolites contain channels with circular openings that are 7.4 Å in diameter that open into supercages that are about 13 Å in diameter.

Carbonaceous adsorbents are more effective for emerging organic contaminant removal than high-silica zeolites. This result was primarily attributed to the fact that activated carbons exhibit a broader micropore size distribution, in which compounds of different shapes and sizes can be effectively accommodated. In contrast, high-silica zeolites, with their uniform pore sizes, appear to be effective if the removal of a specific organic contaminant is targeted (e.g. MTBE, Knappe and Rossner (2005)), but they do not appear to be effective when the removal of a broad mixture of contaminants is targeted.

The effects of initial contaminant concentration and the presence of other contaminants in the mixture on contaminant removal percentages obtained with carbonaceous adsorbents were also investigated in this study. For this purpose, sulfamethoxazole (SMX) adsorption isotherm data for Ambersorb 563 and CC-602 were collected in LMW at an initial concentration of 100 μg/L and compared to SMX adsorption isotherm data obtained with an initial SMX concentration of 426 ng/L in the presence of 24 other emerging organic contaminants that were stable over the 3-week equilibration time. As shown in Figure 7, removal percentages of SMX at a given adsorbent dose were similar for the two initial concentrations. The similarity in removal percentages at initial SMX concentrations that differed by 2.5 orders of magnitude was somewhat surprising for an anionic contaminant (pK_a of the sulfonamide group of SMX is 5.6) because it was anticipated that electrostatic effects would become more pronounced as the initial concentration of trace organic contaminant decreases. However, the results obtained here are similar to previous observations for many neutral organic contaminants (e.g., Knappe et al. 1998, Graham et al. 2000, Westerhoff et al. 2005). To obtain 90% SMX removal in LMW, the results in Figure 7 suggest that ~7 mg/L of CC-602 or ~11.5 mg/L Ambersorb 563 would be required if adsorption equilibrium can be obtained.

Figure 8 summarize adsorption isotherm data for contaminants in the emerging contaminant mixture on CC-602 and Ambersorb 563. Isotherm data are presented by plotting the percentage of the contaminant remaining in solution as a function of adsorbent dose, a format that eliminates the initial concentration dependence of the trace organic contaminant

isotherm in the presence of NOM. For CC-602, the shaded area bracketed by the isotherms for triclosan and diclofenac includes isotherms for 19 of the 23 remaining compounds (panel a). Thus, the results in Figure 8 suggest that CC-602 doses between ~1 and 8 mg/L would be required to achieve 99% removal for 21 of the 25 tested emerging contaminants. The remaining four compounds, iopromide, sulfamethoxazole, meprobamate, and ibuprofen, were not as efficiently removed. For the most poorly adsorbed compound, iopromide, a CC-602 dose of 10 mg/L would have led to ~78% removal from LMW.

For Ambersorb 563, the shaded area bracketed by the isotherms for fluoxetine and ethynylestradiol includes isotherms for 10 of the 23 remaining compounds (panel b). Thus, the results in Figure 8 suggest that Ambersorb 563 doses between ~3 and 10 mg/L would be required to achieve 99% removal for 12 of the 25 tested emerging contaminants. Two compounds, triclosan and oxybenzone, were more adsorbable than fluoxetine and would require Ambersorb 563 doses < 3 mg/L to obtain 99% removal from LMW. On the other hand, 8 compounds (iopromide, meprobamate, dilantin, sulfamethoxazole, diclofenac, hydrocodone, ibuprofen, and carbamazepine) were not as adsorbable as ethynylestradiol. At an Ambersorb 563 dose of 10 mg/L, iopromide removal was <10%; at the same Ambersorb 563 dose, removal of the second-most poorly adsorbed compound, meprobamate, was ~70%.

CONCLUSIONS

Overall, the results obtained for the emerging contaminant mixture suggest that activated carbon adsorption processes provide an effective tool for the removal of antimicrobial compounds, EDCs and other pharmaceuticals from water. For the tested coconut-shell-based activated carbon, a dose of 10 mg/L was sufficient to achieve ≥98% contaminant removal for 24 of the 25 stable compounds in the mixture. Thus, an activated carbon dose that might typically be added by a utility for taste and odor control is sufficient to achieve a 2-log removal of many emerging organic contaminants. The greater effectiveness of activated carbon relative to the carbonaceous resin was primarily related to GAC's larger volume of pores with widths in the 6-9 Å range. Finally, the results obtained with the zeolites showed that this adsorbent class with its uniform pores does not provide an effective broad-spectrum barrier against the wide variety of compound classes that a utility might want to remove from its source water.

REFERENCES

Adams, C.; Wang, Y.; Loftin, K.; and M. Meyer. 2002. "Removal of antibiotics from surface and distilled water in conventional water treatment processes." *J. Environ. Engrg. – ASCE* 128(3): 253-260.

Choi, K.J.; Kim, S.G.; Kim, C.W.; and J.K. Park. 2006. "Removal efficiencies of endocrine disrupting chemicals by coagulation/flocculation, ozonation, powdered/granular

activated carbon adsorption, and chlorination." *Korean Journal of Chemical Engineering* 23(3): 399-408.

Dodd, M.C.; M.O. Buffle; and U. von Gunten. 2006. "Oxidation of antibacterial molecules by aqueous ozone: Moiety-specific reaction kinetics and application to ozone-based wastewater treatment." *Environ. Sci. Tech.* 40(6): 1969-1977.

Graham, M.R.; Summers, R.S.; Simpson, M.R.; and B.W. Macleod. 2000. "Modeling equilibrium adsorption of 2-methylisoborneol and geosmin in natural waters." *Water Research* 34: 2291-2300.

Karanfil, T. and S.A. Dastgheib. 2004. "Trichloroethylene adsorption by fibrous and granular activated carbons: aqueous phase, gas phase, and water vapor adsorption studies." *Environ. Sci. Tech.* 38: 5834-5841.

Kolpin, D.W.; Furlong, E.T.; Meyer, M.T.; Thurman, E.M.; Zaugg, S.D.; Barber, L.B.; and H.T. Buxton. 2002. "Pharmaceuticals, hormones, and other organic wastewater contaminants in US streams, 1999-2000: A national reconnaissance." *Environ. Sci. Tech.* 36(6):1202-1211.

Knappe, D.R.U.; Matsui, Y.; Snoeyink, V.L.; Roche, P.; Prados, M.J.; and M.M. Bourbigot. 1998. "Predicting the capacity of powdered activated carbon for trace organic compounds in natural waters." *Environ. Sci. Tech.* 32: 1694-1698.

Knappe, D.R.U.; L. Li; P.A. Quinlivan; and T.B. Wagner. 2003. *Effects of Activated Carbon Surface Chemistry and Pore Structure on the Adsorption of Trichloroethene and Methyl Tertiary-Butyl Ether from Natural Water*. American Water Works Association Research Foundation: Denver, Colorado.

Knappe, D.R.U. and A.A. Rossner Campos. 2005. "Effectiveness of High-Silica Zeolites for the Adsorption of Methyl Tertiary-Butyl Ether from Natural Water." *Water Sci. Tech. – Water Supply* 5(5): 83-91.

Knappe, D.R.U., A. Rossner, S.A. Snyder, and C. Strickland. 2006. *Alternative Adsorbents for the Removal of Polar Organic Contaminants.* American Water Works Association Research Foundation: Denver, Colorado.

Kümmerer, K. 2001. "Present knowledge and need for further research." In *Pharmaceuticals in the Environment*, Kümmerer, K., ed. Springer Verlag: Heidelberg, pp. 239-245.

Leitner, N.K.V.; Papailhou, A.L.; Croue, J.P.; Peyrot, J.; and M. Dore. 1994. "Oxidation of methyl tert-butyl ether by ozone and combined ozone hydrogen-peroxide." *Ozone Sci. Eng.* 16(1): 41-54.

Li, L.; Quinlivan, P.A.; and D.R.U. Knappe. 2002. "Effects of activated carbon surface chemistry and pore structure on the adsorption of organic contaminants from aqueous solution." *Carbon* 40(12): 2085-2100.

Liang, S.; Palencia, L.S.; Yates, R.S.; M.K. Davis; Bruno, J.M.; and R.L. Wolfe. 1999. "Oxidation of MTBE by ozone and peroxone processes." *Journal AWWA* 91(6): 104-114.

McCusker, L.B. and C. Baerlocher. 2001. "Zeolite structures." In *Introduction to Zeolite Science and Practice, 2nd Completely Revised and Expanded Edition*, van Bekkum, H., E.M. Flanigen, P.A. Jacobs, and J.C. Jansen, eds. Elsevier Science, Amsterdam, pp. 37-67.

Montes-Moran, M.A.; Suarez, D.; Menendez, J.A.; and E. Fuente. 2004. "On the nature of basic sites on carbon surfaces: An overview." *Carbon* 42: 1219-1225.

Newcombe, G.; Drikas, M.; and R. Hayes. 1997. Influence of characterized natural organic material on activated carbon adsorption: II. Effect on pore volume distribution and adsorption of 2-methylisoborneol. *Water Research* 31: 1065-1073.

Quinlivan, P.A.; L. Li; and D.R.U. Knappe. 2005. "Effects of activated carbon characteristics on the simultaneous adsorption of aqueous organic micropollutants and natural organic matter." *Water Research* 39(8): 1663-1673.

Pfenninger, A. 1998. "Manufacture and use of zeolites for adsorption processes." In *Molecular Sieves: Science and Technology*, Vol. 2, Karge, H.G. and J. Weitkamp, eds. Springer-Verlag, Berlin, pp. 163-198.

Rouquerol, F.; Rouquerol, J.; and K. Sing. 1999. *Adsorption by Powders and Porous Solids*. Academic Press, San Diego, CA.

Snyder, S.A.; Westerhoff, P.; Yoon, Y.; and D.L. Sedlak. 2003. "Pharmaceuticals, personal care products, and endocrine disruptors in water: Implications for the water industry." *Environmental Engineering Science*. 20(5): 449-469.

Szostak, R. 1998. *Molecular sieves: principles of synthesis and identification*. 2nd ed. Blackie Academic & Professional: New York, NY.

Ternes, T.A.; Meisenheimer, M.; McDowell, D.; Sacher, F.; Brauch, H.J.; Haist-Gulde, B.; Preuss, G.; Wilme, U.; and N. Zulei-Seibert. 2002. "Removal of Pharmaceuticals during Drinking Water Treatment." *Environmental Science and Technology* 36: 3855-3863.

Vanderford, B.J.; Pearson, R.A.; Rexing, D.J.; and S.A. Snyder. 2003. "Analysis of Endocrine Disruptors, Pharmaceuticals, and Personal Care Products in Water Using

Liquid Chromatography/Tandem Mass Spectrometry." *Analytical Chem.* 75: 6265-6274.

Westerhoff, P.; Yoon, Y.; Snyder, S.; and E. Wert. 2005. "Fate of endocrine-disruptor, pharmaceutical, and personal care product chemicals during simulated drinking water treatment processes." *Environ. Sci. Tech.* 39(17): 6649-6663.

Yoon, Y.; Westerhoff, P.; Snyder, S.A.; and M. Esparza. 2003. "HPLC-fluorescence detection and adsorption of bisphenol A, 17β-estradiol, and 17α-ethynyl estradiol on powdered activated carbon." *Water Research* 37: 3530-3537.

Yoon, Y.; Westerhoff, P.; and S.A. Snyder. 2005. "Adsorption of ^{3}H-Labeled 17-β Estradiol on Powdered Activated Carbon." *Water, Air, and Soil Pollution* 166: 343-351.

Table 1. Adsorbate characteristics

Compound name	CAS #	Use	MW	pK_a	C_s (g/L)[§]	Diameter (Å)[‡]
acetaminophen	103-90-2	analgesic	151.2	9.4[⌂], 9.5[*] [0/-][‡]	10	6.5
androstenedione	63-05-8	steroid[+]	286.4	-	0.0578[⌂]	8.4
atrazine	1912-24-9	herbicide[+]	215.7	1.7[⌂], 1.2[*] [+/0][†]	0.0347[⌂]	7.4
caffeine	58-08-2	stimulant	194.2	<0[*] [+/0]	3.7	6.9
carbamazepine	298-46-4	analgesic	236.3	-	0.078	7.6
DEET	134-62-3	insect repellent	191.3	1.0[*] [+/0]	1	7.5
diazepam	439-14-5	anti-anxiety	284.8	3.4[⌂], 3.6[*] [+/0]	.02	7.9
diclofenac sodium	15307-79-6	arthritis	318.1	4.2[⌂], 4.1[*] [0/-]	44	7.7
dilantin	57-41-0	anti-convulsant	252.3	8.3[⌂], 8.4[*] [0/-]	0.14	7.6
estradiol	50-28-2	steroid[+]	272.4	10.5[*] [0/-]	0.003	8.3
estriol	50-27-1	steroid[+]	288.4	10.5[*] [0/-]	0.015	8.3
estrone	53-16-7	steroid[+]	270.4	10.5[*] [0/-]	0.0051	8.2
ethynylestradiol	57-63-6	birth control[+]	296.4	10.5[*] [0/-]	0.002	8.4
fluoxetine	54910-89-3	anti-depressant	309.3	9.5[*] [+/0]	0.49	8.2
gemfibrozil	25812-30-0	anti-cholesterol	250.3	4.5[*] [0/-]	35	8.1
hydrocodone	125-29-1	pain reliever	299.4	9.1[*] [+/0]	0.57	8.3
ibuprofen	15687-27-1	pain reliever	206.3	4.9[⌂], 4.5[*] [0/-]	120	7.6
iopromide	73334-07-3	x-ray contrast media	791.1	6.5[*] [0/-]; 12.6[*] [-/--]	280	9.5
meprobamate	57-53-4	anti-anxiety	218.3	12.0[*] [0/-]	4.7[⌂]	7.5
naproxen	22204-53-1	analgesic	230.3	4.2[⌂], 4.5[*] [0/-]	39	7.6
oxybenzone	131-57-7	sunscreen	228.2	10.2[*] [0/-]	0.8	7.4
pentoxifylline	6493-05-6	blood viscosity control	278.3	0.1[*] [+/0]	0.78	8.0
progesterone	57-83-0	steroid[+]	314.5	-	0.0088[⌂]	8.8
sulfamethoxazole	723-46-6	antibiotic	253.3	1.7, 1.8[*] [+/0] 5.6, 9.1[*] [0/-]	25	7.4
tri(2-chloroethyl) phosphate (TCEP)	115-96-8	fire retardant	285.5	-	7[⌂]	7.5
testosterone	58-22-0	steroid[+]	288.4	-	0.0234[⌂]	8.5
triclosan	3380-34-5	antibiotic	289.6	8.0[*] [0/-]	0.011	7.4
trimethoprim	738-70-5	antibiotic	290.3	7.1[⌂], 6.6[*] [+/0]	0.49	8.1

[⌂] experimentally determined values listed in EPI Suite v. 3.20 database (http://www.epa.gov/oppt/exposure/pubs/episuite.htm)

[§] at pH 8, calculated values listed in SciFinder Scholar unless otherwise noted (values were calculated with Advanced Chemistry Development (ACD/Labs) Software v. 8.14)

[‡] surface volumes computed with CAChe WorkSystem Pro Version 6.1.8; diameters calculated assuming spherical molecules

[*] values estimated with SPARC v. 4.2 (http://ibmlc2.chem.uga.edu/sparc/) – N species were treated as acids and bases

[+] known or suspected endocrine disrupting compound

[‡] [0/-] = functional group goes from neutral to anionic form

[†] [+/0] = functional group goes from cationic to neutral form

Table 2. Physical characteristics of carbonaceous adsorbents

Adsorbent	BET Surface Area (m^2/g)	Micropore Volume* (cm^3/g)	DFT Mesopore Volume+ (cm^3/g)	BJH Mesopore Volume‡ (cm^3/g)
CC-602	1160	4.37×10^{-1}	2.94×10^{-2}	6.01×10^{-2}
Ambersorb 563	546	2.01×10^{-1}	2.80×10^{-1}	3.18×10^{-1}

* Micropore volume calculated by density functional theory (DFT) for pores with widths less than 20 Å

+ Mesopore volume calculated by density functional theory (DFT) for pores with widths ranging from 20 to 360 Å (upper limit for DFT model)

‡ Mesopore volume calculated by Barrett, Joyner, and Halenda (BJH) method for pores with widths ranging from 20 to 500 Å

Table 3. Zeolite characteristics

Framework type	Manufacturer's ID code	Pore dimensions	Exchangeable cation*	SiO_2/Al_2O_3 ratio*	BET surface area (m^2/g)
Mordenite	HSZ-690HOA	0.65 nm*0.70 nm (12-ring)	H^+	230	505
Y	HSZ-390HUA	0.74 nm*0.74 nm (12-ring)	H^+	810	806

* Information provided by manufacturer

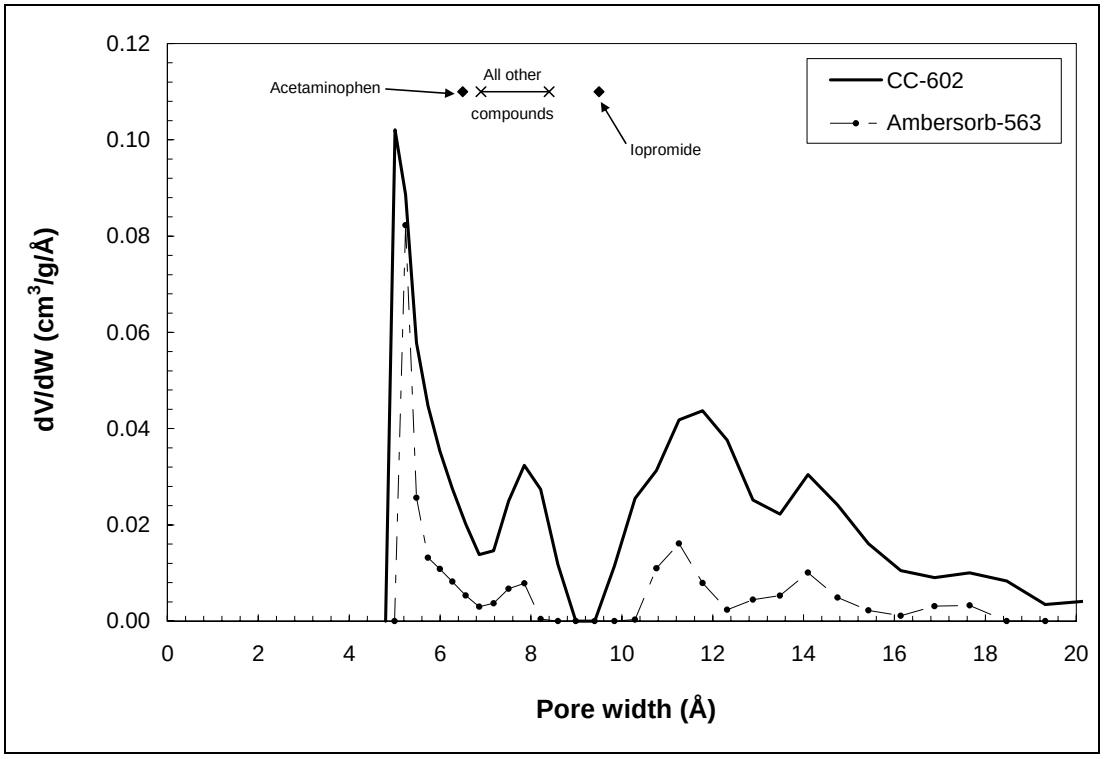

Figure 1. Micropore size distribution of carbonaceous adsorbents (y-axis represents differential pore volume [V] in cm^3/g adsorbent per unit pore width [W] in Å).

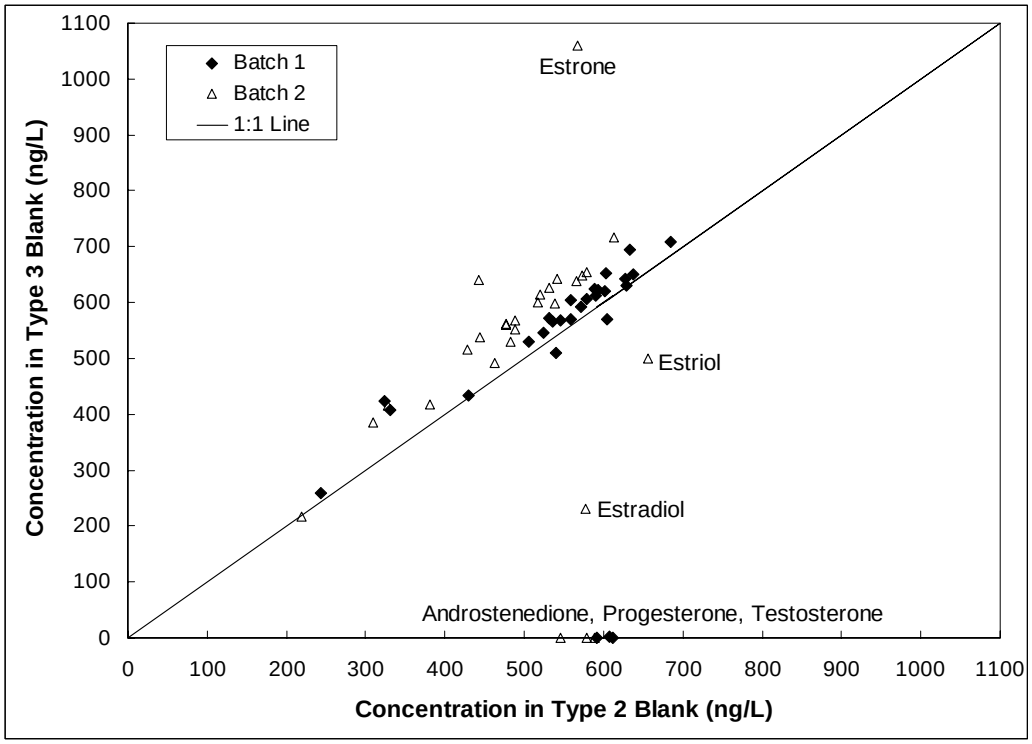

Figure 2. Stability of emerging organic contaminants over the three-week equilibration time. Type 2 blanks were analyzed immediately upon preparation, type 3 blanks were mixed for 3 weeks prior to analysis.

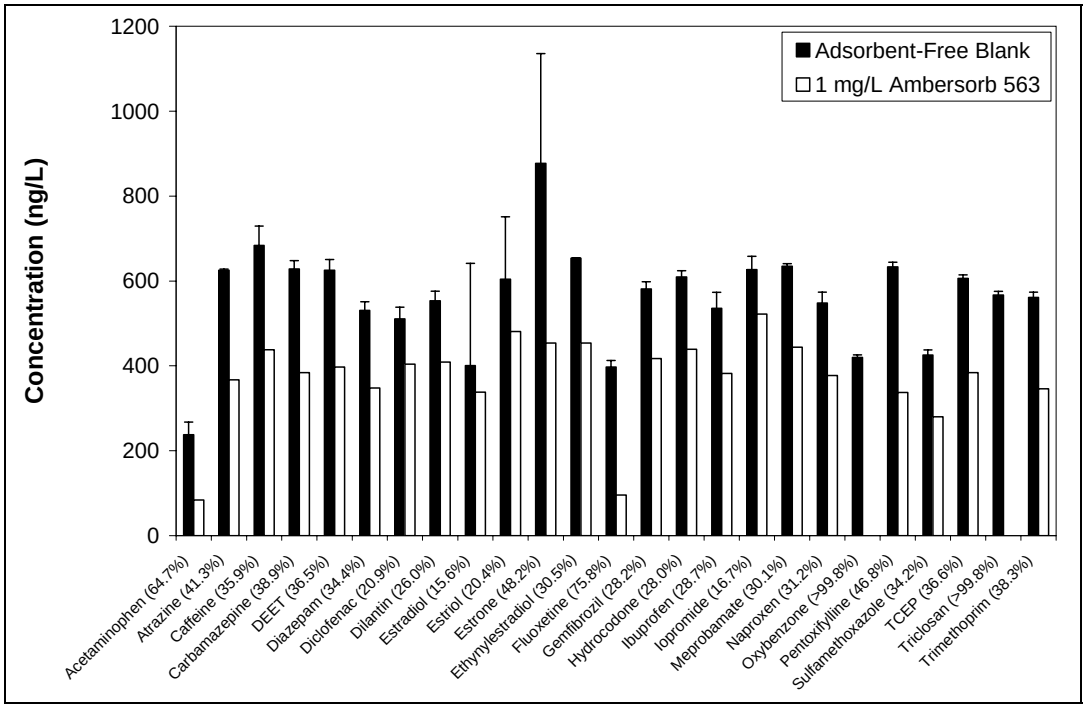

Figure 3. Removal of 25 emerging organic contaminants from Lake Mead water by 1 mg/L Ambersorb 563. Error bars represent standard deviations of duplicates. Removal percentages are shown in the x-axis labels.

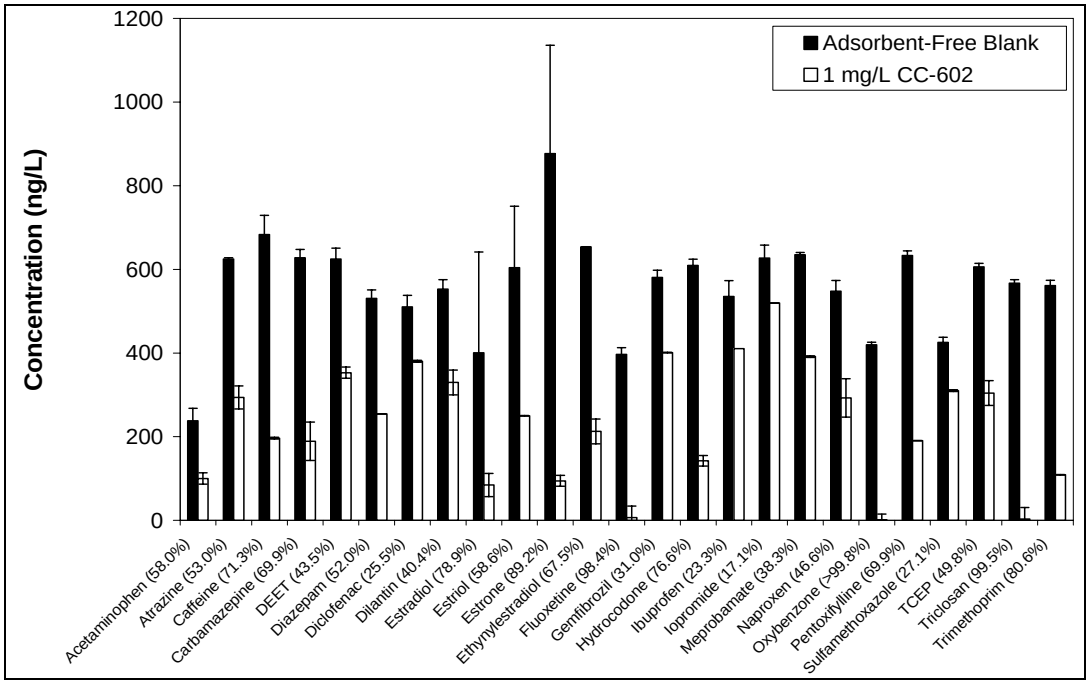

Figure 4. Removal of 25 emerging organic contaminants from Lake Mead water by 1 mg/L CC-602. Error bars represent standard deviations of duplicates. Removal percentages are shown in the x-axis labels.

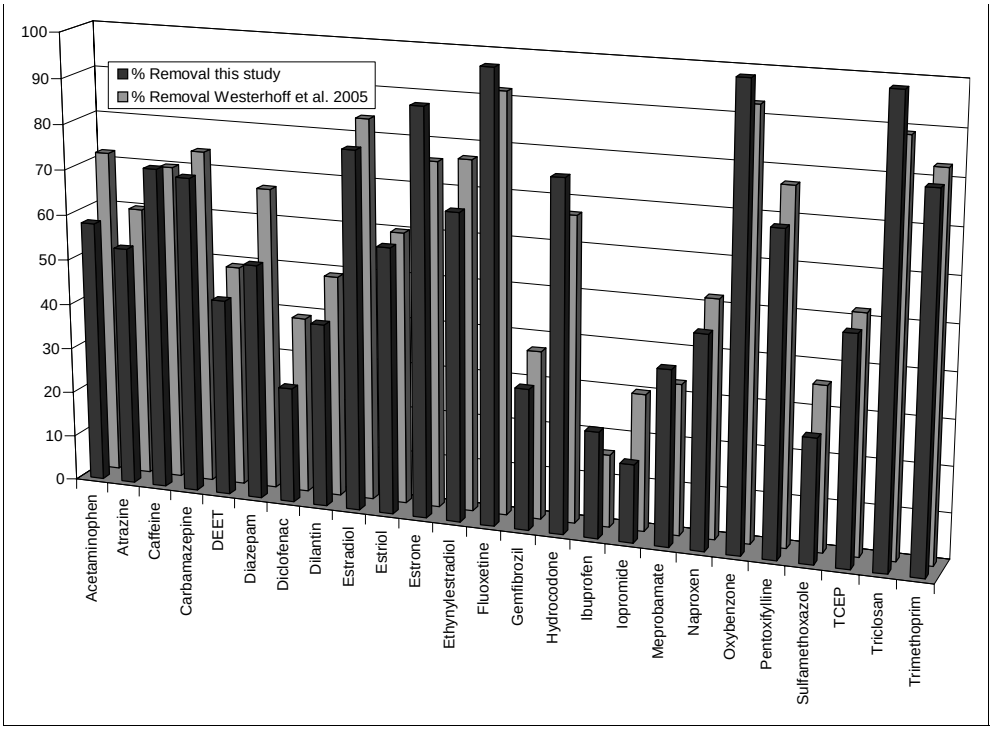

Figure 5. Comparison of percentage removal of the different emerging compounds studied in this work with results of Westerhoff et al. 2005. Removal percentages correspond to 1 mg/L dose of activated carbon CC-602 and three weeks contact time in this study and 5 mg/L dose of activated carbon WPM and 4 hours contact time of Westerhoff et al. 2005.

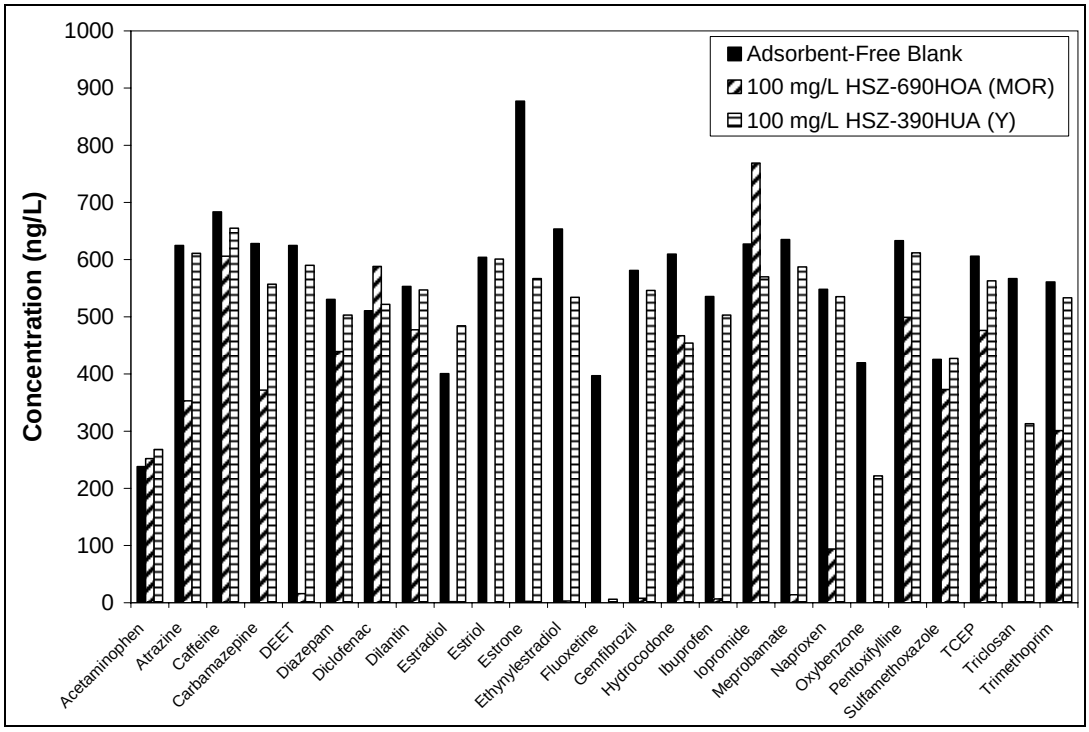

Figure 6. Removal of 25 emerging organic contaminants from Lake Mead water by 100 mg/L mordenite or Y zeolites.

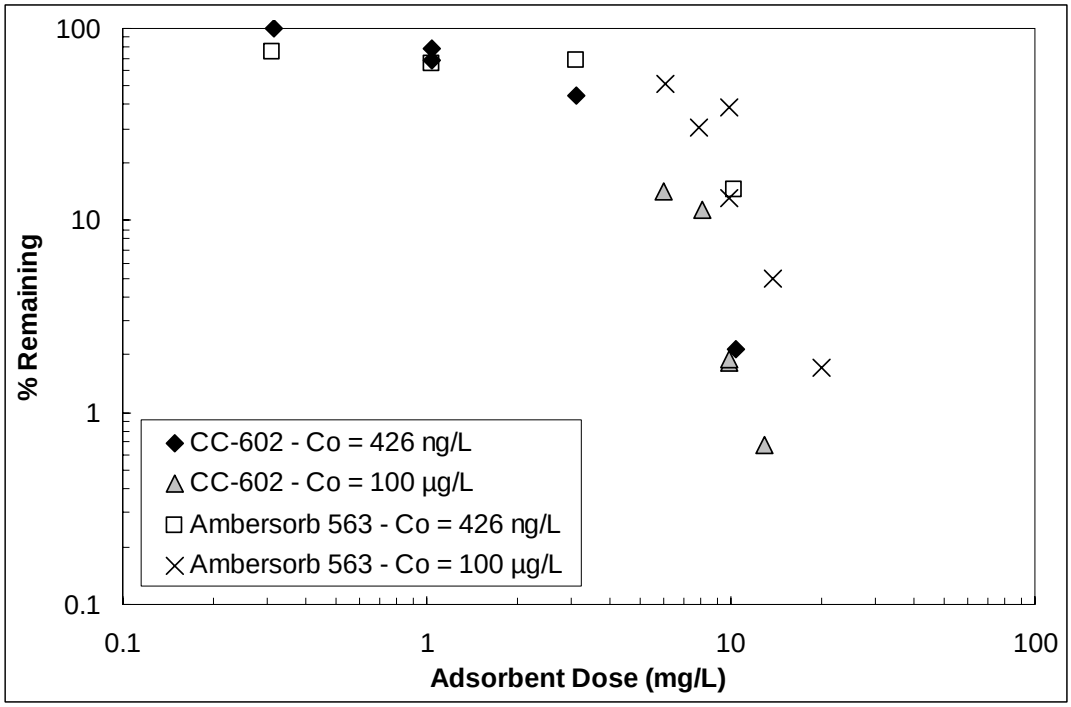

Figure 7. Effect of initial SMX concentration and presence of trace level emerging contaminants in Lake Mead water on SMX removal by activated carbon CC-602 and carbonaceous resin Ambersorb 563.

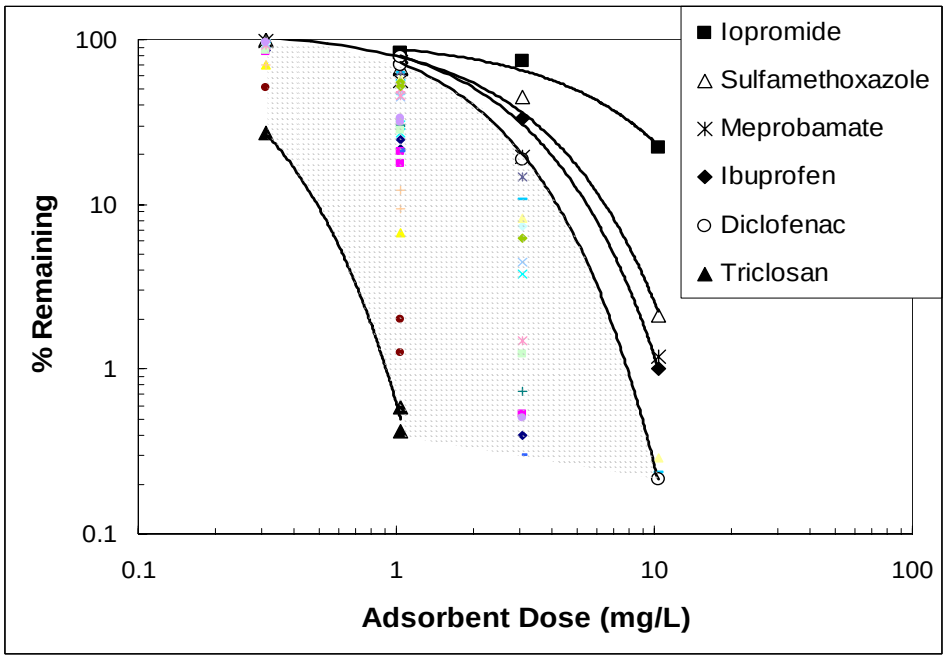

(a)

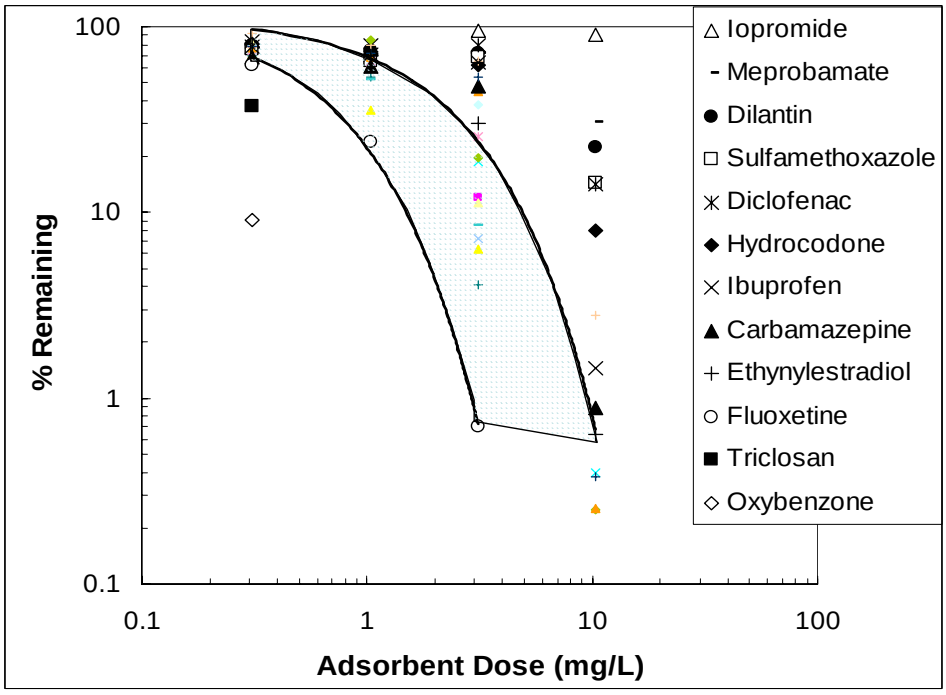

(b)

Figure 8. Percent removal of EPOCs from Lake Mead water as a function of (a) activated carbon and (b) carbonaceous resin dose.

CHAPTER 4

Activated carbon adsorption of ionizable organic compounds – Effects of adsorbent, adsorbate, and background water characteristics

INTRODUCTION

Removal of organic pollutants from drinking water is frequently achieved by activated carbon adsorption processes. Although adsorption of organic contaminants by activated carbon has been studied extensively, the heterogeneous pore structure and surface chemistry of activated carbons and the complex nature of the aqueous solutions containing the contaminants, makes it difficult to apply a general model for different drinking water treatment scenarios. The removal of organic contaminants from drinking water by activated carbon adsorption is affected by three interactions: (1) adsorbate – adsorbent interactions, (2) solvent (water) – adsorbent interactions, and (3) adsorbate – solvent interactions (Knappe 2006). The magnitude with which these interactions will affect the adsorption process will depend on: (a) chemical and physical properties of the adsorbent (functional groups, surface area and pore size distribution, ash content), (b) chemical and physical properties of the adsorbate (functional groups, polarity, hydrophobicity, molecular weight and size, solubility and pK_a or pK_b), and (c) solution conditions (pH, temperature, adsorbate concentration,

polarity of solvent and presence of co-adsorbing solutes that can compete with the adsorbate for adsorption sites) (Radovic et al. 1997).

Interactions between the molecular or ionized compounds and the surface of the activated carbon are largely controlled by non-specific dispersive or van der Waals forces and polar interactions that are always present for any organic chemical. Dispersive interactions are always attractive and their strength tends to increase with increasing adsorbate molecular size, polarizability (ability to develop uneven electron distributions in the molecule in response to imposed electric fields), dipole moment and planarity of the molecule (Belfort 1979, Schwarzenbach et al. 2003, Cornelissen et al. 2004). These interactions occur primarily between the molecular or ionized compound and the basal planes of the activated carbon. In the adsorption of aromatic compounds π-π dispersive interactions are important, and a decrease in π-electron density on the activated carbon basal planes decreases the affinity of the activated carbon surface for the aromatic compound (Radovic et al. 1997). In addition, ionic species in the aqueous solution can be attracted by coulombic or electrostatic interactions at surface sites exhibiting the opposite charge. These interactions are strongly influenced by solution pH and ionic strength. The solution pH affects (1) the protonation or deprotonation of functional groups of ionizable organic compounds in solution and (2) the surface charge density of activated carbon. Therefore, solution pH determines whether the electrostatic interactions are repulsive, when they are counter-ions or attractive, when they are co-ions (Knappe 2006, Müller et al. 1980, 1985). The increase in ionic strength compresses the electric double layer surrounding the activated carbon particle,

reducing the importance of electrostatic interactions. Therefore, at low surface coverage, when the charge of the adsorbed, ionized organic molecules is smaller than the original surface charge, an increase in ionic strength enhances the adsorption of co-ions and decreases the adsorption of counter-ions (Müller et al. 1985). In general, dispersive interactions govern over electrostatic interactions when conducting experiments at pH values near the point of zero charge of the activated carbon surface (pH at which the activated carbon surface has a net charge of zero), where electrostatic interactions are minimized (Radovic et al. 1997). Furthermore, other interactions may be present in the adsorption process; e.g., reactive moieties on the carbon surface and in the adsorbate structure can form electron donor-acceptor complexes such as hydrogen bonds (Schwarzenbach et al. 2003).

Interactions between water and the activated carbon surface are dominated by the presence of surface functional groups with which the water can interact via hydrogen bonding. In contrast, water adsorption is low on the hydrophobic basal planes of the carbon surface because the disruption of hydrogen bonds between water molecules is not energetically favored relative to the adsorption of water on a hydrophobic surface (Knappe 2006). However, an increase of functional groups containing oxygen facilitates hydrogen bonding of water molecules with the activated carbon surface. Additional water molecules can bond to the water molecules adsorbed on the surface forming water clusters around the hydrophilic sites and extending over the hydrophobic surface (Pendleton et al. 1997). Therefore, in aqueous solutions, for adsorption of organic micropollutants to occur, water molecules need to be displaced from the carbon surface, and if the hydrophilicity of the

carbon surface increases, the adsorption of the micropollutant is energetically less favored (Pendleton et al. 1997, Karanfil and Kilduff 1999). An increase in water affinity decreases the capacity of the activated carbon to adsorb organic micropollutants (Karanfil and Kilduff 1999, Li et al. 2002, 2005, Karanfil and Dastgheib 2004).

In aqueous solutions, adsorbate – solvent interactions depend on the size and shape of the molecule and its H-donor and/or H-acceptor properties (Schwarzenbach et al. 2003). The bigger the molecular size of the organic molecule, the more water molecules are needed for the solvation of the molecule, which lowers the solubility of the organic compound in water. The H-donor and/or H-acceptor properties of a certain compound enable it to form hydrogen bonds with water molecules. An increase in hydrogen bonding with water increases the affinity of the organic compound for water and decreases its hydrophobicity. In general, the more hydrophobic the organic compound, the more favored it is to adsorb on an activated carbon surface. For neutral organic contaminants the variation in adsorbability that is attributable to adsorbate – water interactions can be overcome by normalizing the aqueous phase adsorbate concentration in an adsorption isotherm by the solubility of the compound at the temperature and solution pH of the experiment (Knappe 2006). For weak organic acids and bases, the solubility changes with pH (as determined by the compound's dissociation constant), and the affinity of the compound for the activated carbon surface is therefore pH-dependent.

Taking into account all of the above facts, the adsorption of ionizable organic compounds from aqueous solutions and its dependence on solution pH is a complex process that is difficult to fully explain theoretically and to describe by a simple model. Ward and Getzen (1970) made the first attempt to describe quantitatively the influence of pH on the adsorption of weak organic acids. They used the Langmuir isotherm to describe the experimental data for the molecular and ionic species and observed that the maximum adsorption capacity was reached at a pH equal to the pK_a for phenoxyacetic acid. These findings were attributed to pH-related changes in the solution conditions and the influence of pH on the activated carbon surface charge was not considered. A more complete description of the adsorption of ionizable organic compounds on activated carbon was developed by Müller et al. (1980, 1985), who considered the adsorption potential due to dispersive interactions between the heterogeneous carbon surface and the molecular and ionic adsorbate species as well as the influence of coulombic forces between charged surface sites and the ionic adsorbate species. The Langmuir isotherm model for competitive adsorption was used by Müller et al. (1985), and the adsorption of neutral and ionic adsorbate species was treated separately.

Electrostatic interactions, which depend on solution pH (since it determines the (de)protonation of weak electrolytes and the net surface charge of the carbon), are important in the adsorption process of ionizable organic compounds, because counter-ions will be attracted to a charged activated carbon surface and co-ions will be repelled. Co-ions can adsorb when the adsorption potential at a given adsorption site due to attractive dispersive

interactions is higher than the repulsive electrostatic interaction between the co-ion solute and the charged adsorption site (Müller et al. 1980, 1985). Müller et al. (1980, 1985) explained the appearance of maximum adsorption of an ionizable compound at a pH = pK_a occurs only if considerable ionization of the solutes take place while the surface still carries charge opposite to that of the ionic solute. This means that, for a weak organic acid, it is necessary for the slope of the solute-dissociation curve to be larger than that of the surface potential curve for a given increase in pH.

Radovic et al. (1997) showed the importance of electrostatic and dispersive interactions for the adsorption of aniline (weak base pK_b = 4.6) on an acidic carbon (pH_{PZC} = 3), an as-received carbon (pH_{PZC} = 6.5), and a basic carbon (pH_{PZC} = 10). At low pH, anilinium cation adsorption can be improved by carbon oxidation (acidic carbon), because of attractive electrostatic interactions between the negatively charged surface and the anilinium cation. However, at high pH, when neutral aniline is dominant in solution, the acidic carbon exhibited a lower adsorption capacity because carbon oxidation reduced the π-electron density in the graphene layers of the basal plane and decreased the dispersive interaction potential. For basic carbons, the anilinium cation adsorption at low pH was low because of repulsive electrostatic interactions between the positively charged carbon surface and the anilinium cation; however, the greater π-electron density in the graphene layers of the basal planes increased the dispersive interaction energy and thus the adsorption of the aniline molecule (Radovic et al. 1997).

While, the model of Müller et al. (1980, 1985) and Radovic et al. (1997) effectively describes experimental data for the adsorption of ionizable organic compounds, this model is complex and numerous parameters (n^a_{max}, maximum number of adsorption sites on the activated carbon surface, K_0, adsorption equilibrium constant for the neutral organic solute on a neutral homogeneous surface, n, heterogeneity parameter, and U_0, adsorption potential for homogeneous surface) need to be determined experimentally before the prediction of adsorption isotherms is possible at different solution pH values.

Hu et al. (1998) used the Freundlich isotherm model ($q = K\ C^{1/n}$) to describe adsorption data for acidic and basic pesticides at different solution pH values. The data of Hu et al. (1998) showed that the adsorption capacity of the carbon, as expressed by the Freundlich K-value, was log-linearly related to the pH-dependent octanol water partition coefficient ($\log K_{ow}^{pH}$) of the pesticides. This result suggests that the pH-related change in hydrophobicity, as the pesticide transitioned from its neutral to its ionic form, was the dominant variable affecting the pH-dependent adsorption uptake of weak organic acids and bases.

HYPOTHESIS AND OBJECTIVES

When plotting adsorption isotherms for neutral organic compounds, it is common to normalize for adsorbate – water interactions by dividing the equilibrium liquid phase concentration of the adsorbate (C) by its aqueous solubility (C_s). This normalization has not been applied yet to describe the adsorption of ionizable organic compounds. In recent years, software packages have become available, that are capable of predicting the dependence of C_s on solution pH. Figure 1 depicts the p-nitrophenol (PNP) adsorption isotherm data obtained of Müller et al. (1980) as originally presented (Figure 1a) and following normalization with the pH-dependent aqueous solubility (C_s^{pH}) (Figure 1b), where C_s^{pH} values for PNP were predicted using ACD/Labs software (as reported in SciFinder Scholar 2006). PNP is a weak organic acid with a pK_a of 7.23, consequently at pH < 6.8 the neutral form of PNP was dominant in solution, whereas at pH 9.7 the anionic form of PNP prevailed. Figure 1 illustrates that this normalization procedure effectively accounted for the differences in PNP adsorption uptake observed in Figure 1a.

Therefore, the principal hypothesis that was tested in this chapter was that adsorption isotherm data for ionizable organic contaminants that are sparingly soluble in water can be normalized by C_s^{pH}. In other words, the pH-induced change in aqueous solubility is the principal variable that affects the pH-dependent adsorption capacity of ionizable organic contaminants. While Figure 1 suggest that dispersive and electrostatic interactions play a

secondary role, this hypothesis needed to be verified with additional ionizable contaminants as well as with activated carbons exhibiting a range of surface chemistries.

The principal objective of this research was to identify activated carbon, contaminant, and background water characteristics that affect the pH-dependent adsorption capacity of ionizable organic contaminants. Specific objectives included (1) to predict pH-dependent aqueous solubilities of ionizable organic contaminants, for which adsorption isotherm data at different pH values are available in the literature and for model compounds that were used in the experimental portion of the research, (2) verify solubility predictions for selected compounds and utilize aqueous solubilities to normalize literature adsorption isotherm data, (3) determine the importance of pH-mediated changes in contaminant and activated carbon surface ionization on the adsorption process.

This research is relevant to the drinking water treatment industry because many emerging contaminants and non-regulated organic contaminants are ionizable. Finding a simple way to predict the pH-dependent adsorption capacity of ionizable organic contaminants will therefore facilitate the design and operation of activated carbon adsorption processes when ionizable organic contaminant removal is an important treatment objective. Results will also provide activated carbon selection criteria for utilities that need to identify effective activated carbons for the removal of ionizable organic contaminants.

MATERIALS AND METHODS

Normalization of literature isotherm data

Data published for ionizable compounds at different solution pHs were selected for normalization (Snoeyink et al. 1969, Müller et al. 1980, 1985, Hu et al. 1998, Derylo-Marczewska and Marczewski 1999). Published isotherm plots were first digitized using DataThief III software. Then the equilibrium liquid-phase concentrations at the different solution pHs were divided by the pH-dependent solubility of the compound, which yielded a normalized isotherm curve depicting the equilibrium solid-phase concentration (q_e) as a function of C/C_s^{pH}.

Adsorbate characterization

Using ACD/Labs software, aqueous solubilities were calculated as a function of solution pH for compounds, for which pH-dependent adsorption isotherm data were available (p-nitrophenol, aniline, MCPB, imazalil, benzoic acid, phenol) in the literature as well as for two antibiotics [sulfamethoxazole (SMX) and trimethoprim (TMP)] that were used in the experimental portion of the research. Figure 3 illustrates the molecular structures of SMX and TMP and the functional groups where protonation or deprotonation occurs as solution pH changes. Aniline, p-nitrophenol, MCPB, imazalil, benzoic acid, phenol, SMX, and TMP properties are summarized in Table 1.

To assess the accuracy of ACD/Labs software solubility predictions, solubility as a function of pH was also determined experimentally for SMX and TMP. C_s^{pH} values at 25°C were measured in the pH range of 2 to 10 using the shake-flask method (EPA method OPPS 830.7840, USEPA 1998). An equal amount of the compound was placed in three glass centrifuge tubes. Hydrochloric acid and sodium hydroxide were used to adjust the solution pH to the targeted value. The closed vessels were then agitated at 30°C in a temperature-controlled shaker. After a mixing time of five days, one of the vessels was re-equilibrated at 25°C for 24 hours. The sample was centrifuged for 15 minutes at 3500 rpm and the supernatant analyzed by UV spectrophotometry. The other two samples were treated similarly after initial equilibration at 30°C for six and seven days, respectively. The test results were considered satisfactory if at least the last two samples agreed within the required reproducibility (<15%).

Adsorbent characterization

One carbonaceous resin and four activated carbons were utilized in this study. The characteristics that were measured for each adsorbent were (1) Brunauer, Emmett and Teller (BET) surface area, (2) micropore volume and pore size distribution, (3) mesopore volume, (4) point of zero charge (pH_{PZC}), (5) acid and base neutralization capacities, (6) elemental composition, and (7) ash content.

BET surface area and pore size distribution

BET surface areas were determined from N_2 adsorption isotherm data collected at 77 K (Autosorb-1-MP, Quantachrome Corporation, Boynton Beach, FL). Prior to analysis, adsorbent samples were outgassed for 24 hours at 423 K. Samples of 0.1 g were used to collect data in the relative pressure range of 0.01 to 0.1. A glass rod was used during the analysis to decrease the void volume of the sample holder.

Pore size distributions of carbonaceous adsorbents were determined by conducting N_2 adsorption experiments in two separate phases: (1) For the high pressure phase, N_2 adsorption isotherms were constructed from 86 data points in the relative pressure range of 0.0005 to 1 using a sample mass of 0.04 g of pulverized adsorbent; (2) for the low pressure phase, N_2 adsorption isotherms were constructed from 41 data points in the relative pressure range of 10^{-6} to 0.01 using a sample mass of 0.01 g of pulverized adsorbent. Adsorption isotherms from both high and low pressure phases were combined to produce one isotherm. The adsorbent sample mass used in the low pressure phase was adjusted such that the volume adsorbed in the 0.0005 to 0.01 relative pressure range matched that obtained in the high pressure phase in the same relative pressure range.

Micropore volume, mesopore volume and pore size distribution were computed from N_2 adsorption isotherm data using the Density Functional Theory (DFT) with the N2_carb1.gai kernel (PC software version 1.51, Quantachrome, Boynton Beach, FL). In addition, the mesopore volume was computed using the Barrett, Joyner, and Halenda (BJH)

method because this method captures the entire mesopore range (20 to 500 Å) while the DFT method is only able to calculate a mesopore volume for pores with widths in the range of 20 to 360 Å.

Elemental composition and ash content

C, H and N contents of the activated carbons were determined using a CHN Elemental Analyzer (Perkin-Elmer Corp., Norwach, CT) in the Soil Science Department at North Carolina State University. The accuracy of the CHN analyzer was checked with a NIST standard reference material (Trace Elements in Coal – Bituminous, SRM Number 1632c) and Table 2 compares measured and accepted values for this sample.

Oxygen content was determined by Huffman Laboratories (Golden, CO) according to ASTM D5622. Ash content was determined following ASTM D 2866.

Mass titration

Mass titrations were performed to determine the pH_{PZC} of the adsorbents. The pH_{PZC} is the pH value at which a given adsorbent possesses a net surface charge of zero. In this study the method proposed by Noh and Schwarz (1989) was used to determine the pH_{PZC}. The method relies on the principle that the suspension pH reaches a constant value after addition of excess solid in the presence of an electrolyte.

Adsorbent masses in the range of 1 to 12% (w/w) were added to 30 mL 0.1 N sodium chloride (NaCl) solution, and the resulting pH values were measured after one week of

equilibration time. Prior to use in pH_{PZC} determinations, adsorbents were washed with UPW until no pH change was observed. The NaCl solution was prepared with degassed ultrapure water (UPW), and the preparation of the samples and final pH measurements were performed under a nitrogen environment in a glove box.

Boehm titration

The total acid neutralization capacity, the concentrations of acidic surface functional groups, and the total base neutralization capacity of the adsorbent surface were determined by Boehm titrations (Boehm et al. 1964). This method consists of acid/base titrations of acidic or basic centers on the activated carbon surface. For these tests, 0.5 g of adsorbent was contacted with 30 mL of 0.1 N sodium bicarbonate ($NaHCO_3$), sodium carbonate (Na_2CO_3), sodium hydroxide (NaOH), and hydrochloric acid (HCl), and equilibrated for 3 weeks. After equilibration, the samples were centrifuged, and 10 mL of the supernatant were extracted and titrated with 0.05 N carbonate-free NaOH or HCl under nitrogen to measure the unreacted or unadsorbed acid or base remaining in solution. To calculate the number of surface acidic sites, it was assumed that $NaHCO_3$ neutralizes only strong carboxylic acid groups, Na_2CO_3 strong and weak carboxylic acid and lactonic groups, and NaOH strong and weak carboxylic, lactonic and phenolic groups. The number of basic surface sites was calculated from the amount of hydrochloric acid that reacted with the adsorbent.

Prior to Boehm titration experiments, adsorbents were washed with UPW until no pH change was observed. $NaHCO_3$ and Na_2CO_3 solutions were prepared with degassed UPW.

The 0.05 N HCl and NaOH solutions were obtained from Ricca Chemical and Fisher Scientific, respectively.

Adsorption Isotherm Experiments

Single-solute adsorption isotherm experiments were conducted in UPW with two adsorbates (SMX and TMP) and five adsorbents: four as-received activated carbons (one coconut shell-based carbon, two coal-based carbons, and one wood-based carbon) and one carbonaceous resin. Experiments were conducted at solution pH values that were at least two pH units below (pH = 3.6) and above (pH = 7.6 and 10 for SMX and pH = 9.1 for TMP) the pK_a/pK_b of the adsorbate such that the pollutant was present either predominantly in the neutral or ionic form. Another pH value that was evaluated matched the adsorbate pK_a/pK_b. The solution pH was maintained with 1 mM inorganic buffers (phosphate and borate buffer). Initial contaminant concentrations and adsorbent doses were such that isotherm data overlapped over a broad range of C/C_s^{pH} values.

Additional experiments were performed with SMX and TMP in Tar River water (TRW) and Lake Mead water (LMW) at ambient pH to quantify the adsorption competition exerted by NOM and compare it against pH-induced changes in adsorption capacity. Initial contaminant concentration (100 μg/L) was lower than in single-solute adsorption experiments (1-10 mg/L) to observe competition between NOM and the contaminant.

Batch reactors for adsorption isotherm experiments were mixed on a rotary tumbler for 3 to 4 weeks, a time that was sufficient to reach adsorption equilibrium. Upon equilibration, samples were filtered through 0.22-μm MAGNA nylon membrane filters (Osmonics/MSI, Westboro, MA) and analyzed with a Waters Breeze HPLC system that was equipped with a C18-AQ HPLC column (5 μm, 4.6 x 250 mm, Alltima HP, Grace) and a dual-wavelength UV detector. Samples were eluted at a flow rate of 1.0 mL/min using a binary mobile phase (70% mobile phase A, 30% mobile phase B). Mobile phase A contained 25 mM ammonium acetate buffer (pH 5, 1.26 g/L ammonium acetate and 2.96 ml/L of 3 M acetic acid) in UPW, and mobile phase B was 100% acetonitrile. The detector wavelengths were set at 266 and 238 nm, which represents the wavelengths of maximum absorbance for SMX and TMP, respectively.

RESULTS

Normalization of literature isotherm data

To test the hypothesis that the pH-dependent adsorption uptake of ionizable organic contaminants is largely controlled by pH-dependent changes in aqueous solubility, adsorption isotherm data were obtained from several journal publications (Snoeyink et al. 1969, Müller et al. 1980, 1985, Hu et al. 1998, Derylo-Marczewska and Marczewski 1999), and the liquid phase concentration was normalized by the pH-dependent solubility (C_s^{pH}). Figure 1 shows adsorption isotherm data of p-nitrophenol (weak organic acid, pK_a = 7.23) originally published by Müller et al. (1980). Panel a of Figure 1 presents the data as originally published by the authors and panel b shows the same data following normalization of the x-axis by C_s^{pH}. Values of C_s^{pH} of the compound were predicted using ACD/Labs software. Figure 1 clearly illustrates that the pH-induced change in aqueous solubility was the principal variable that affected the pH-dependent adsorption uptake of p-nitrophenol and that electrostatic and dispersive interactions played a secondary role in the adsorption process. Similar results were obtained for MCPB (weak organic acid, pK_a = 4.58), imazalil (weak organic base, pK_b = 6.75), benzoic acid (weak organic acid, pK_a = 4.2), and phenol (weak organic acid, pK_a = 9.99). These results are presented in Appendix A. For aniline (weak organic base, pK_b = 4.61), experiments conducted at pH 3.14, 4, and 10.85 also yielded results that agree with the proposed hypothesis (Figure 2). At pH 2, however, the adsorption isotherm of anilinium cations was shifted to lower equilibrium solid-phase

concentrations and did not follow the hypothesized trend. This shift can be attributed to increasing repulsive coulombic interactions between the positively charged surface and anilinium cations. Müller et al. (1985) determined that the pH_{PZC} of the activated carbon was 6.7. Therefore, at pH 2 the activated carbon surface charge was positive and more than 99% of the aniline in solution was in the cationic form, which increased the repulsive coulombic interactions between the carbon surface and cations. At pH 3.14 (96.7% of the aniline is cationic) and 4 (80.3% of the aniline is cationic), this situation is also occurring, but it appears that preferential adsorption of molecular aniline from solution followed by subsequent re-equilibration between aqueous aniline and anilinium occurred at these pH values.

Adsorbate characterization

Figure 4 depicts the pH-dependent aqueous solubility of TMP and SMX. Both panels show that the experimentally determined aqueous solubilities of both compounds are similar to the values predicted by the model in the pH regions, in which both compounds are sparingly soluble (<10,000 mg/L). At pH values at which the compounds became more soluble in water, the model predicted aqueous solubilities that differed from the experimentally determined values. For TMP in the cationic form, aqueous solubility values differed by a factor of about 15 at pH 3.6 (7.9 g/L determined experimentally compared to 118 g/L predicted by the model) and for SMX in the anionic form by a factor of about 4 (43 g/L predicted by the model compared to 189 g/L determined experimentally).

Adsorbent characterization

Physical properties

Micropore volumes of the fresh activated carbons ranged from approximately 0.20 to 0.50 cm^3/g and BJH mesopore volumes from 0.06 to 0.66 cm^3/g (Table 3). Mesopore volumes were similar for the adsorbents Ambersorb 563, F600, and UC830, smallest for the coconut-shell-based AC1230C GAC, and largest for the wood-based Picazine GAC. Micropore volumes were smallest for Ambersorb 563 and largest for the Picazine GAC.

Figure 5 depicts micropore size distributions of the five carbonaceous adsorbents used in this study. For organic trace contaminant removal from water, adsorbents with a large pore volume in a size range similar to the molecular size of the targeted contaminant are more effective (Newcombe et al. 1997, Li et al. 2002, Karanfil and Dasthgeib 2004). Thus, from a pore size distribution stand point, for SMX and TMP, which have molecular diameters of approximately 7.4 and 8.1 Å (considering the molecule as a sphere), activated carbon AC1230C appears to be the most suitable among the carbons being evaluated in this study because this adsorbent exhibited the largest pore volume in the 7-9 Å range (Figure 5).

Chemical properties

The results shown in Table 4 illustrate that the five carbonaceous adsorbents used in this research exhibited a wide range of ash and oxygen contents. Picazine had an oxygen content of almost 16%, which renders the surface of this carbon acidic (pH_{PZC} = 2.18, Table

5). A high oxygen content enhances the hydrophilicity of activated carbons and results in lower adsorption capacities for both polar and non-polar organic contaminants. Oxygen is primarily present on the surface as part of acidic surface functional groups such as carboxylic acid and phenolic groups that are located at the edges of the polyaromatic basal plane sheets. In contrast, the basic character of activated carbons is often attributed to the high density of delocalized π-electrons on the basal plane (Montes-Moran *et al*. 2004). However, some surface oxygen groups (e.g. pyrone groups) and ash may also affect the basic character of activated carbons (Montes-Moran *et al*. 2004).

Table 5 summarizes the pH_{PZC} values and acid/base neutralization capacities for the five carbonaceous adsorbents used in this research. As expressed by their pH_{PZC} values, both Picazine and Ambersorb 563 (2.18 and 2.4, respectively) are very acidic. Picazine had high concentrations of all types of acidic groups, which explains its low pH_{PZC}. Hence, this carbon is expected to be very hydrophilic and to exhibit lower organic contaminant uptake than may be expected based on physical characteristics alone. Compared to Picazine, Ambersorb 563 had much smaller concentrations of acidic groups and an unexpected low pH_{PZC}. Additionally, Table 5 shows data for the basic activated carbons AC1230C, F600 and UC830 (pH_{PZC} ranged from 8.3 - 8.9) with UC830 being slightly less basic than AC1230C and F600. Among the three basic carbons, UC830 had the highest concentrations of both basic and acidic sites. This result suggests that electrostatic interactions (attractive or repulsive) with

ionic adsorbates will play a more important role with UC830 than with AC1230C and F600, the latter of which exhibiting the lowest concentration of basic and acidic sites (Table 5).

Effects of activated carbon surface chemistry on the adsorption of ionizable organic contaminants at different solution pH values

Figure 6 compares TMP adsorption isotherms on the five adsorbents in UPW amended with 1 mM borate buffer at pH 9.1. At this solution pH, the TMP adsorption capacity of Ambersorb 563 was considerably smaller than those of the activated carbons. Among the activated carbons AC1230C was most effective for TMP removal. TMP adsorption isotherm data were also collected in UPW amended with 1 mM phosphate buffer at pH 3.6 and 7.0. TMP, a weak organic base with a pK_b of about 7.0, is primarily cationic (>99.9%) at pH 3.6, 50% cationic and 50% neutral at pH 7.0, and predominantly neutral (>99% neutral) at pH 9.1. Figure 7a summarizes TMP adsorption isotherm data collected with activated carbon UC830 (coal-based carbon) at pH 3.6, 7.0, and 9.1. Analogous data for the four other adsorbents are shown in Figures 1-4 of Appendix B. Figure 7a shows that the TMP adsorption capacity at pH 7.0 was similar to that at pH 9.1, and similar results were obtained for the other two basic carbons (AC1230C and F600, see Figures 1 and 2 in Appendix B). The absence of an adsorption maximum at pH = pK_a agrees with the thesis of Müller et al. (1980, 1985) who proposed that such a maximum only occurs if considerable ionization of the compounds takes place while the carbon surface still carries a charge opposite to the ionized compound. In the case of the three basic activated carbons, the carbon

surface carried a positive charge at pH 7.0 while TMP was present in both cationic and neutral forms. Therefore, the absence of attractive electrostatic interactions precluded the possibility of an adsorption maximum at pH = pK_a. For Picazine, on the other hand, a maximum in TMP adsorption capacity was observed at pH = pK_a. This carbon carries a strong negative charge at pH 7.0, which is opposite in charge to the TMP cations, thus enhancing the adsorption at pH = pK_a (Figure 3, Appendix B). However, Ambersorb 563, another acidic adsorbent, did not follow this trend (Figure 4, Appendix B). At pH = pK_a the TMP adsorption capacity was similar to that at pH 9.1, which was not expected, since Ambersorb 563 surface carries a net negative charge and 50% of TMP was present in cationic form. For all tested adsorbents, TMP adsorption isotherms measured at pH 3.6 fell below those measured at pH 7.0 and 9.1, illustrating that at solution pHs, at which the cationic form dominates, the effectiveness of adsorption processes for TMP removal from water is lower. Table 6 compares solid-phase TMP concentrations at equilibrium liquid-phase concentrations of 1 and 100 μg/L at pH 3.6 and 9.1. Solid-phase concentrations were calculated using the Freundlich isotherm parameters shown in Figure 7a and Figures 1-4 (Appendix B). Relative to the TMP adsorption capacity at pH 9.1, the percentage of the TMP adsorption capacity at pH 3.6, at which the cationic form of TMP dominates, was higher for the acidic adsorbents Picazine and Ambersorb 563 and lower for the three basic activated carbons. These results suggest that electrostatic interactions did play a role at solution pHs at which the cationic form of TMP dominated.

To assess the importance of the pH-dependent aqueous TMP solubility on TMP adsorption, the TMP isotherm data in Figure 7a were normalized by C_s^{pH} values obtained from model predictions (Figure 7b) and from the experimentally determined solubilities (Figure 7c). Figure 7b clearly illustrates that the normalization procedure accounts for the pH-dependency of the adsorption capacity of the activated carbon tested. Figures 1-4 (Appendix B) confirm the same result for all the adsorbents tested. However, Figure 7c illustrates that the TMP adsorption isotherm at pH 3.6 is shifted towards lower equilibrium solid-phase concentrations. Similar results are exhibited by the other two basic activated carbons (see Figures 1 and 2, Appendix B). The latter results can be explained by repulsive coulombic interactions between the positively charged carbon surface and the cationic form of TMP at pH 3.6. At pH 3.6 more than 99% of TMP molecules are in the cationic form and the activated carbon surface is positive (e.g., pH_{PZC} of UC830 is 8.28). In contrast, at pH 9.1 the net surface charge is nearly zero for the basic carbons and less than 1% of the TMP in solution is in the cationic form; therefore, TMP adsorption is mainly occurring through dispersive interactions. Whether or not coulombic interactions played a role in the adsorption of TMP at pH 3.6 cannot be stated unambiguously because of the uncertainty associated with the C_s^{pH} value at pH 3.6.

Figure 8 depicts SMX adsorption isotherm data for the five adsorbents in UPW amended with phosphate buffer at pH 3.6. Results show that the SMX adsorption capacity of Picazine was considerably smaller than the rest of the adsorbents. As was the case for TMP, AC1230C was the most effective adsorbent for SMX removal. SMX adsorption isotherm

data were also collected in UPW at pH 7.6, 10 as well as at pH ~6 for the basic GACs and at pH 1.75 for the acidic adsorbents. SMX is a weak organic acid with a pK_a of about 5.6. Thus, SMX is predominantly neutral (~99%) at pH 3.6, 50% neutral and 50% anionic at pH 5.6, predominantly anionic (~99%) at pH 9.1, and almost completely anionic at pH 10. Experiments were performed at pH 1.75 for the acidic adsorbent, because SMX also has a pK_a at pH ~1.80, at which the neutral form is in equilibrium with the cationic form (Table 1). These experiments were conducted to quantify the importance of electrostatic interactions between a positively charged adsorbent surface and SMX cations. Figure 9a summarizes pH-dependent SMX adsorption isotherm data collected with activated carbon UC830. Additional SMX isotherm data collected for the basic activated carbons AC1230C and F600, the acidic activated carbon Picazine and the carbonaceous resin Ambersorb 563 are presented in Appendix B (Figures 5-8). SMX results for the basic carbons did not show a maximum in SMX adsorption capacity at pH = pK_a, instead the SMX adsorption capacity near the pH = pK_a was similar to that at pH 3.6.

For the acidic carbons, the adsorption capacity at pH 1.75 was lower than at pH 3.6. This result reflects the increase in solubility of SMX at pH 1.75 compared to pH 3.6, which rendered SMX less adsorbable. In addition, repulsive interactions between the positively charged adsorbent surface and SMX cations may have affected the results.

Table 7 compares SMX adsorption capacities at pH 3.6, 7.6 and 10 at equilibrium liquid-phase concentrations of 1 and 100 μg/L. This comparison supports the observation that

SMX is more adsorbable at pH values at which the neutral form dominates. Solid-phase concentrations were calculated using the Freundlich isotherm parameters shown in Figure 9a and Figures 5-8 (Appendix B). Relative to the SMX adsorption capacity at pH 3.6, the decrease in SMX adsorption capacity that was measured at pH 7.6 and 10, at which the anionic form of SMX dominated, was not uniform among the adsorbents. The percentage reduction of SMX adsorption at pH 7.6 and 10 was higher for the acidic adsorbents Picazine and Ambersorb 563 and lower for the three basic activated carbons. These results suggest that electrostatic interactions played a role at solution pHs at which the anionic form of SMX dominated. Picazine was the adsorbent for which an increase in solution pH had the largest detrimental effect on SMX adsorption. This result reflects the high concentration of acidic surface functional groups and the repulsive interactions between the negatively charged activated carbon surface and SMX anions.

To assess the importance of the pH-dependent aqueous SMX solubility on SMX adsorption, the SMX isotherm data in Figure 9a were normalized by C_s^{pH} values obtained from model predictions (Figure 9b) and from the experimentally determined solubilities (Figure 9c). Apart from the pH 10 data, the SMX isotherm data could be effectively normalized by dividing the equilibrium liquid phase concentrations by C_s^{pH} (Figure 9b and Figures 5-8 panels b and c). Only in Figure 9c, the data at pH 10 did not show a shift towards lower equilibrium solid-phase concentrations. The much smaller adsorption capacity of all tested activated carbons at pH 10 was likely the result of repulsive coulombic interactions between negatively charged adsorbent surfaces and the anionic form of SMX. At pH 7.6

repulsive interactions can also be present, because some of the carbons were negatively charged and around 99% of the SMX molecules were in the anionic form; however, repulsive interactions at this pH seem to be unimportant. A probable explanation for this result is that the neutral form is more readily adsorbed than anionic form. Therefore, the neutral form (present at 1% of the total SMX concentration) adsorbed preferentially, which was followed by re-equilibration between aqueous SMX molecules and anions. This process continued until the final equilibrium solid-phase concentration was reached.

To further test if the TMP and SMX isotherm data could be effectively normalized by dividing the equilibrium liquid phase concentration by C_s^{pH}, the Dubinin-Astakhov (D-A) isotherm model was used to describe the normalized isotherm data. Normalized data collected at different solution pHs were pooled for this purpose. The D-A isotherm model is based on Dubinin's theory of micropore volume filling and has the form shown in equation 1

$$q_e = q_m \cdot \exp\left[-\left(\frac{A}{E}\right)^n\right] \qquad \text{(eq. 1)}$$

where A is the adsorption potential (J/mol):

$$A = RT \cdot \ln\left(\frac{C_{sat}}{C_e}\right) \qquad \text{(eq. 2)}$$

q_m, n, E are the three adjustable parameters of the DA isotherm model, R is the ideal gas constant (8.314 J mol-1 K-1), T is the absolute temperature (K), and C_{sat} is the aqueous solubility of the compound (in this case SMX and TMP, which vary with pH). The adjustable parameters of the model represent physical characteristics of the adsorbate and adsorbent.

The maximum adsorption capacity, q_m, represents the filling of adsorbent micropores, E is the adsorption potential at which the capacity is 36.8% of the maximum capacity, and the parameter n represents the heterogeneity of the adsorbent pores and describes the curvature of the isotherm.

It was observed that small changes in the initial guesses of the parameters affected the final values of the three parameters and, therefore, a unique set of D-A isotherm parameters could not be identified. Consequently, a different approach was employed. Parker (1995) found that q_m (= $V_m \cdot \rho$) can be predicted from the micropore volume (V_m obtained from N_2 adsorption data, Table 3) of the adsorbent and the liquid density of the adsorbate (ρ). The remaining two fitting parameters of the D-A isotherm model were determined using GraphPad Prism, Version 5.01. The D-A isotherm parameters are shown in Tables 8 and 9 for TMP and SMX, respectively. The R^2 values suggest that the D-A isotherm well described the adsorption of SMX and TMP on carbonaceous adsorbents at different solution pH values and that the pH-dependent solubility of the compounds was the main variable affecting the pH-dependent adsorption uptake of SMX and TMP. Additionally, it was observed that the values of E for the adsorption of TMP on Ambersorb 563 and SMX on Picazine were smaller than for the remaining adsorbents. This result agrees with the fact that the adsorption capacity of the carbonaceous resin and the wood-base activated carbon for TMP and SMX, respectively, was the lowest among the studied adsorbents.

Effect of co-adsorbing NOM on adsorption of ionizable organic compounds

To evaluate the effect of NOM on the adsorption of SMX and TMP, adsorption isotherm experiments were completed in TRW and LMW for adsorbents AC1230C, Ambersorb 563, F600 and UC830 (Figure 7a and Figure 1,2 and 4, Appendix B). For the tested adsorbents, TMP adsorption capacities were similar in TRW (TOC = 6.1 mg/L) and LMW (TOC = 2.5 mg/L). In general, TMP adsorption capacities in TRW and LMW were lower than (AC1230C, F600, Ambersorb 563) or similar to (UC830) the TMP adsorption capacity measured at pH 3.6. This result suggests that co-adsorption of NOM more severely affected TMP adsorption capacity than pH effects, since the majority of TMP in the natural waters was present in the neutral form (pH_{TRW} = 7.3, pH_{LMW} = 8.4).

SMX adsorption isotherm results obtained in TRW and LMW are depicted in Figure 9a and Figures 5-7 (Appendix B). Comparing NOM effects on SMX adsorption capacities, the results obtained with all three activated carbons showed that higher adsorption capacities were obtained in LMW than in TRW. In contrast, similar SMX adsorption capacities were obtained with the carbonaceous resin in both natural waters. The pH of TRW was 7.5 and that of LMW 8.1, suggesting that SMX was mostly present in the anionic form in both natural waters. The higher pH of LMW also suggests that the surface charge of the activated carbons was more negative or less positive in LMW than in TRW, which should have adversely affected the adsorption of SMX anions. However, the results in Figure 9a indicate

that differences in the competitive nature of NOM between TRW and LMW dominated over electrostatic effects as a result of pH differences between TRW and LMW.

CONCLUSIONS

- For both TMP and SMX, adsorption capacities were highest at solution pHs at which the neutral form dominated.
- The reduction of the TMP adsorption capacity at pH 3.6 relative to the TMP adsorption capacity at pH 9.1 was higher for the three basic activated carbons and lower for the two acidic adsorbents, suggesting that electrostatic interactions played a role at solution pHs at which the cationic form of TMP dominated.
- Relative to the SMX adsorption capacity at pH 3.6, the reduction of SMX adsorption capacity at pH 7.6 and 10, at which the anionic form of SMX dominated, was not uniform among the adsorbents. This reduction was higher for the two acidic adsorbents and lower for the three basic adsorbents, suggesting that electrostatic interactions are important at solution pHs at which the anionic SMX dominated.
- The activated carbon AC1230C was the most effective among the adsorbents studied to remove TMP and SMX from UPW, TRW, and LMW. This was attributed to the fact that AC1230C exhibited the largest micropore volume in the 7-9 Å range; i.e. the size range that encompassed the molecular diameters of SMX and TMP.

- The hypothesis that the pH-dependent adsorption uptake of ionizable organic contaminants is largely controlled by pH-dependent changes in aqueous solubility was validated over a limited pH range for a wide range of ionizable organic pollutants, for which data were available in literature. This result suggests that the adsorptive removal of ionizable organic compounds is largely controlled by adsorption of the neutral species, even at pH values at which the ionic form begins to dominate. An exception to this result was the data set describing the adsorption of aniline at pH 2. At this solution pH aniline is almost completely in the cationic form, and electrostatic interactions therefore became important.

- TMP isotherm data normalized by ***model-predicted*** C_s^{pH} values showed that the normalization procedure accounted for the pH-dependence of the adsorption capacity of the tested activated carbons and suggests that coulombic interactions played a secondary role in the adsorption of TMP at pH values at which the cationic form prevailed in solution. However, the TMP isotherm data at pH 3.6 for the three basic activated carbons shifted to lower equilibrium solid-phase concentrations when the experimental data was normalized by the ***experimentally determined*** C_s^{pH} values. This result suggests that electrostatic interactions between the positively charged surface of the basic activated carbons and TMP cations do play an important role. Thus, uncertainty in C_s^{pH} values precludes an unambiguous determination of the importance of coulombic interactions on the adsorption of TMP at pH 3.6.

- SMX isotherm data were effectively normalized by C_s^{pH} for solution pH values in the range of 3.6 to 7.6. In contrast, the data at pH 10 was shifted towards lower equilibrium solid-phase concentrations. This shift was likely the result of repulsive electrostatic interactions between the negatively charged activated carbon surface and SMX anions.

- TMP adsorption capacities were similar in TRW and LMW and lower than in UPW at similar pH values. Generally, the competitive effect of NOM on TMP and SMX adsorption capacities was stronger than pH-dependent changes in TMP and SMX adsorption capacities that were measured in UPW.

REFERENCES

G. Belfort. 1979. "Selective adsorption of organic homologues onto activated carbon from dilute aqueous solutions. "Solvophobic interaction approach and correlations of molar absorptivity with physicochemical parameters." *Environmental Science & Technology* 13(8): 939-946.

Boehm, H.P.; Diehl, E.; Heck, W.; and R. Sappok. Surface Oxides of Carbon. Angew. Chem. Internat. Edit. 1964; 3:669-677.

Cornelissen, G.; Elmquist, M.; Groth, I.; and Ö. Gustafsson. 2004. "Effect of sorbate planarity on environmental black carbon sorption." *Environmental Science & Technology* 38(13): 3574-3580.

Derylo-Marczewska, A.; and A.W. Marczewski. 1999. "Nonhomogeneity effects in adsorption from gas and liquid phases on activated carbons." *Langmuir* 15: 3981-3986.

Hu, J.Y.; Aizawa, T.; Ookubo, Y.; Morita, T.; and Y. Magara. 1998. "Adsorptive characteristics of ionogenic aromatic pesticides in water on powdered activated carbon." *Water Research* 32(9): 2593-2600.

Karanfil, T.; and S.A. Dastgheib. 2004. "Trichloroethylene adsorption by fibrous and granular activated carbons: aqueous phase, gas phase, and water vapor adsorption studies." *Environmental Science & Technology* 38(22): 5834-5841.

Karanfil, T.; and J.E. Kilduff. 1999. "Role of granular activated carbon surface chemistry on the adsorption of organic compounds. 1. Priority pollutants." *Environmental Science & Technology* 33(18): 3217-3224.

Kilduff, J.E.; Karanfil, T.; and W.J. Weber Jr. 1998. "Competittive effects of nondisplaceable organic compounds on trichloroethylene uptake by activated carbon. I. Thermodynamic predictions and model sensitivity analyses." *Journal of Colloid and Interface Science* 205: 271-279.

Kilduff, J.E.; Srivastava, R.; and T. Karanfil. 2002. "Preloading of GAC by natural organic matter: effect of surface chemistry on TCE uptake." *Studies in Surface Science and Catalysis* 144: 553-560.

Knappe, D.R.U. "Chapter 9 - Surface Chemistry Effects in Activated Carbon Adsorption of Industrial Pollutants." In Interface Science in Drinking Water Treatment - Theory and Applications, Newcombe, G. and Dixon, D. (Eds.), Academic Press: Oxford, UK, 2006.

Li, L.; Quinlivan, P.A.; and D.R.U. Knappe. 2002. "Effects of activated carbon surface chemistry and pore structure on the adsorption of organic contaminants from aqueous solution." *Carbon* 40(12): 2085-2100.

Li, L.; Quinlivan, P.A.; and D.R.U. Knappe. 2005. "Predicting adsorption isotherms for aqueous organic micropollutants from activated carbon and pollutant properties." *Environmental Science and Technology* 39(9): 3393-3400.

McKay, G.; and B. Al Duri. 1989. "Prediction of multicomponent adsorption equilibrium data using empirical correlations." *The Chemical Engineering Journal* 41: 9-23.

Montes-Morán, M.A.; Suárez, D.; Menéndez, J.A; and E. Fuente. 2004. "On the nature of basic sites on carbon surfaces: An overview." *Carbon* 42: 1219-1225.

Morris, G.; and G. Newcombe. 1993. "Granular activated carbon: The variation of surface properties with the adsorption of humic substances." *Journal of Colloid and Interface Science* 159: 413-420.

Müller, G.; Radke, C.J.; and J.M. Prausnitz. 1980. "Adsorption of weak organic electrolytes from aqueous solution on activated carbon. Effect of pH." *The Journal of Physical Chemistry* 84: 369-376.

Müller, G.; Radke, C.J.; and J.M. Prausnitz. 1985. "Adsorption of weak organic electrolytes from dilute aqueous solution onto activated carbon. Part 1. Single-solute systems." *Journal of Colloid and Interface Science* 103(2): 466-483.

Newcombe, G. 1994. "Activated carbon and soluble humic substances: Adsorption, desorption, and surface charge effects." *Journal of Colloid and Interface Science* 164: 452-462.

Newcombe, G.; Drikas, M.; and R. Hayes. 1997. "Influence of characterized natural organic material on activated carbon adsorption: II. Effect on pore volume distribution and adsorption of 2-methylisoborneol." *Water Research* 31: 1065-1073.

Noh, J.S.; and J.A. Schwarz. 1989. "Estimation of the point of zero charge of simple oxides by mass titration." *Journal of Colloid and Interface Science* 130(1): 157-164.

Parker, G. R. (1995). ''Optimum isotherm equation and thermodynamic interpretation for aqueous 1,1,2-trichloroethene adsorption isotherms on three adsorbents.'' *Adsorption*, 1(1), 113–132.

Pelekani, C.; and V.L. Snoeyink. 1999. "Competitive adsorption in natural water: role of activated carbon pore size." *Water Research* 33(5): 1209-1219.

Pendleton, P.; Wong, S.H.; Schumann, R.; Levay, G.; Denoyel, R.; and J. Rouquerol. 1997. "Properties of activated carbon controlling 2-methylisoborneol adsorption." *Carbon* 35(8): 1141-1149.

Radovic, L.R.; Silva, I.F.; Ume, J.I.; Menendez, J.A.; Leon y Leon, C.A.; and A.W. Scaroni. 1997. "An experimental and theoretical study of the adsorption of aromatics possessing electron-withdrawing and electron-donating functional groups by chemically modified activated carbons." *Carbon* 35(9): 1339-1348.

Schwarzenbach, R.P.; Gschwend, P.M.; and D.M. Imboden. Environmental Organic Chemistry, 2nd ed. John Wiley & Sons, Hoboken, NJ, 2003.

SciFinder Scholar. 2006. Version 2006. American Chemical Society, Washington, DC.

USEPA. 1998. Product Properties Test Guidelines – OPPTS 830.7840 – Water Solubility: Column Elution Method; Shake Flask Method. EPA 712-C-98-041. Washington, DC.

Ward, T.M.; and F.W. Getzen. 1970. "Influence of pH on the adsorption of aromatic acids on activated carbon." *Environmental Science and Technology* 4(1): 64-67.

Table 1. Properties of selected compounds

Compound	CAS #	MW (g/mol)	C_s in water (mg/L)[&]	Log K_{OW}[&]	pK_a
Aniline	62-53-3	93.1	32,000	0.94	4.61 (+/0)[*]
Benzoic acid	65-85-0	122.1	4,000	1.90	4.20 (0/-)[$]
Imazalil	35554-44-0	297.2	14	3.58	6.75 (+/0)[*]
MCPB	94-81-5	228.7	190	3.42	4.58 (0/-)[$]
Phenol	108-95-2	94.1	103,000	1.48	9.86 (0/-)[$]
p-nitrophenol	100-02-7	139.1	4,200	1.57	7.23 (0/-)[$]
Sulfamethoxazole	723-46-6	253.3	430	400	(1) 1.6-1.85 (+/0)[*] (2) 5.57-5.7 (0/-)[$]
Trimethoprim	738-70-5	290.3	0.89	0.91	(1) 6.6-7.34 (+/0)[*]

[&] determined for neutral form at 25°C
[*] (+/0) = moiety goes from cationic to neutral form;
[$] (0/-) = moiety goes from neutral to anionic form

Table 2. Measured and accepted values of C, H and N for NIST standard reference material

	%C	%H	%N
Measured value	77.03	4.88	1.52
Accepted value	77.45 ± 0.25	5.11 ± 0.12	1.54 ± 0.06

Table 3. Physical characteristics of as-received activated carbons and carbonaceous resin

Adsorbent	BET Surface Area (m^2/g)	Micropore Volume[a] (cm^3/g)	DFT Mesopore Volume[b] (cm^3/g)	BJH Mesopore Volume[c] (cm^3/g)
AC1230C	1160	4.37×10^{-1}	2.94×10^{-2}	6.01×10^{-2}
Ambersorb 563	546	2.01×10^{-1}	2.80×10^{-1}	3.18×10^{-1}
F600	820	2.66×10^{-1}	2.66×10^{-1}	3.05×10^{-1}
Picazine	1680	4.96×10^{-1}	5.62×10^{-1}	6.55×10^{-1}
UC830	1030	3.56×10^{-1}	2.20×10^{-1}	2.70×10^{-1}

[a] Micropore volume calculated by density functional theory (DFT) for pores with widths less than 20 Å

[b] Mesopore volume calculated by density functional theory (DFT) for pores with widths ranging from 20 to 360 Å (upper limit for DFT model)

[c] Mesopore volume calculated by Barrett, Joyner, and Halenda (BJH) method for pores with widths ranging from 20 to 500 Å

Table 4. Chemical characteristics of carbonaceous adsorbents

Adsorbent	%C	%H	%N	%O	%Ash
AC1230C	97.41	0.70	0.19	3.75	3.14
Ambersorb 563	84.26	2.01	0.06	4.81	0.80
F600	92.50 [a]	0.61 [a]	0.41 [a]	2.60 [a]	1.84 [a]
Picazine	76.92 [a]	0.40 [a]	0.03 [a]	15.88 [a]	3.37 [a]
UC830	89.95	0.81	0.33	2.28	11.32

[a] from Li et al. (2002)

Table 5. Acid/base characteristics of carbonaceous adsorbents

Adsorbent	Total basic groups (meq/100g)	Total acidic groups (meq/100g)	Strong carboxylic groups (meq/100g)	Weak carboxylic groups (meq/100g)	Phenolic groups (meq/100g)	pH_{PZC}
AC1230C	62.0	28.5	0	8.6	19.9	8.77
Ambersorb 563	13.4	28.1	11.1	14.5	2.5	2.40
F600	45.7	14.1	0	6.7	7.4	8.88
Picazine	6.3	191.0	65.4	46.7	78.9	2.18
UC830	65.4	34.1	0.9	13.2	20.0	8.28

Table 6. Effect of TMP dissociation on single-solute adsorption capacities of carbonaceous adsorbents

Adsorbent	pH	q_{10} (mg/g)*	% of q_{10} at pH 9.1	q_{100} (mg/g)+	% of q_{100} at pH 9.1
AC1230C	9.1	164.0		240.3	
	3.6	78.6	47.9	115.1	47.9
Ambersorb 563	9.1	26.9		35.1	
	3.6	15.1	56.1	21.4	61.0
F600	9.1	119.7		146.3	
	3.6	46.7	39.0	68.1	46.5
Picazine	9.1	102.7		158.3	
	3.6	70.1	68.2	100.8	63.4
UC830	9.1	141.9		190.6	
	3.6	51.2	36.1	78.0	40.9

* solid-phase concentration at an equilibrium liquid phase concentration of 10 µg/L
+ solid- phase concentration at an equilibrium liquid phase concentration of 100 µg/L

Table 7. Effect of SMX dissociation on single-solute adsorption capacities of carbonaceous adsorbents

Adsorbent	pH	q_{10} (mg/g)	% of q_{10} at pH 3.6	q_{100} (mg/g)	% of q_{100} at pH 3.6
AC1230C	3.6	144.7		284.1	
	7.6	59.3	41.0	115.4	40.6
	10.0	18.6	12.8	39.1	13.8
Ambersorb 563	3.6	71.1		130.3	
	7.6	29.1	40.9	48.6	37.3
	10.0	2.00	2.80	4.40	3.40
F600	3.6	96.8		164.8	
	7.6	46.8	48.3	80.2	48.7
	10.0	13.2	13.6	24.2	14.7
Picazine	3.6	22.8		70.5	
	7.6	4.82	21.1	12.6	17.9
	10.0	1.43	6.30	2.12	3.00
UC830	3.6	92.9		188.8	
	7.6	40.4	43.5	72.5	38.4
	10.0	14.6	15.7	25.8	13.7

Table 8. Dubinin-Astakhov isotherm parameters for normalized TMP adsorption isotherms on carbonaceous adsorbents

Adsorbent	C_s determination	Dubinin-Astakhov isotherm parameters			
		q_m (mg/g)[&]	E (kJ/mol)[%]	n[%]	R^2
AC1230C	Model	547	25.1±0.8	1.48±0.16	0.96
	Experiment[*]	547	24.8±1.1	1.49±0.22	0.95
Ambersorb 563	Model	252	6.1±1.4	0.51±0.08	0.78
	Experiment	252	6.4±1.3	0.57±0.08	0.77
F600	Model	333	25.7±1.1	1.38±0.18	0.88
	Experiment[*]	333	26.2±1.4	0.95±0.22	0.88
Picazine	Model	621	17.7±2.2	0.95±0.18	0.71
	Experiment	621	15.8±2.4	0.94±0.22	0.74
UC830	Model	446	24.6±0.7	1.52±0.12	0.95
	Experiment[*]	446	24.8±1.3	1.34±0.24	0.93

[*] pH 3.6 data were excluded because the normalized isotherm at pH 3.6 deviated from the remaining isotherm data

[&] Calculated from $q_m=V_m \cdot \rho$, where V_m is the micropore volume of the adsorbent estimated from N_2 adsorption data (Table 3) and ρ is the liquid density of TMP at 20ºC as estimated from ChemSketch (1.252 g/cm^3)

[%] interval represents the 95% confidence interval of the parameter

Table 9. Dubinin-Astakhov isotherm parameters for normalized SMX adsorption isotherms on carbonaceous adsorbents

Adsorbent	C_s determination	Dubinin-Astakhov isotherm parameters			
		q_m (mg/g)[&]	E (kJ/mol)[%]	n[%]	R^2
AC1230C	Model[*]	639	22.0±1.0	1.59±0.22	0.90
	Experiment[*]	639	21.1±1.4	1.44±0.26	0.84
Ambersorb 563	Model[*]	294	20.0±0.9	1.38±0.17	0.92
	Experiment[*]	294	19.1±0.9	1.33±0.17	0.91
F600	Model[*]	389	23.6±0.7	1.71±0.19	0.94
	Experiment[*]	389	23.1±1.1	1.57±0.26	0.88
Picazine	Model[*]	726	11.7±0.3	1.50±0.07	0.99
	Experiment[*]	726	10.5±0.3	1.37±0.06	0.99
UC830	Model[*]	521	20.6±1.0	1.70±0.27	0.89
	Experiment	521	19.9±1.3	1.63±0.29	0.82

[*] pH 10 data were excluded because the normalized isotherm at pH 10 deviated from the remaining isotherm data

[&] Calculated from $q_m=V_m \cdot \rho$, where V_m is the micropore volume of the adsorbent estimated from N_2 adsorption data (Table 3) and ρ is the liquid density of SMX at 20ºC as estimated from ChemSketch (1.462 g/cm^3)

[%] interval represents the 95% confidence interval of the parameter

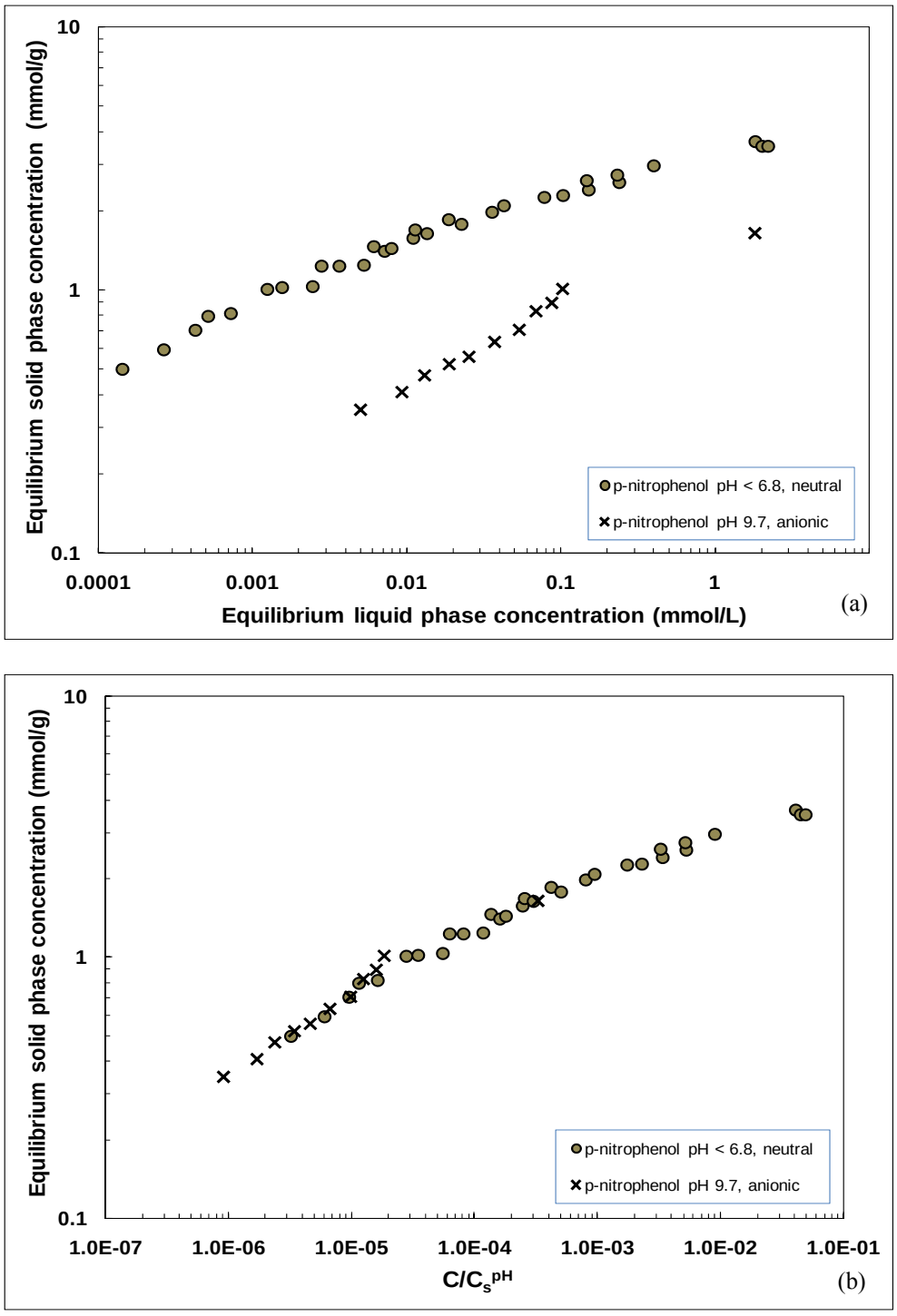

Figure 1. Adsorption isotherm data of p-nitrophenol at different solution pHs; (a) as originally presented by Müller et al. (1980), and (b) following normalization with C_s^{pH}.

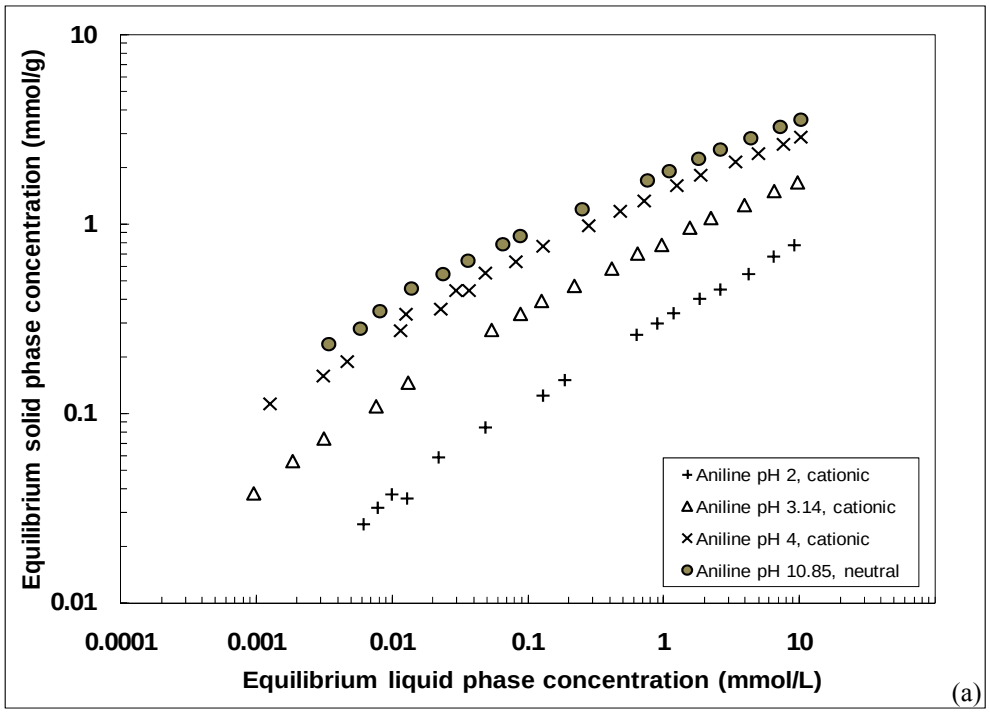

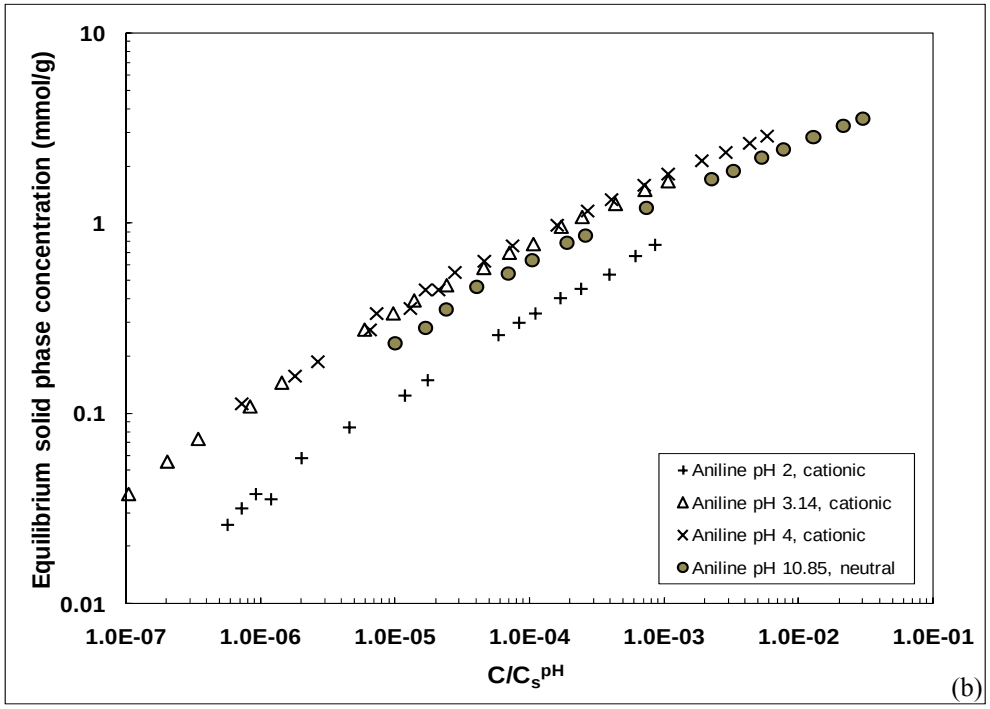

Figure 2. Adsorption isotherm data of aniline at different solution pHs; (a) as originally presented by Müller et al. (1985), and (b) following normalization with C_s^{pH}.

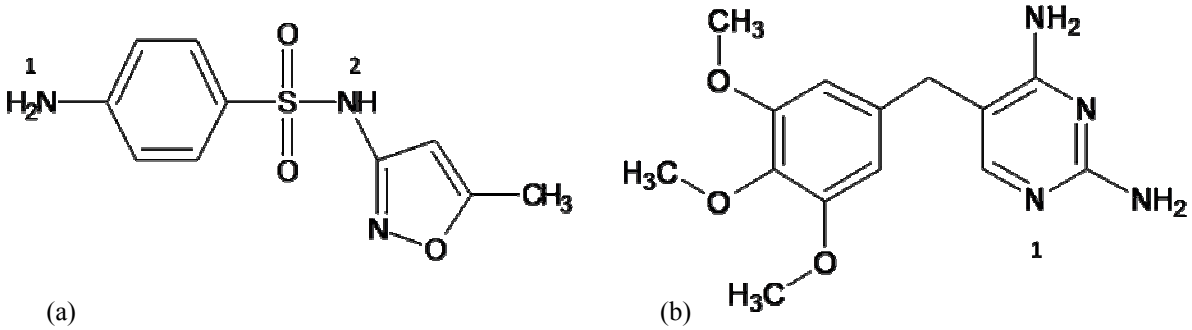

Figure 3. Molecular structures of (a) sulfamethoxazole and (b) trimethoprim. Labels 1 and 2 adjacent to functional groups refer to protonation/deprotonation sites.

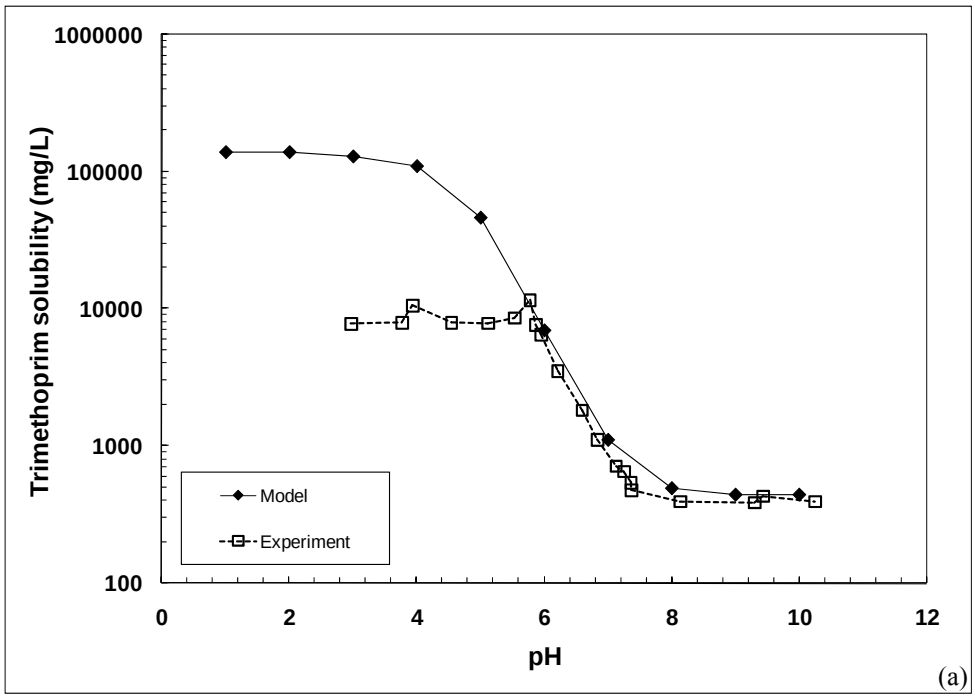

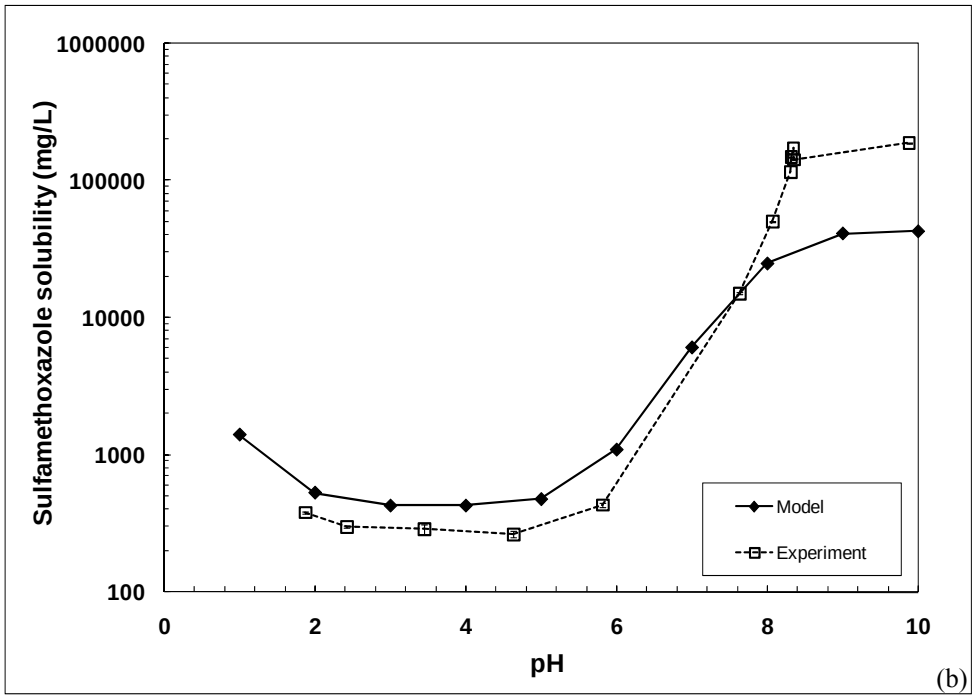

Figure 4. Solubility of ionizable compounds as a function of pH predicted theoretically by ACD/Labs software and determined experimentally; (a) solubility of TMP, and (b) solubility of SMX.

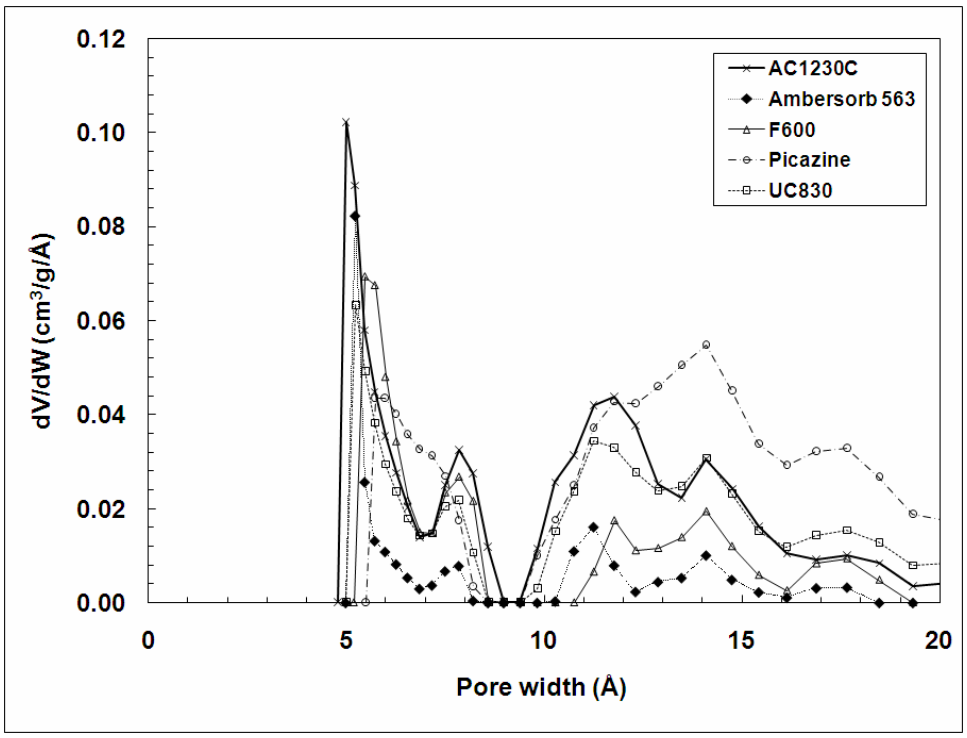

Figure 5. Micropore size distribution of activated carbons and carbonaceous resin (y-axis represents differential pore volume [V] in cm^3/g adsorbent per unit pore width [W] in Å).

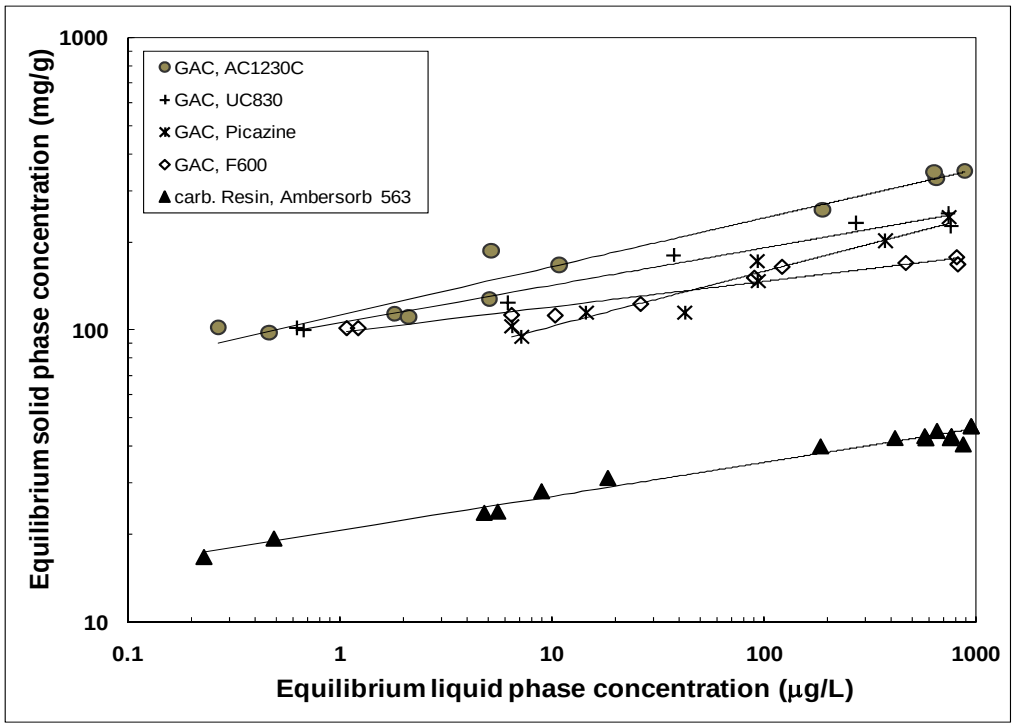

Figure 6. Adsorption isotherms of TMP on carbonaceous adsorbents AC1230C, Ambersorb 563, F600, Picazine, and UC830 in UPW at pH 9.1. Lines represent Freundlich isotherm model fits.

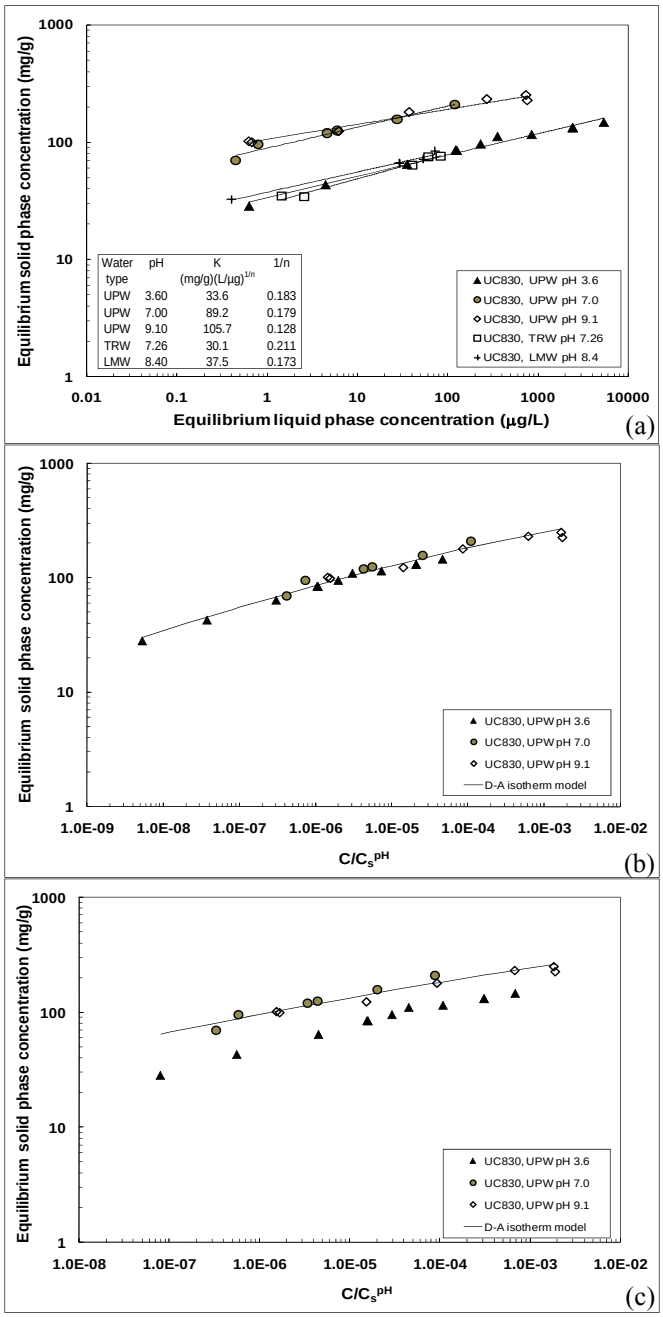

Figure 7. TMP adsorption isotherms on coal-based activated carbon UC830 in UPW at different solution pHs, TRW, and LMW; (a) plotted against the equilibrium liquid phase concentration (table shows Freundlich isotherm parameters), (b) UPW data following normalization with theoretical C_s^{pH} values predicted with ACD/Labs software, and (c) UPW data following normalization with experimental C_s^{pH} values. Lines in panels (b) and (c) represent Dubinin-Astakhov isotherm model fits.

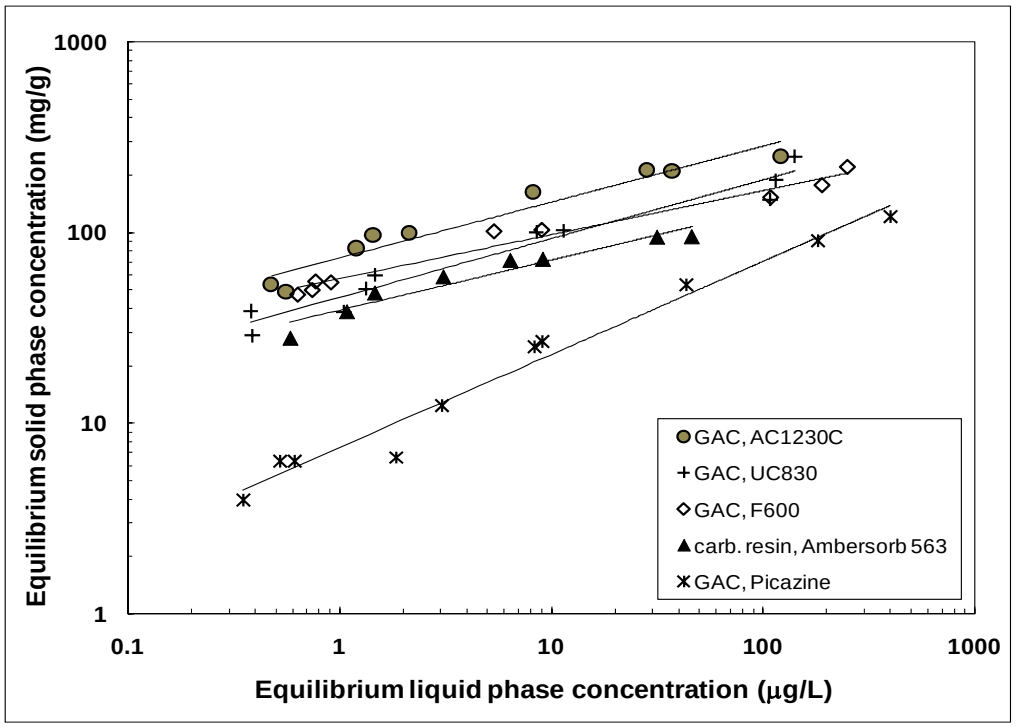

Figure 8. Adsorption isotherms of SMX on carbonaceous adsorbents AC1230C, Ambersorb 563, F600, Picazine, and UC830 in UPW at pH 3.6. Lines represent Freundlich isotherm model fits.

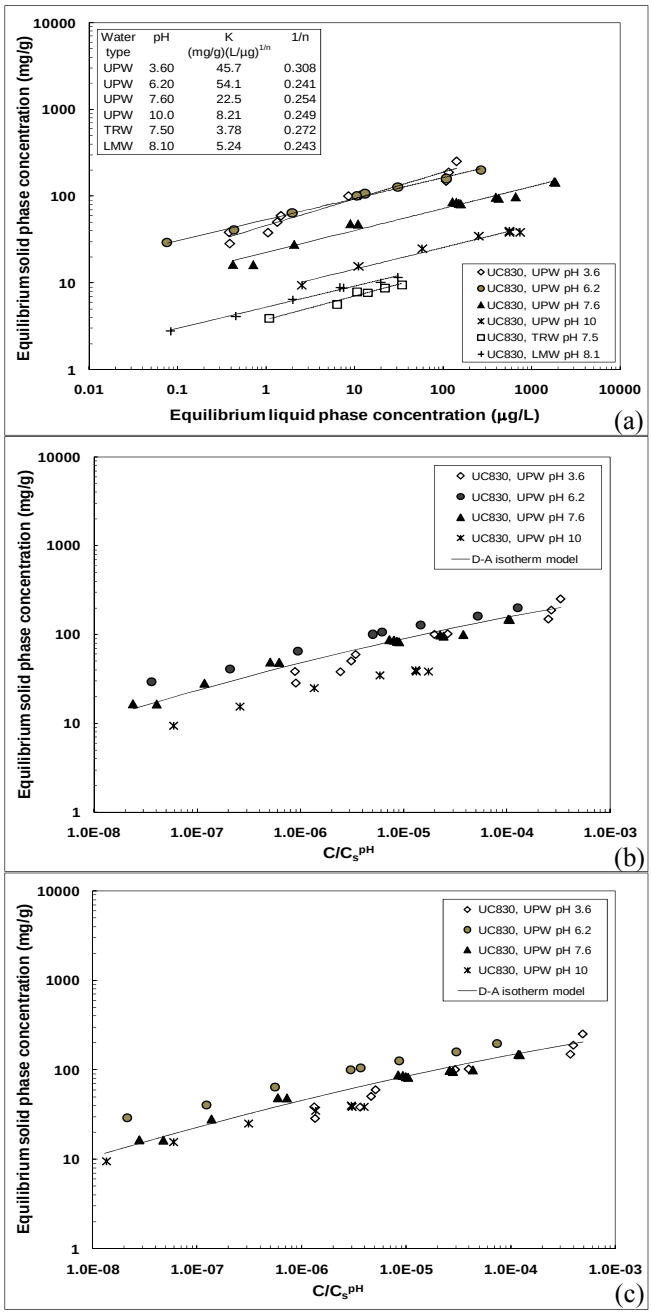

Figure 9. SMX adsorption isotherms on coal-based activated carbon UC830 in UPW at different solution pHs, TRW, and LMW; (a) plotted against the equilibrium liquid phase concentration (table shows Freundlich isotherm parameters), (b) UPW data following normalization with theoretical C_s^{pH} values predicted with ACD/Labs software, and (c) UPW data following normalization with experimental C_s^{pH} values. Lines in panels (b) and (c) represent Dubinin-Astakhov isotherm model fits.

CHAPTER 5

Effect of preloading time and pH on the adsorption of ionizable organic compounds with activated carbon

INTRODUCTION

Activated carbon adsorption is an effective technology for the removal of ionizable organic micropollutants from water. However, different background water constituents such as natural organic matter (NOM) hinder the adsorption process efficiency. NOM is ubiquitous in natural waters and is formed primarily from biodegradation of plant and animal matter. Typical constituents of NOM are fulvic and humic acids, which contain moieties such as carboxylic acid and phenolic groups. The presence of these functional groups causes NOM molecules to behave as polyelectrolytes in water, and their charge will depend on the solution pH.

NOM adversely affects the activated carbon adsorption of trace organic pollutants because it is usually present at concentrations in surface and ground waters that are 3-6 orders of magnitude higher than the targeted micropollutant. NOM can directly compete with the micropollutant for adsorption sites on the pore surface of the activated carbon and also block or constrict activated carbon pores, such that access to pore volume and surface area is restricted. The dominant mechanism by which NOM interferes with the adsorption of micropollutants depends on (1) the size and shape of the competing species and (2) the pore

size distribution (PSD) of the adsorbent. If pores are large enough for the NOM and micropollutant molecules to access the adsorption sites, the dominant mechanism is direct competition. However, if a significant fraction of the adsorbent pore volume is large enough to admit the micropollutant but not large enough to admit NOM molecules, then pore blockage is the dominant competition mechanism (Kilduff et al. 1998, Pelekani and Snoeyink 1999). Kilduff et al. (1998) in a study of the effects of NOM preloading on TCE adsorption found that at low levels of NOM preloading a loss in high-energy sites occurred, which caused a reduction in the site-energy heterogeneity and adsorption capacity in the low concentration region of the isotherm. Furthermore, they observed that higher NOM preloading levels produced a reduction in the average site energy and maximum adsorption capacity that shifted the whole isotherm to lower equilibrium solid phase concentrations. With respect to pore structure changes that occur as a result of NOM preloading in full-scale adsorbers, Moore et al. (2001) found that the greatest reduction in pore volume occurred in the size range of 5 to 30 Å and took place primarily during the first 30 days of operation. In contrast, the mesopore volume changed only slightly over a period of 1 year of operation.

Furthermore, preloading NOM can change the surface chemistry of activated carbons because NOM functional groups tend to be negatively charged at typical water treatment plants operating pHs. Newcombe (1994) conducted surface titrations of a virgin activated carbon and activated carbon with different levels of NOM loading. This study showed that all NOM-loaded activated carbons exhibited a higher negative surface charge than the virgin sample and the pH_{PZC} converged from a value of ~7.5 for the virgin activated carbon to a

value of 4.50 ± 0.25 for activated carbons with high NOM loadings. At typical water treatment plant operating pH values, the adsorbed NOM on the activated carbon surface will carry a negative charge that can interact through repulsive or attractive forces with ionic adsorbates, depending on the charge of the adsorbate.

While the effects of NOM preloading on the adsorption of neutral organic contaminants has been study extensively, studies are lacking that have systematically evaluated the effects of NOM preloading on the adsorption of ionizable organic contaminants. The principal objective of this study, therefore, was to determine the effects of NOM preloading on physical and chemical GAC characteristics and the adsorption of two ionizable organic contaminants, the antimicrobial compounds sulfamethoxazole (SMX), a weak organic acid, and trimethoprim (TMP), a weak organic base. An additional objective was to evaluate the effects of solution pH on SMX adsorption by fresh and preloaded activated carbons and to assess the importance of electrostatic interactions at different levels of SMX deprotonation.

MATERIALS AND METHODS

Adsorbates

Adsorption isotherm data were obtained for the ionizable antimicrobial compounds sulfamethoxazole (SMX) and trimethoprim (TMP). SMX and TMP (Sigma-Aldrich) purity

was >99%. Figure 1 illustrates the molecular structures of SMX and TMP and the functional groups where protonation or deprotonation occurs as solution pH changes. Table 1 summarizes some properties of both compounds. SMX is a weak organic acid with a pK_{a2} of ~5.6 and TMP is weak organic base with a pK_{b2} of ~7.0. Therefore, at typical water treatment plant pHs, SMX will be predominantly anionic while TMP will occur in both neutral and cationic forms.

Adsorbents

To examine how NOM preloading affects the adsorption of ionizable organic compounds, three GAC samples were taken from a pilot-scale GAC adsorber that was operated at the Zurich Water Works (WW Lengg, Switzerland). The three samples were collected after 3 days (F400 – 3), 32 days (F400 – 32) and 298 days (F400 – 298) of adsorber operation. GAC samples were collected from the filter bed surface (upper 5 cm), drained and stored in 200-ml screw-capped glass flasks at 4°C in darkness. The GAC adsorber was fed with ozonated Lake Zurich water (Q = 13.5 m^3/day, EBCT = 1.65 min, v_f = 8m/h, DOC = 0.96 mg/L). The 0.125 - 0.71 mm grain size fraction of Filtrasorb® 400 (Chemviron) was used. Furthermore, one GAC sample was collected from a full-scale GAC filter treating ozonated Lake Zurich water. The GAC in this filter was ROW 0.8 SUPRA (Norit), and the sample was collected after 20 years of operation (Norit – 20 years preloaded). In addition, fresh Filtrasorb® 400 (F400 - Fresh) and ROW 0.8 SUPRA (Norit – Fresh) samples were evaluated for comparison with the preloaded counterparts.

Adsorbent characterization

The characteristics that were measured for each adsorbent were (1) Brunauer, Emmett and Teller (BET) surface area, (2) micropore volume and pore size distribution, (3) mesopore volume, (4) point of zero charge (pH_{PZC}), (5) acid and base neutralization capacities, (6) elemental composition, and (7) ash content.

BET surface area and pore size distribution

BET surface areas were determined from N_2 adsorption isotherm data collected at 77 K (Autosorb-1-MP, Quantachrome Corporation, Boynton Beach, FL). Prior to analysis, adsorbent samples were outgassed for 24 hours at 423 K. Samples of 0.1 g were used to collect data in the relative pressure range of 0.01 to 0.1. A glass rod was used during the analysis to decrease the void volume of the sample holder.

Pore size distributions of carbonaceous adsorbents were determined by conducting N_2 adsorption experiments in two separate phases: (1) For the high pressure phase, N_2 adsorption isotherms were constructed from 86 data points in the relative pressure range of 0.0005 to 1 using a sample mass of 0.04 g of pulverized adsorbent; (2) for the low pressure phase, N_2 adsorption isotherms were constructed from 41 data points in the relative pressure range of 10^{-6} to 0.01 using a sample mass of 0.01 g of pulverized adsorbent. Adsorption isotherms from both high and low pressure phases were combined to produce one isotherm. The adsorbent sample mass used in the low pressure phase was adjusted such that the volume

adsorbed in the 0.0005 to 0.01 relative pressure range matched that obtained in the high pressure phase in the same relative pressure range.

Micropore volume, mesopore volume and pore size distribution were computed from N_2 adsorption isotherm data using the Density Functional Theory (DFT) with the N2_carb1.gai kernel (PC software version 1.51, Quantachrome, Boynton Beach, FL). In addition, the mesopore volume was computed using the Barrett, Joyner, and Halenda (BJH) method because this method captures the entire mesopore range (20 to 500 Å) while the DFT method is only able to calculate a mesopore volume for pores with widths in the range of 20 to 360 Å.

Elemental composition and ash content

Oxygen content was determined by Huffman Laboratories (Golden, CO) according to ASTM D5622. Ash content was determined following ASTM D 2866.

Mass titration

Mass titrations were performed to determine the pH_{PZC} of the adsorbents. The pH_{PZC} is the pH value at which a given adsorbent possesses a net surface charge of zero. In this study the method proposed by Noh and Schwarz (1989) was used to determine the pH_{PZC}. The method relies on the principle that the suspension pH reaches a constant value after addition of excess solid in the presence of an electrolyte.

Adsorbent masses in the range of 1 to 12% (w/w) were added to 30 mL 0.1 N sodium chloride (NaCl) solution, and the resulting pH values were measured after one week of equilibration time. Prior to use in pH_{PZC} determinations, adsorbents were washed with UPW until no pH change was observed. The NaCl solution was prepared with degassed ultrapure water (UPW), and the preparation of the samples and final pH measurements were performed under a nitrogen environment in a glove box.

Boehm titration

The total acid neutralization capacity, the concentrations of acidic surface functional groups, and the total base neutralization capacity of the adsorbent surface were determined by Boehm titrations (Boehm et al. 1964). This method consists of acid/base titrations of acidic or basic centers on the activated carbon surface. For these tests, 0.5 g of adsorbent was contacted with 30 mL of 0.1 N sodium bicarbonate ($NaHCO_3$), sodium carbonate (Na_2CO_3), sodium hydroxide (NaOH), and hydrochloric acid (HCl), and equilibrated for 3 weeks. After equilibration, the samples were centrifuged, and 10 mL of the supernatant were extracted and titrated with 0.05 N carbonate-free NaOH or HCl under nitrogen to measure the unreacted or unadsorbed acid or base remaining in solution. To calculate the number of surface acidic sites, it was assumed that $NaHCO_3$ neutralizes only strong carboxylic acid groups, Na_2CO_3 strong and weak carboxylic acid and lactonic groups, and NaOH strong and weak carboxylic, lactonic and phenolic groups. The number of basic surface sites was calculated from the amount of hydrochloric acid that reacted with the adsorbent.

Prior to Boehm titration experiments, adsorbents were washed with UPW until no pH change was observed. $NaHCO_3$ and Na_2CO_3 solutions were prepared with degassed UPW. The 0.05 N HCl and NaOH solutions were obtained from Ricca Chemical and Fisher Chemical, respectively.

Effects of NOM preloading on the adsorption capacity of ionizable organic contaminants

To evaluate the effects of preloaded NOM on ionizable organic contaminant removal, two fresh and four preloaded activated carbons were used. A portion of each preloaded adsorbent was used to quantify changes in physical and chemical characteristics (see adsorbent characterization for a list of parameters that were measured), while another portion was used for adsorption isotherm experiments. SMX and TMP adsorption isotherm experiments were conducted in UPW amended with 1mM phosphate buffer at pH 7.8 to mimic the pH of Lake Zürich (Switzerland) water. In addition, SMX adsorption isotherms were collected at pH 3.6 and 5.6 to measure the adsorbability of SMX at pH values at which the neutral form dominated in solution (pH 3.6) and at which both the neutral and anionic forms were present in equal proportions (pH = pK_a). For the SMX experiments at pH 7.8 mixing times of 6, 12, and 20 weeks were tested to determine that adsorption equilibrium was reached.

To quantify the amount of dissolved organic carbon (DOC) that desorbed from the preloaded activated carbon samples during the adsorption isotherm tests, samples were

filtered through a 0.45-μm membrane filters that were previously cleaned with UPW. Sample pH values were adjusted with HCl to pH 2-3 prior to analysis (Model TOC – 5000A, Shimadzu, Columbia, MD).

RESULTS AND DISCUSSION

Adsorbent characterization

Table 2 summarizes BET surface areas and the micropore and mesopore volumes of the studied activated carbon samples. As expected, BET surface area and micropore volume decreased as the NOM preloading time increased. After a preloading time of 298 days, remaining BET surface area and micropore volume were 73 and 76% of the corresponding values for fresh F400 GAC. After 20 years of operation, decreases in BET surface area and micropore volume were more pronounced, and the remaining BET surface area and micropore volume were only 34 and 25% of the corresponding values for fresh Norit GAC. Interestingly, the reduction in BJH mesopore volume of the Norit sample that had been preloaded for 20 years (5.8% reduction) was comparable to that of the F400 samples after 3 and 32 days of preloading (7.6 and 4.8% reduction, respectively). However, after 298 days of preloading, the F400 sample had lost 25.6% of the BJH mesopore volume measured for the fresh F400; i.e. the mesopore volume loss of the F400 GAC after ~10 months of operation was much higher than that of the Norit GAC after 20 years of operation. Moore et al. (2001)

showed that NOM preloading only slightly changed the mesopore volume of F400 GAC in filters operated with Ohio River water for a period of 1 year.

The change in micropore volume as a function of pore size and preloading time is illustrated in Figure 2. For the F400 series, there was a small decrease in micropore volume after 3 and 32 days of preloading and a considerable reduction for the sample collected after 298 days preloading. Figure 2 clearly shows that the Norit sample after 20 years of preloading had lost a substantial amount of micropores in the 5 to 20Å range, a result that is also reflected in the BET surface area data.

Table 3 summarizes the oxygen and ash contents and Table 4 the physical characteristics of the as-received and preloaded activated carbons. Table 3 shows a dramatic increase in oxygen content with preloading time. This result suggests an increase in surface acidity, which was corroborated with the acid/base results presented in Table 4. The total acid groups increased as preloading time increases. High oxygen content can increase the hydrophilicity of activated carbons. Generally, the higher the hydrophilicity of the activated carbons, the lower the adsorption capacity for both polar and non-polar organic contaminants. The higher oxygen content can be related in part to adsorbed NOM, which is rich in carboxylic acid and phenolic functional groups. Table 4 further shows that there was a substantial increase in weak carboxylic and phenolic groups in the preloaded activated carbons, while the strong carboxylic groups maintained fairly constant. The pH_{PZC} decreased to 6 as the NOM preloading time increased for the F400 series. This is in agreement with

Newcombe (1994), who found a continuous decrease in pH_{PZC} for an increase in NOM loading in the low NOM loading range. At higher loadings the pH_{PZC} stayed unchanged. Another interesting result presented in Table 4 is that basic groups increased for the two most preloaded activated carbon samples. One explanation for this result is that metals can precipitate over or adsorb on the surface of the activated carbon. For example, calcium carbonate ($CaCO_3$) and calcium oxide (CaO) can precipitate on the GAC surface, and the presence of carbonate and oxide salts is a probable reason for the increase in basic groups. However, neither NOM adsorption nor the accumulation of carbonate and oxide salts can explain the dramatic increase in oxygen content that took place in the pilot-scale GAC adsorber. One additional factor that led to an increase in the GAC oxygen content was the presence of residual ozone (~0.2 -0.3 mg/L) in the adsorber influent. Ozone readily reacts with GAC surfaces and adds oxygen-containing functional groups to the edges of activated carbon basal planes.

Experiments were also conducted to measure the amount of NOM that desorbed from the preloaded activated carbon samples when preloaded carbons were placed into UPW. Samples for DOC analysis were taken after a contact time of 6 weeks, after which time the non-purgeable organic carbon concentration was measured in the aqueous phase. Table 5 summarizes DOC concentrations for the different activated carbon samples and illustrates that DOC release increased as the preloading time increased. The samples taken from batch reactors containing fresh GAC and GAC that had been preloaded for 3 days exhibited DOC concentrations similar to that of the blank that contained only 100 µg/L SMX in solution. In

contrast, DOC release from the GAC sample that had been in service for 20 years approached 5 mg/g.

Effect of preloading time on activated carbon adsorption of ionizable organic compounds

Figure 3 depicts SMX adsorption isotherms for the fresh and preloaded activated carbons in UPW amended with 1 mM phosphate buffer at pH 7.8. Samples were collected after mixing times of 6 and 12 weeks. In experiments in which considerable concentration differences were observed for the 6 and 12 week mixing times, another sample was analyzed after a mixing time of 20 weeks. This was the case for the two most heavily preloaded activated carbons (F400-298 days preloaded and Norit-20 years preloaded) and suggests that these activated carbons needed a long equilibration time due to greater intra-particle diffusion limitations caused by NOM restricting the access to adsorption sites. Freundlich parameters showed considerable differences between data collected at 6, 12 and 20 weeks for these two preloaded activated carbons (Table 6); while the K-value increased, the 1/n value decreased. Table 6 further shows that for the F400 series, K-values decreased as preloading time increased. In addition, the 1/n-value increased considerably from the fresh F400 sample to the F400 sample that was preloaded for 3 days; however, for longer preloading periods, the 1/n value remained approximately constant. This result agrees with those of Kilduff et al. (1998), who found that low NOM loadings caused a decrease in TCE adsorption capacity in the low concentration region while higher NOM loadings caused the entire isotherm to shift

to lower equilibrium solid-phase concentrations. An increase in 1/n shows a loss of heterogeneity in adsorption site energies, which is manifested in a decrease of high-energy sites, where the adsorption of small organic pollutants is favored.

Figure 4 depicts the results of TMP adsorption isotherm data on fresh and preloaded activated carbons in UPW at pH 7.8. After a GAC service time of 3 days, the effect of preloading/GAC adsorber operation on the remaining TMP adsorption capacity was similar to that observed for SMX (~65% reduction compared to ~58% for SMX, considering F400-Fresh and F400-3 days preloaded results). However, little additional decrease in the TMP adsorption capacity was observed as the preloading time increased from 3 to 32 days and even to 298 days. It is possible that the continued oxidation of the activated carbon surface as a result of an ozone residual in the GAC influent created sufficient quantities of negatively charged functional groups that served as ion exchange sites for cationic TMP; however, additional experiments are required to substantiate this hypothesis. As was the case for SMX, the remaining TMP adsorption capacity of the Norit sample after 20 years of preloading was very low (Figure 4).

Effect of solution pH on adsorption of ionizable organic compounds

Figure 5a summarizes SMX adsorption isotherm data in UPW at solution pH values of 3.6, 5.8 and 7.8 for the fresh F400 sample and the F400 sample that was preloaded with NOM for a period of 32 days. To assess the importance of the pH-dependent aqueous SMX solubility (C_s^{pH}) on SMX adsorption, the SMX isotherm data in Figure 5a were normalized

by C_s^{pH} values obtained from model predictions (Figure 5b) and from the experimentally determined solubilities (Figure 5c). Similar isotherm results were obtained at pH 3.6 and 5.8. At pH 5.8, the fresh F400 activated carbon carried a net positive charge while approximately 61% of SMX was present in the anionic form. This result suggests, according to Müller et al. (1980 and 1985), that a maximum adsorption capacity should be obtained at a pH near the pK_a; however, an adsorption maximum was not observed here. Müller et al. (1980 and 1985) proposed that such a maximum only occurs if considerable ionization of the compound takes place while the carbon surface still carries a charge opposite to the ionized compound. At pH 7.8 the SMX adsorption capacity of the fresh activated carbon is considerably lower than at pH 3.6 and 5.8. Division of aqueous SMX concentrations by C_s^{pH} effectively normalized SMX adsorption isotherms at pH 3.6, 5.8, and 7.8. This result suggests that SMX adsorption was primarily controlled by non-specific dispersive interactions and that pH-related changes in SMX adsorbability are primarily related to changes in the pH-dependent aqueous solubility of SMX.

In contrast to the results for the fresh F400 activated carbon, results for the preloaded activated carbon showed that the SMX adsorption capacity at pH 6.0 was lower than that at pH 3.6 (Figure 5a). Also, compared to the pH 3.6 data, the reduction in SMX adsorption capacity measured at pH 7.8 was higher for the preloaded carbon than for the fresh carbon. For fresh F400, the reduction was ~50% at an equilibrium liquid-phase concentration of 1 µg/L while it was ~73% for the preloaded activated carbon. The data at pH 7.8 suggest that repulsive electrostatic interactions between the anionic form of SMX and the preloaded

activated carbon surface (pH_{PZC} = 5.76) may have affected the adsorption of SMX. However, division of the SMX equilibrium liquid-phase concentrations by the pH-dependent SMX solubility (C_s^{pH}) again effectively normalized the SMX adsorption isotherms at the three tested solution pH values (Figures 5b and 5c). As was the case for fresh GAC, it has to be argued that the pH-dependent SMX adsorption uptake on preloaded activated carbons was primarily related to changes in aqueous solubility while coulombic interactions played only a secondary role.

Finally, the Dubinin-Astakhov isotherm model was fitted to the normalized SMX adsorption isotherm data obtained at different solution pH values. R^2 values in Table 7 illustrate that the normalized isotherm data followed a similar trend at different solution pHs and could be effectively described by a unique set of D-A isotherm parameters. Table 7 also shows that the E values for the preloaded GAC are lower than those for the fresh GAC, a result that illustrates the loss of high-energy adsorption sites due to NOM preloading.

CONCLUSIONS

The principal objective of this study was to determine the effects of NOM preloading on physical and chemical GAC characteristics and the remaining adsorption capacities of the antimicrobial compounds sulfamethoxazole (SMX), a weak organic acid, and trimethoprim (TMP), a weak organic base. An additional objective was to evaluate the effects of solution

pH on SMX adsorption by fresh and preloaded activated carbons and to assess the importance of electrostatic interactions at different levels of SMX deprotonation.

NOM preloading decreased BET surface area and micropore volume of the tested activated carbons. Approximately 75% of the initial BET surface area and micropore volume remained after 10 months of service (F400 GAC) while approximately 30% remained after 20 years of service (Norit GAC). Increasing GAC service time also altered the surface chemistry of the activated carbons. An ozone residual concentration that was present in the GAC adsorber influent, from which preloaded GAC samples were obtained, as well as NOM adsorption contributed to an increase in GAC oxygen content, a decrease in the pH_{PZC}, and an increase in acidic functional groups on the GAC surface. Changes in GAC surface chemistry were most dramatic during the first month the GAC was in service.

At pH 7.8, SMX adsorption capacities of F400 GAC decreased with increasing preloading time while TMP adsorption capacities was relatively constant at preloading times of 3, 32, and 298 days. It is possible that the continued oxidation of the activated carbon surface as a result of an ozone residual in the GAC influent created sufficient quantities of negatively charged functional groups that served as ion exchange sites for cationic TMP; however, additional experiments are required to substantiate this hypothesis. For the GAC sample that had been in service for 20 years, remaining adsorption capacities for both SMX and TMP were very low.

Regarding the pH-dependent adsorption of SMX on fresh and preloaded GAC, results obtained at pH 7.8 suggest that repulsive coulombic interactions negatively affected SMX adsorption on the preloaded GAC. Nonetheless, when equilibrium liquid-phase SMX concentrations were divided by the pH-dependent solubility of SMX, SMX adsorption isotherm data at pH 3.6, 5.8-6.0, and 7.8 were effectively normalized. Therefore, the pH-dependent aqueous solubility of SMX appeared to be the most important variable affecting the pH-dependent adsorption uptake of SMX on both fresh and preloaded GACs over the studied pH range.

REFERENCES

Boehm, H.P.; Diehl, E.; Heck, W.; and R. Sappok. Surface Oxides of Carbon. Angew. Chem. Internat. Edit. 1964; 3:669-677.

Cannon, F.S.; Knappe, D.R.U.; Snoeyink, V.L.; Lee, R.G.; DeWolfe, J.R.; and G. Dagois. The effect of metals on thermal regeneration of granular avtivated carbon. AWWARF, Denver, Colorado, 1994.

Kilduff, J.E.; Karanfil, T.; and W.J. Weber Jr. 1998. "Competittive effects of nondisplaceable organic compounds on trichloroethylene uptake by activated carbon. I. Thermodynamic predictions and model sensitivity analyses." *Journal of Colloid and Interface Science* 205: 271-279.

Kilduff, J.E.; Srivastava, R.; and T. Karanfil. 2002. "Preloading of GAC by natural organic matter: effect of surface chemistry on TCE uptake." *Studies in Surface Science and Catalysis* 144: 553-560.

Moore, B.C.; Cannon, F.S.; Westrick, J.A.; Metz, D.H.; Shrive, C.A; DeMarco, J.; and D.J. Hartman. 2001. “Changes in GAC pore structure during full-scale water treatment at Cincinnati: a comparison between virgin and thermally reactivated GAC.” Carbon 39: 789–807.

Müller, G.; Radke, C.J.; and J.M. Prausnitz. 1980. “Adsorption of weak organic electrolytes from aqueous solution on activated carbon. Effect of pH.” *The Journal of Physical Chemistry* 84: 369-376.

Müller, G.; Radke, C.J.; and J.M. Prausnitz. 1985. “Adsorption of weak organic electrolytes from dilute aqueous solution onto activated carbon. Part 1. Single-solute systems.” *Journal of Colloid and Interface Science* 103(2): 466-483.

Newcombe, G. 1994. “Activated carbon and soluble humic substances: Adsorption, desorption, and surface charge effects.” *Journal of Colloid and Interface Science* 164: 452-462.

Noh, J.S.; and J.A. Schwarz. 1989. “Estimation of the point of zero charge of simple oxides by mass titration.” *Journal of Colloid and Interface Science* 130(1): 157-164.

Pelekani, C.; and V.L. Snoeyink. 1999. “Competitive adsorption in natural water: role of activated carbon pore size.” *Water Research* 33(5): 1209-1219.

Table 1. Properties of SMX and TMP

	SMX	**TMP**
CAS #	723-46-6	738-70-5
Molecular Weight (g/mol)	253.3	290.3
Solubility in Water (neutral form)	610 mg/L (at 37°C)	400 mg/L (at 25°C)
Log K_{OW} (neutral form)	0.89	0.91
pK_a (+/0) = moiety goes from cationic to neutral form; (0/-) = moiety goes from neutral to anionic form	(1) 1.6-1.85 (+/0) (2) 5.57-5.7 (0/-)	(1) 6.6-7.34 (+/0)

Table 2. Physical characteristics of fresh and preloaded activated carbons

Adsorbent	NOM exposure (d)	BET Surface Area (m^2/g)	Micropore Volume[a] (cm^3/g)	DFT Mesopore Volume[b] (cm^3/g)	BJH Mesopore Volume[c] (cm^3/g)
F400-Fresh	--	1084	$3.70x10^{-1}$	$2.68x10^{-1}$	$2.89x10^{-1}$
F400-3 days preloaded	3	1088	$3.59x10^{-1}$	$2.44x10^{-1}$	$2.67x10^{-1}$
F400–32 days preloaded	32	994	$3.37x10^{-1}$	$2.48x10^{-1}$	$2.75x10^{-1}$
F400–298 days preloaded	298	792	$2.82x10^{-1}$	$1.90x10^{-1}$	$2.15x10^{-1}$
Norit-Fresh	--	946	$3.31x10^{-1}$	$2.46x10^{-1}$	$2.57x10^{-1}$
Norit-20 years preloaded	~7300	318	$8.42x10^{-2}$	$2.28x10^{-1}$	$2.42x10^{-1}$

[a] Micropore volume calculated by density functional theory (DFT) for pores with widths less than 20 Å

[b] Mesopore volume calculated by density functional theory (DFT) for pores with widths ranging from 20 to 360 Å (upper limit for DFT model)

[c] Mesopore volume calculated by Barrett, Joyner, and Halenda (BJH) method for pores with widths ranging from 20 to 500 Å

Table 3. Chemical characteristics of fresh and preloaded activated carbons

Adsorbent	%O	%Ash
F400-Fresh	5.31	10.2
F400-3 days preloaded	7.28	10.7
F400–32 days preloaded	9.87	11.4
F400-298 days preloaded	10.95	11.2
Norit-Fresh	7.64	6.43
Norit-20 years preloaded	22.84	15.6

Table 4. Acid/base characteristics of fresh and preloaded activated carbons

Adsorbent	Total basic groups (meq/100g)	Total acidic groups (meq/100g)	Strong carboxylic groups (meq/100g)	Weak carboxylic groups (meq/100g)	Phenolic groups (meq/100g)	pH_{PZC}
F400-Fresh	61.4	45.9	6.9	18.4	19.4	7.95
F400-3 days preloaded	57.6	56.2	1.6	22.9	31.7	6.28
F400–32 days preloaded	62.9	79.9	2.9	39.2	37.8	5.76
F400–298 days preloaded	71.8	88.9	1.3	50.5	37.1	6.03
Norit-Fresh	111.7	64.1	0	22.9	41.2	8.50
Norit-20 years preloaded	263.9	123.6	2.7	87.2	33.7	7.18

Table 5. Release of DOC from preloaded activated carbons

Carbon sample	Carbon dose (mg/L)	DOC (mg/L)	Dose-normalized DOC release (mg DOC/g activated carbon)
Blank 100 µg/L SMX	---	0.20	---
F400-Fresh	20	0.21	0.5
Norit-Fresh	20	0.22	1.0
F400-3 days preloaded	90	0.23	0.3
F400-32 days preloaded	350	1.24	3.0
F400-298 days preloaded	560	2.47	4.1
Norit-20 years preloaded	560	2.82	4.7

Table 6. Freundlich isotherm parameters describing the adsorption of SMX in UPW at pH 7.8 on fresh and preloaded activated carbons

Adsorbent	Equilibration Time (weeks)	Freundlich parameters	
		K $(mg/g)(L/\mu g)^{1/n}$	1/n
F400-Fresh	6	29.4	0.234
F400-Fresh	12	27.5	0.260
F400-3 days preloaded	6-12	11.4	0.408
F400-32 days preloaded	6-12	4.67	0.484
F400-298 days preloaded	6	1.24	0.508
F400-298 days preloaded	12	2.14	0.540
F400-298 days preloaded	20	3.05	0.487
Norit-Fresh	6	22.5	0.217
Norit-Fresh	12	20.7	0.270
Norit-20 years preloaded	6	0.064	0.544
Norit-20 years preloaded	12	0.103	0.496
Norit-20 years preloaded	20	0.123	0.482

Table 7. Dubinin-Astakhov isotherm parameters for normalized SMX adsorption isotherms on fresh and NOM-preloaded GAC

Adsorbent	C_s determination	Dubinin-Astakhov isotherm parameters			
		q_m (mg/g)[&]	E (kJ/mol)[%]	n[%]	R^2
F400-Fresh	Model	541	21.1±0.5	1.66±0.13	0.97
	Experiment	541	19.6±0.7	1.47±0.15	0.96
F400-32 days preloaded	Model	493	13.0±1.2	1.34±0.11	0.96
	Experiment	493	12.1±2.5	1.24±0.22	0.86

[&] Calculated from $q_m=V_m \cdot \rho$, where V_m is the micropore volume of the adsorbent estimated from N_2 adsorption data (Table 2) and ρ is the liquid density of SMX at 20ºC as estimated from ChemSketch (1.462 g/cm^3)

[%] interval represents the 95% confidence interval of the parameter

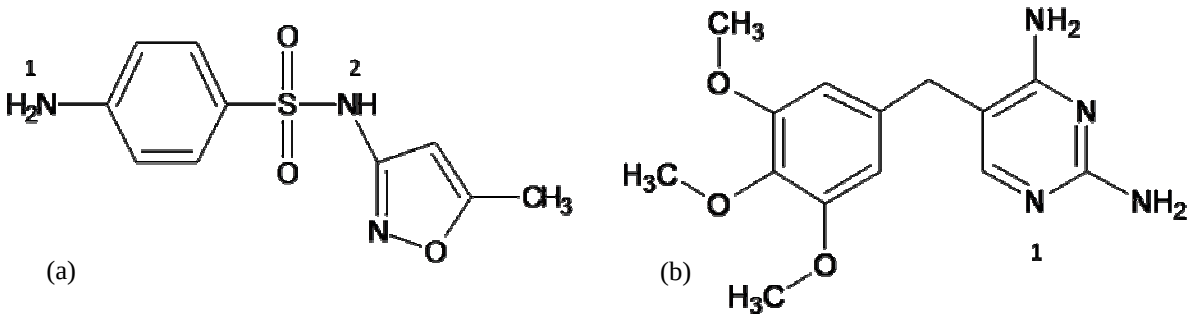

Figure 1. Molecular structures of (a) sulfamethoxazole and (b) trimethoprim. Labels 1 and 2 adjacent to functional groups refer to protonation/deprotonation sites.

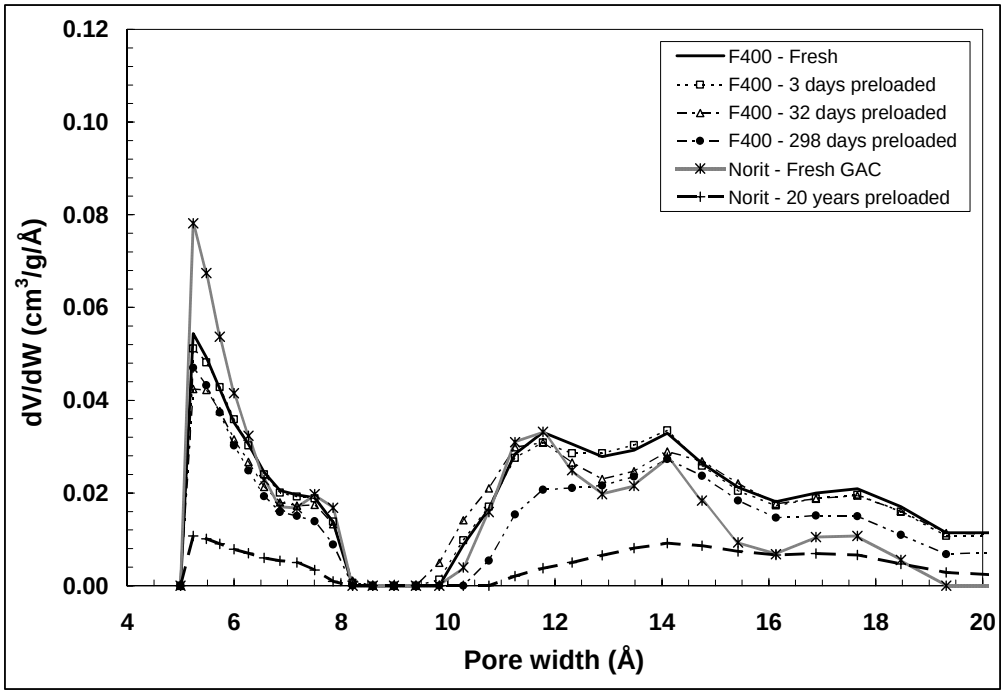

Figure 2. Micropore size distribution of fresh and preloaded activated carbons (y-axis represents differential pore volume [V] in cm^3/g adsorbent per unit pore width [W] in Å).

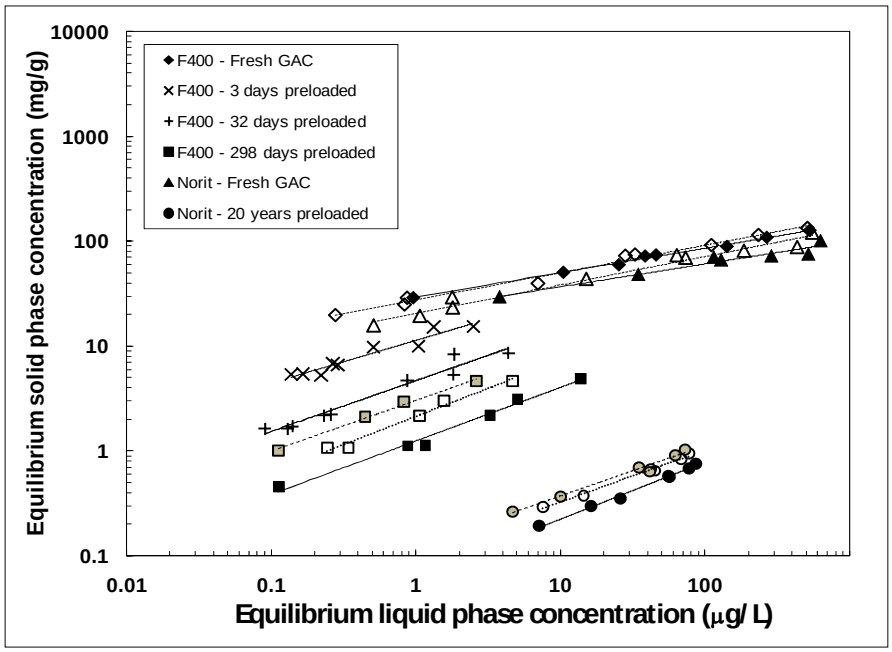

Figure 3. SMX adsorption isotherms on fresh and preloaded GACs in UPW at pH 7.8 and different mixing times. Data with closed symbols - 6 weeks, data with open symbols - 12 weeks, and data with gray filled symbols - 20 weeks. Lines represent Freundlich isotherm fits.

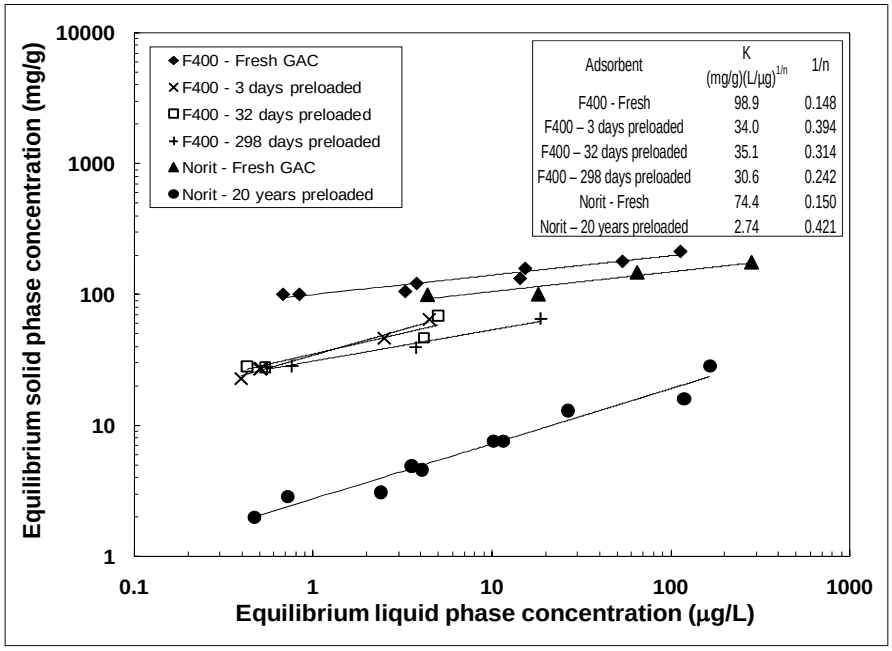

Figure 4. TMP adsorption isotherms on fresh and preloaded GACs in UPW at pH 7.8. Lines represent Freundlich isotherm fits.

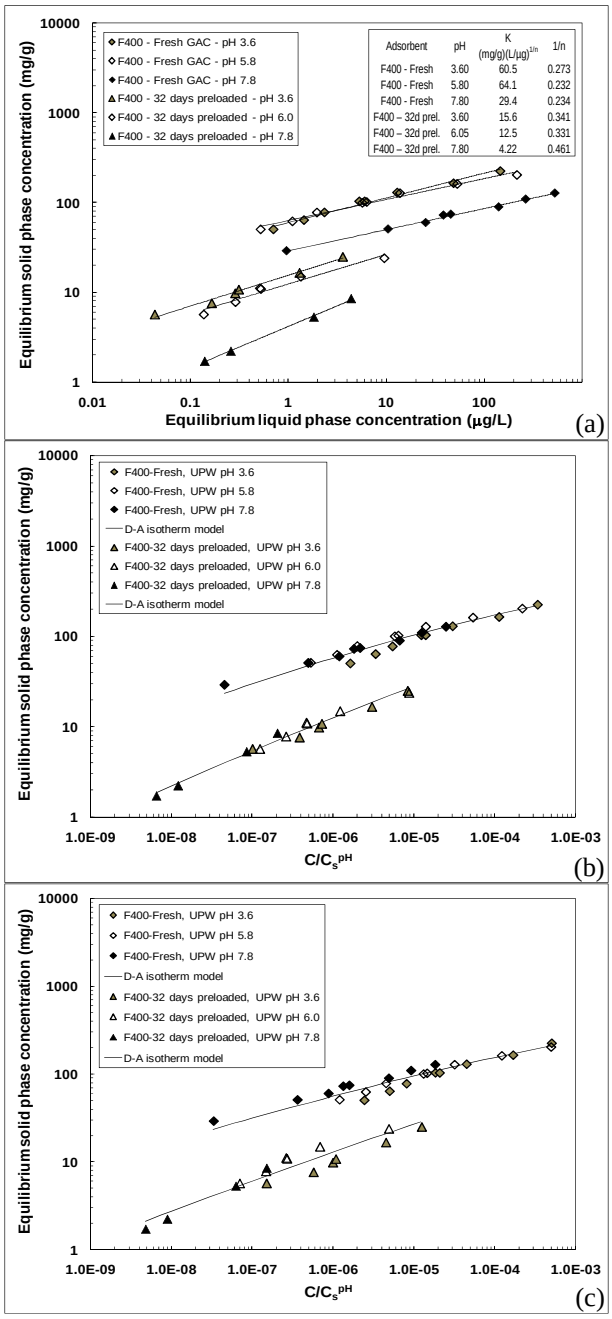

Figure 5. SMX adsorption isotherms on fresh F400 GAC and F400 GAC after 32 days of preloading in UPW at different solution pHs. (a) plotted against the equilibrium liquid phase concentration (table shows Freundlich isotherm parameters), (b) UPW data following normalization with theoretical C_s^{pH} values predicted with ACD/Labs software, and (c) UPW data following normalization with experimental C_s^{pH} values. Lines in panels (b) and (c) represent Dubinin-Astakhov isotherm model fits.

CHAPTER 6

CONCLUSIONS AND RECOMMENDATIONS

The overall objective of this research was to evaluate the effectiveness of alternative adsorbents for the removal of POCs from drinking water and to identify activated carbon, contaminant, and background water characteristics that affect the pH-dependent adsorption uptake of ionizable organic contaminants.

In the first phase of this research, the MTBE removal effectiveness of a silicalite zeolite and a carbonaceous resin was compared to that of a coconut-shell-based GAC. Adsorption isotherm and short bed adsorber tests were completed in UPW and river water to determine equilibrium and kinetic parameters describing the adsorption of MTBE. The results showed that for the silicalite, co-adsorbing NOM had a small effect on the MTBE adsorption uptake but a more pronounced effect on MTBE adsorption kinetics. For the GAC, co-adsorbing NOM had a more pronounced effect on MTBE adsorption uptake but a smaller effect on MTBE adsorption kinetics. The costs associated with silicalite usage were approximately double those associated with GAC usage; however, the useful life of a silicalite adsorber was predicted to be more than 4 times larger than that of a GAC adsorber with the same dimensions. Overall, the results of this study showed that silicalite is an alternative adsorbent that should be considered for full-scale applications that specifically target MTBE removal.

In the second phase of this research, the removal of an emerging contaminant mixture from lake water was compared for two high-silica zeolites (Mordenite and Y), a carbonaceous resin, and a coconut shell-based activated carbon. Isotherm data showed that activated carbon would provide the most effective barrier for the removal of antimicrobial compounds, endocrine disrupting chemicals (EDCs) and other pharmaceuticals from water. The greater effectiveness of activated carbon relative to the carbonaceous resin and the high-silica zeolites was primarily related to its larger micropore volume in the 6-9 Å size range; i.e., in the size range that bracketed the molecular diameters of the compounds in the emerging contaminant mixture.

In the third phase of this research, the effects of adsorbent and solution characteristics on the adsorption of the antimicrobial compounds SMX and TMP were evaluated. SMX is a weak organic acid with a pK_a of 5.6 while TMP is a weak organic base with a pK_b of ~7.0. Among the five studied carbonaceous adsorbents, the coconut shell-based activated carbon AC1230C was the most effective for TMP and SMX removal from UPW, TRW, and LMW, and this result was again attributed to the fact that AC1230C exhibited the largest pore volume in a size range that corresponded to the molecular diameters of SMX and TMP (~7-9 Å). To determine the extent to which pH-dependent adsorption isotherm data of SMX and TMP were controlled by their pH-dependent aqueous solubilities, equilibrium liquid phase concentrations of SMX and TMP were normalized by (1) model-predicted C_s^{pH} values and (2) experimentally determined C_s^{pH} values. TMP isotherm data normalized by model-predicted C_s^{pH} values showed that the normalization procedure accounts for the pH-

dependency of the adsorption uptake by the tested activated carbons and suggests that Coulombic interactions did not play an important role in the adsorption of TMP at pH values at which the cationic form prevailed in solution. However, the TMP isotherm data at pH 3.6 for the three basic activated carbons shifted to lower equilibrium solid-phase concentrations when the experimental data were normalized by the experimentally determined C_s^{pH} values. This result suggests that electrostatic interactions between the positively charged surface of the basic activated carbons and the TMP cation did affect the adsorption of TMP cations. SMX adsorption isotherm data were effectively normalized by C_s^{pH} in the pH range of 3.6 to 7.6; at pH 10, however, normalized isotherms were shifted towards lower equilibrium solid-phase concentrations and did not follow the trend established at lower pH values. This shift was likely the result of repulsive electrostatic interactions between negatively charged activated carbon surfaces and SMX anions.

In the final phase of this research the effect of NOM preloading time on the adsorption of SMX and TMP was studied. It was observed that the adsorbed NOM molecules increased intra-particle diffusion limitations that required equilibration times of up to 20 weeks for the more heavily preloaded GACs. To evaluate the effects of solution pH on the adsorption capacity of SMX and TMP on preloaded GAC, the equilibrium liquid phase concentration of SMX was normalized by (1) model-predicted C_s^{pH} values and (2) experimentally determined C_s^{pH} values. Results showed that for the pH range studied, the pH-dependent solubility of SMX was the most important variable affecting the adsorption process on both fresh and preloaded GAC.

Recommendations for future work

- Regeneration of activated carbon employed in drinking water treatment applications requires energy-intensive thermal methods to oxidize NOM that adsorbs inside of the activated carbon pores. The results of this research showed that NOM adsorption on silicalite was negligible. Therefore, NOM removal from silicalite pores is not required during regeneration, and less energy-intensive regeneration methods such steam or microwave regeneration may suffice to recover the MTBE adsorption capacity of spent silicalite.

- To more clearly establish the importance of electrostatic interactions on the adsorption of ionic organic compounds, surface titrations should be conducted with activated carbons. Knowledge of how the activated carbon surface charge changes with solution pH provides an important basis for future models that incorporate electrostatic interactions. Also, the ion exchange capacity of activated carbons should be determined.

- Develop a mathematical model that permits the prediction of the pH-dependent adsorption uptake of ionizable organic contaminants.

APPENDICES

APPENDIX A. Supplementary information for Chapter 4.

Normalization of literature isotherm data

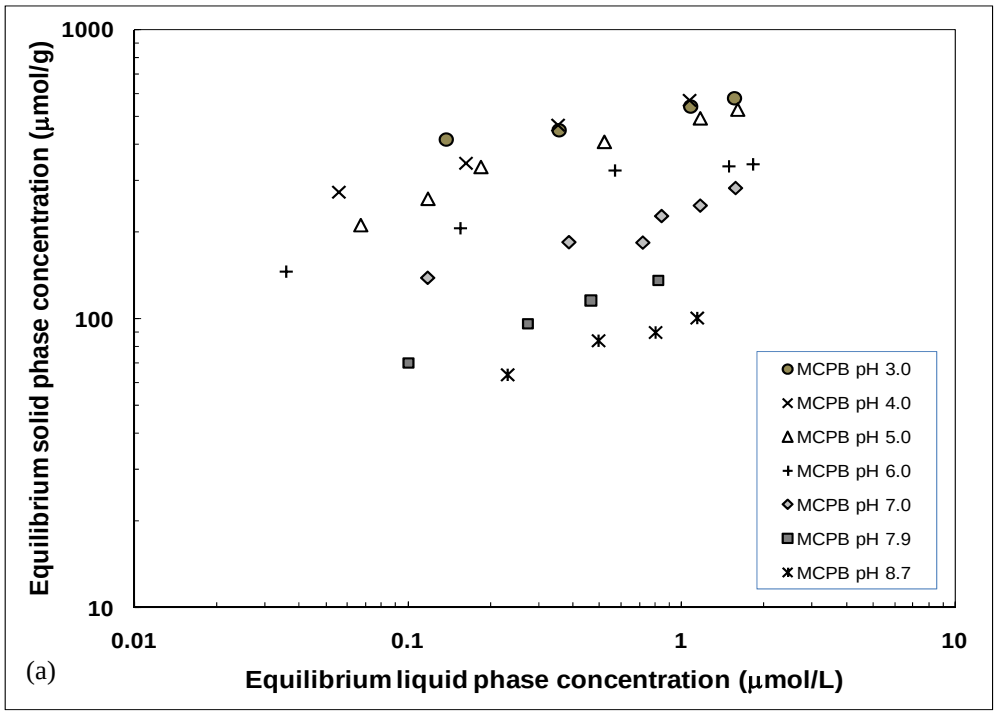

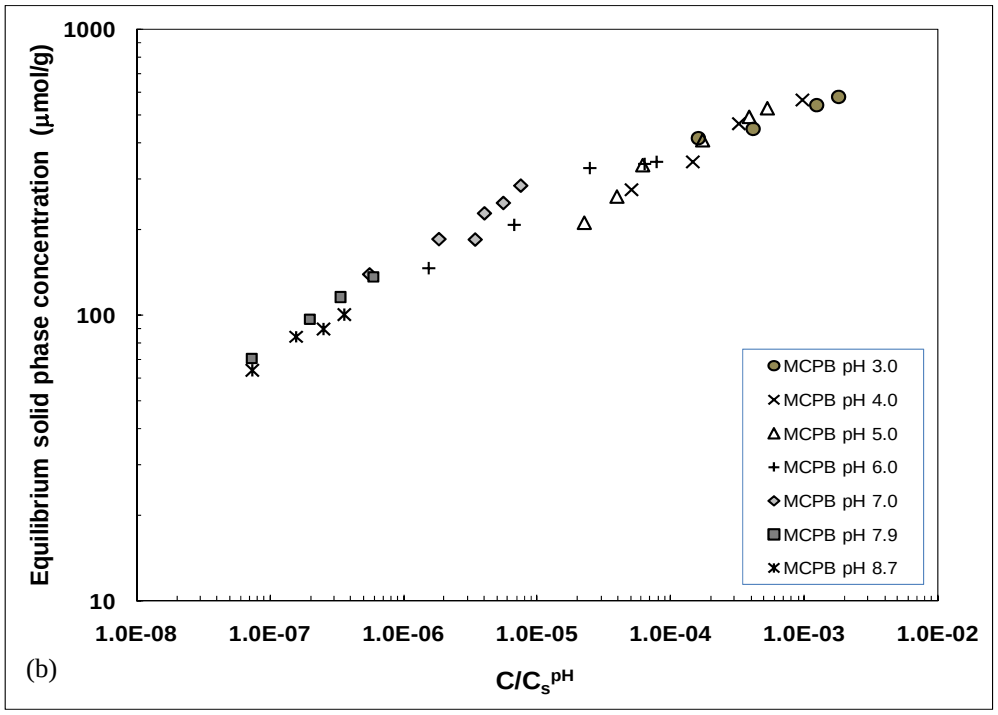

Figure 1. Adsorption isotherm data of MCPB at different solution pHs; (a) as originally presented by Hu et al. (1998), and (b) following normalization with C_s^{pH}.

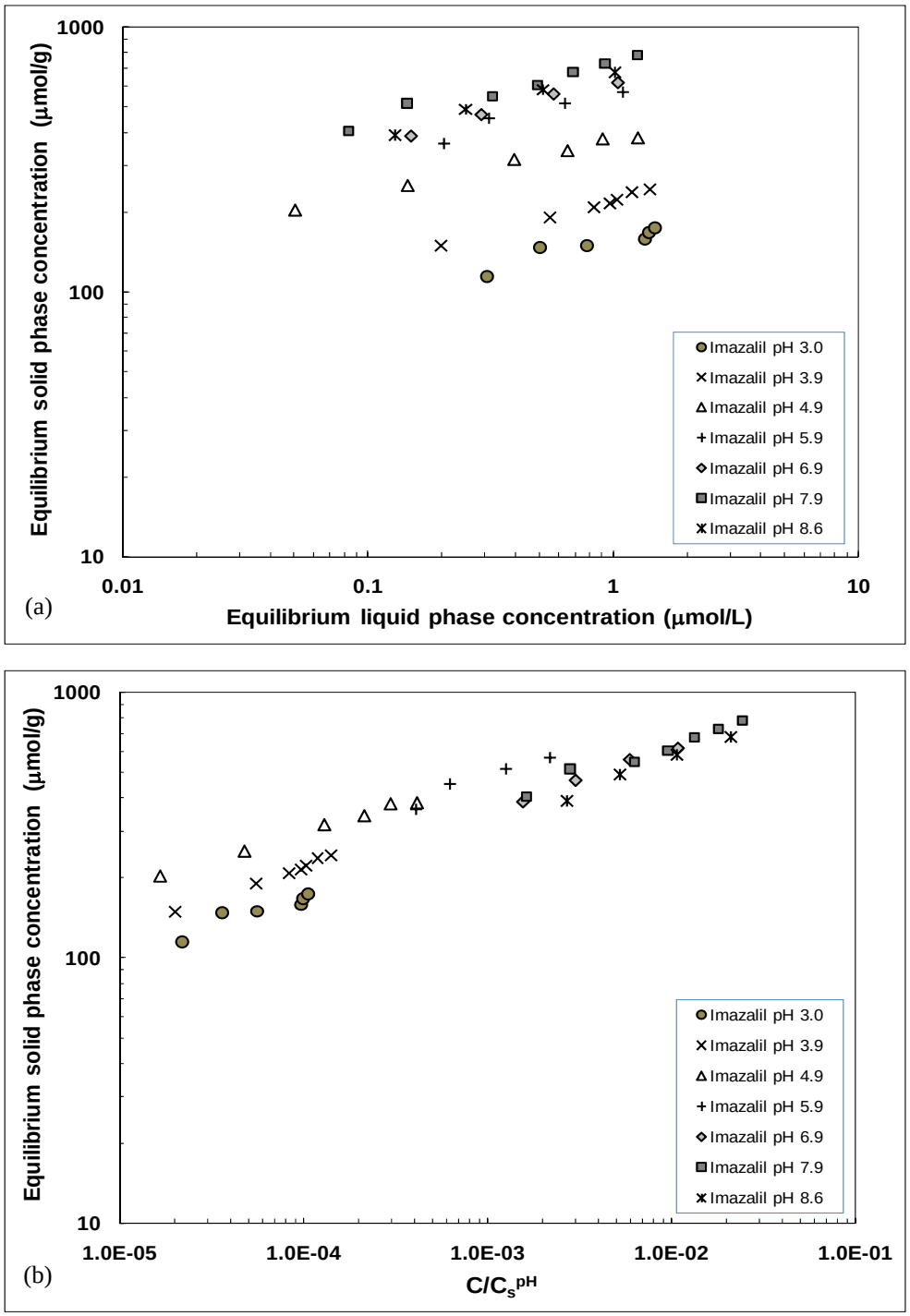

Figure 2. Adsorption isotherm data of imazalil at different solution pHs; (a) as originally presented by Hu et al. (1998), and (b) following normalization with C_s^{pH}.

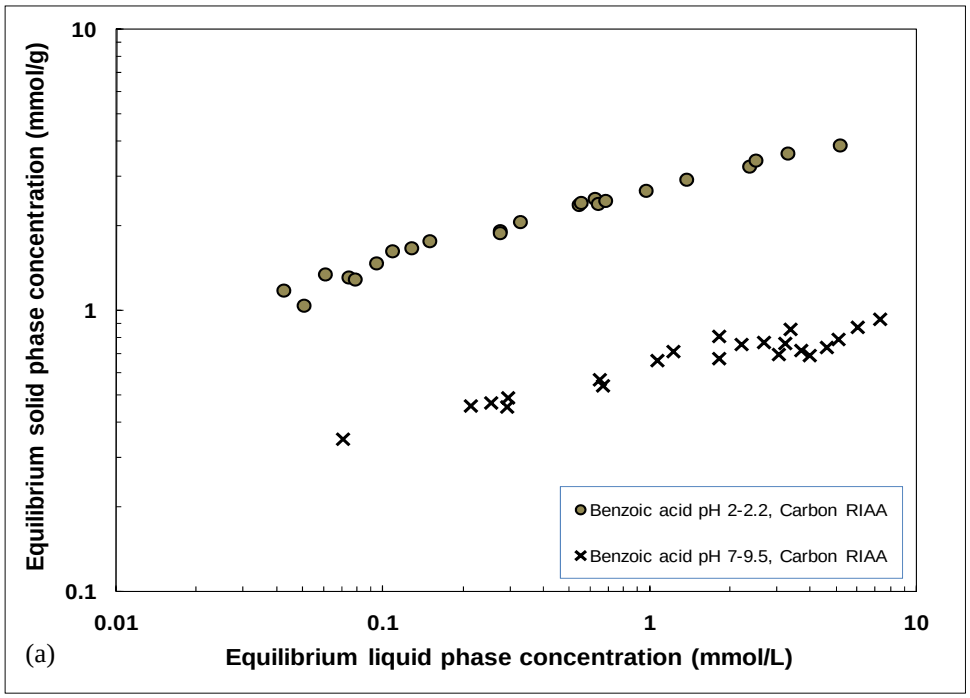

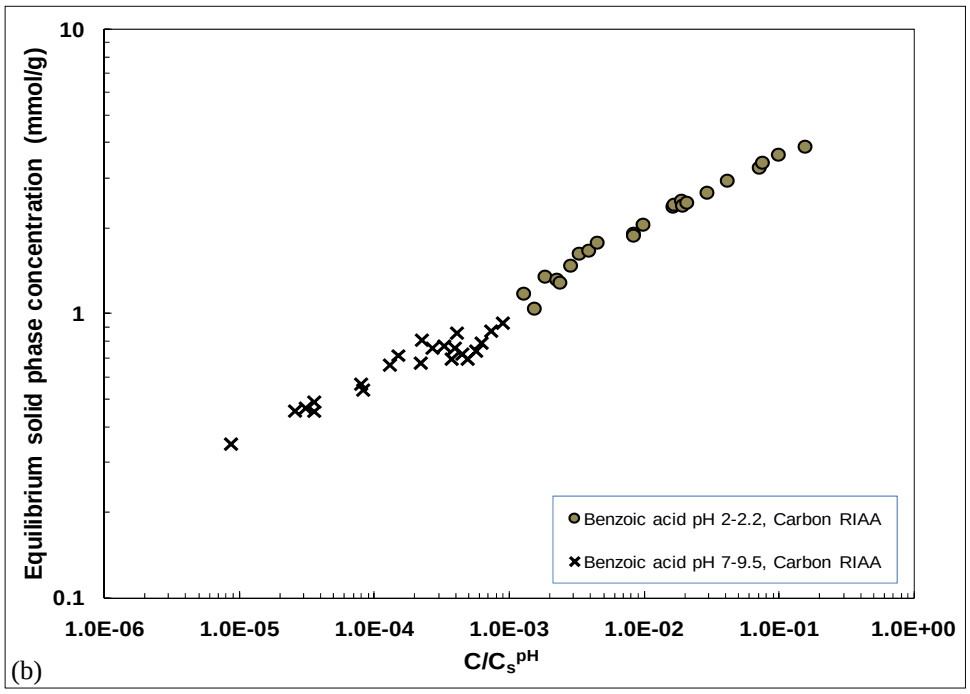

Figure 3. Adsorption isotherm data of benzoic acid at different solution pHs on activated carbon RIAA; (a) as originally presented by Derylo-Marczewska and Marczewski (1999), and (b) following normalization with C_s^{pH}.

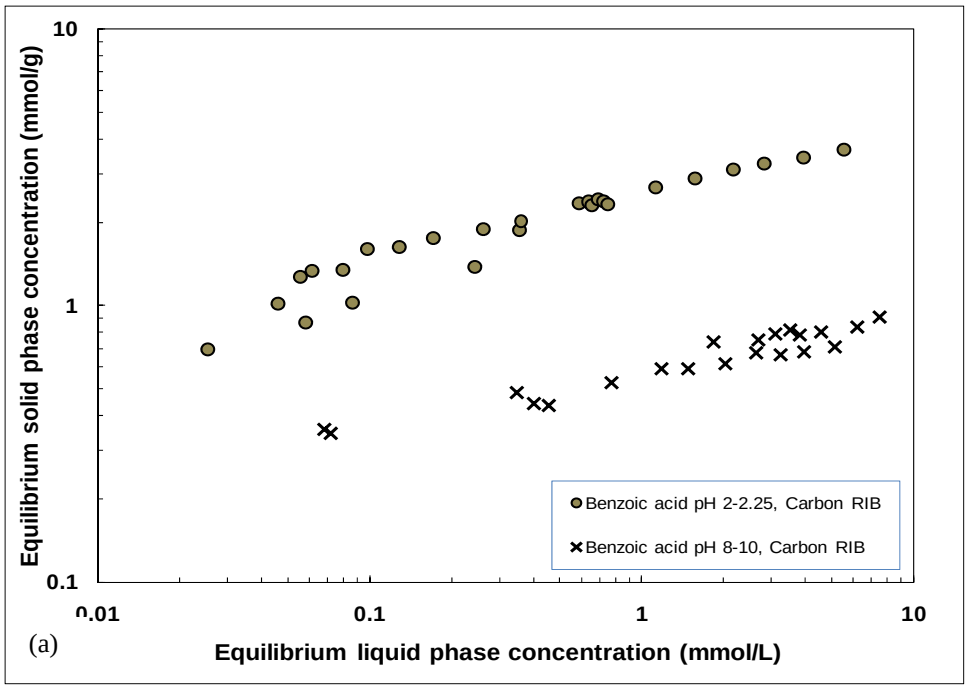

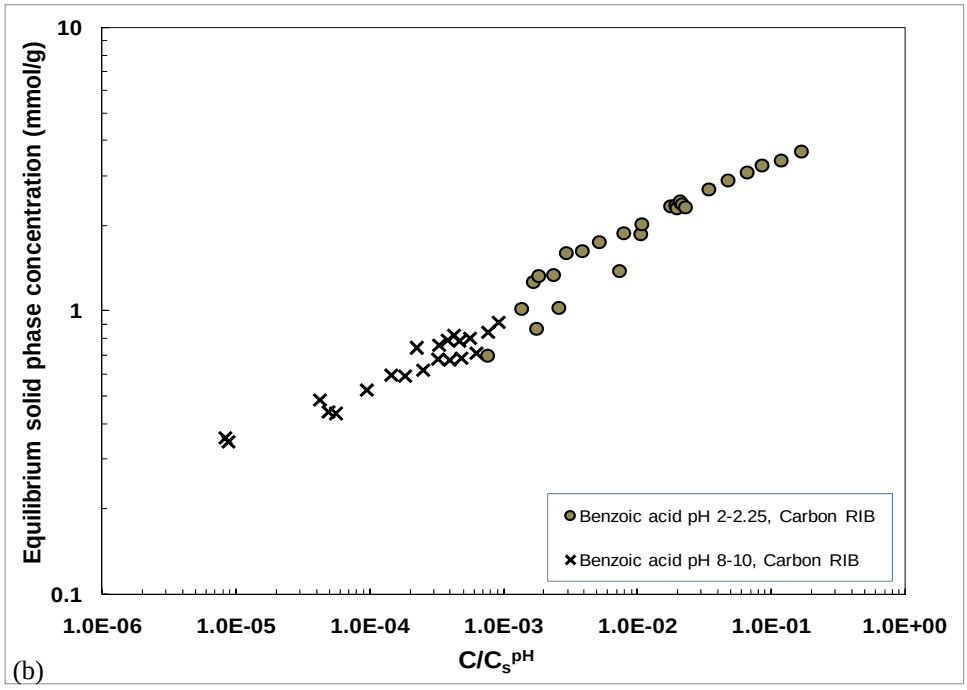

Figure 4. Adsorption isotherm data of benzoic acid at different solution pHs on activated carbon RIB; (a) as originally presented by Derylo-Marczewska and Marczewski (1999), and (b) following normalization with C_s^{pH}.

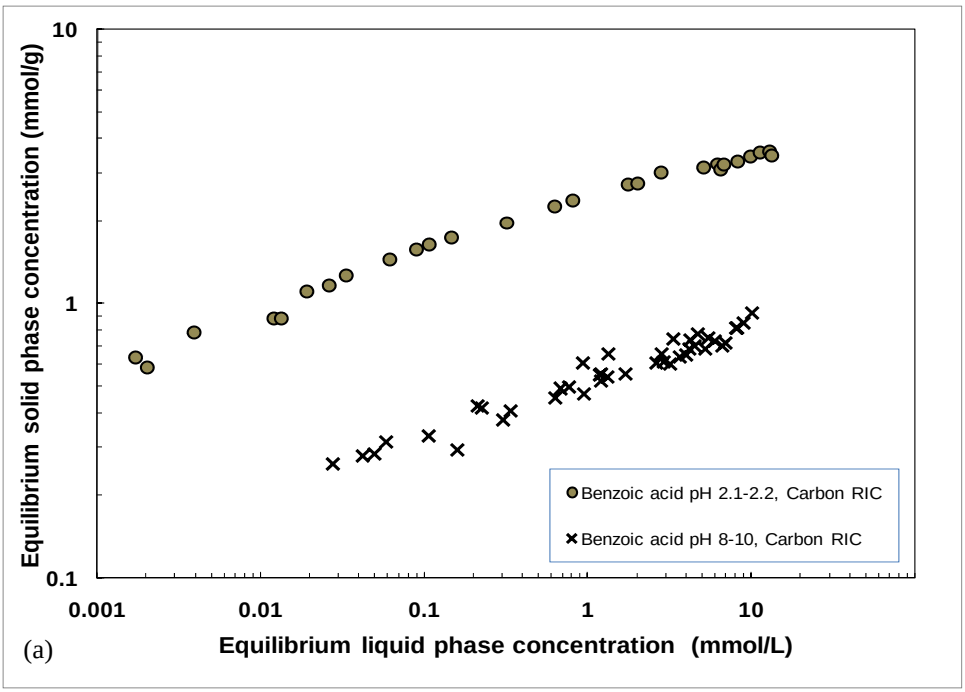

(a)

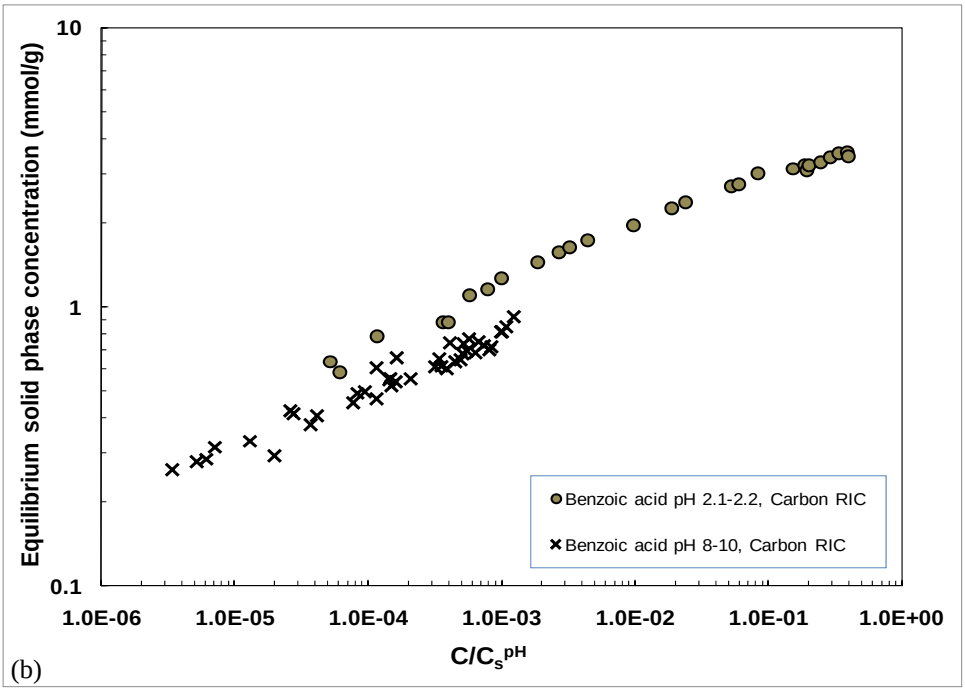

(b)

Figure 5. Adsorption isotherm data of benzoic acid at different solution pHs on activated carbon RIC; (a) as originally presented by Derylo-Marczewska and Marczewski (1999), and (b) following normalization with C_s^{pH}.

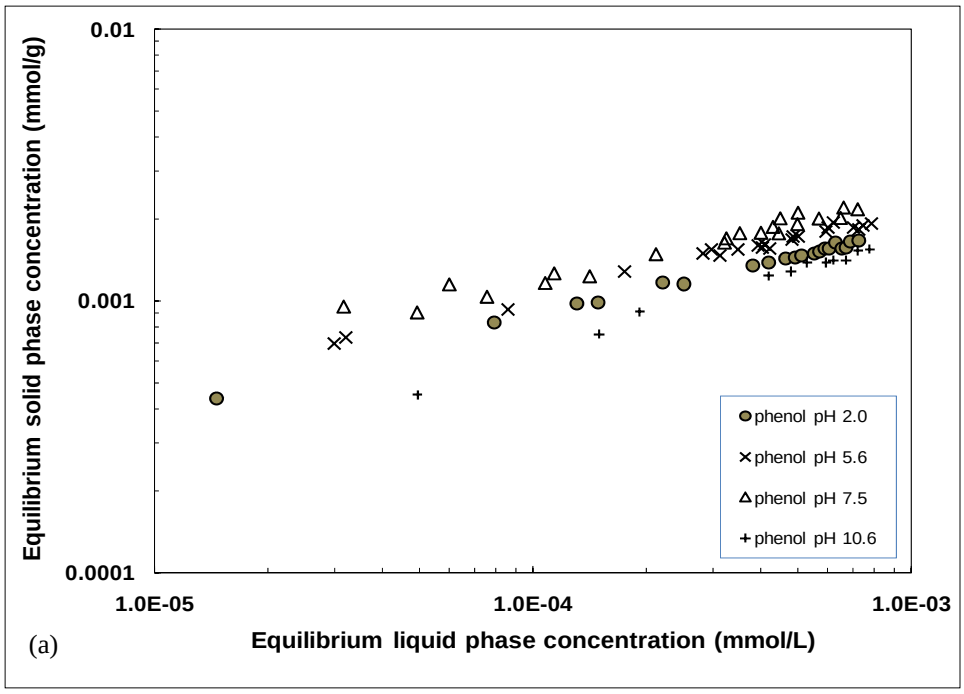

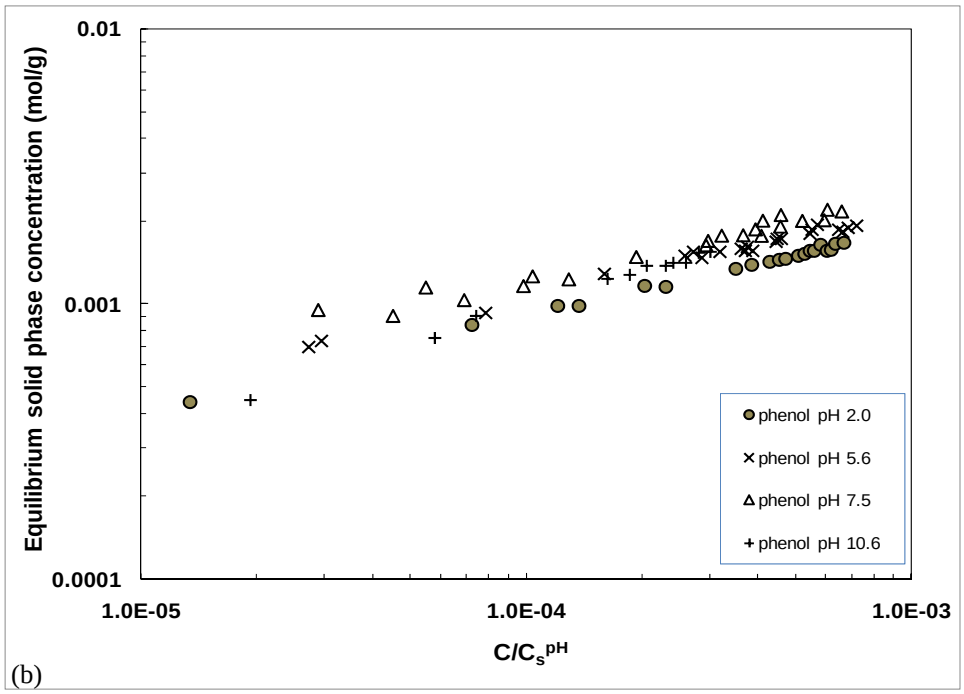

Figure 6. Adsorption isotherm data of phenol at different solution pHs; (a) as originally presented by Snoeyink et al. (1969), and (b) following normalization with C_s^{pH}.

APPENDIX B. Supplementary information for Chapter 4.

SMX and TMP adsorption isotherm at different pHs and normalization procedure with pH-dependent solubility

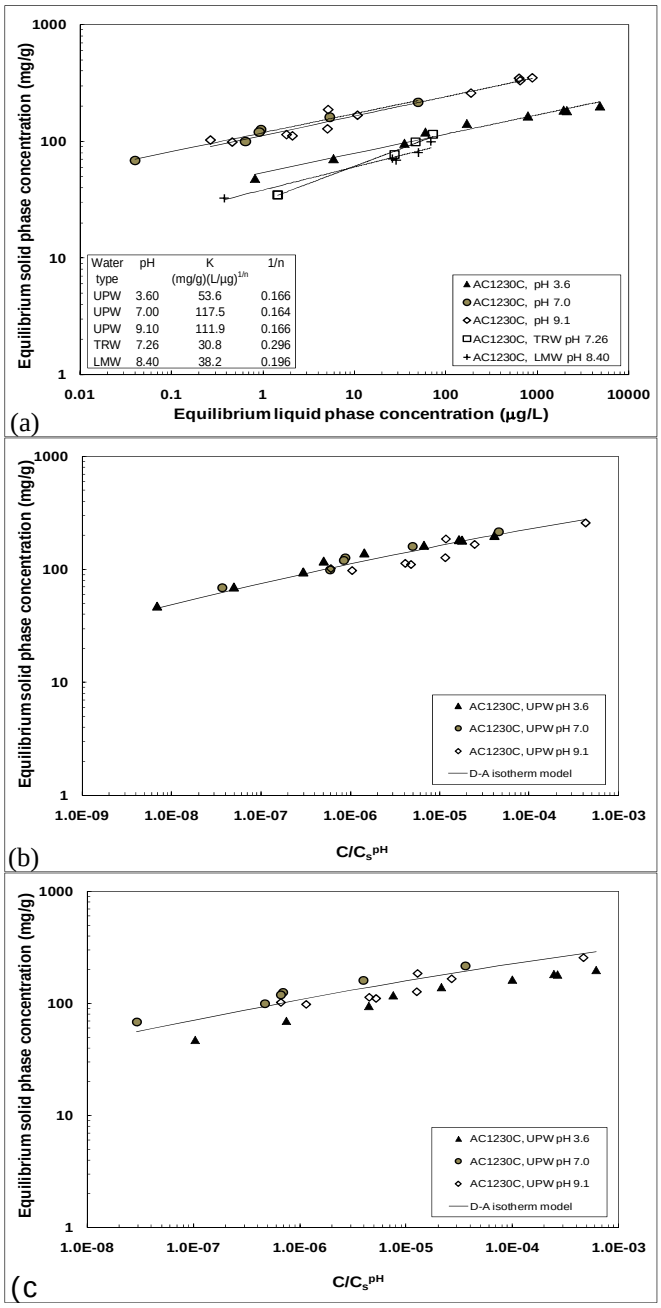

Figure 1. TMP adsorption isotherms on coconut shell-based activated carbon AC1230C in UPW at different solution pHs, TRW, and LMW; (a) plotted against the equilibrium liquid phase concentration (table shows Freundlich isotherm parameters), (b) UPW data following normalization with theoretical C_s^{pH} values predicted with ACD/Labs software, and (c) UPW data following normalization with experimental C_s^{pH} values. Lines in panels (b) and (c) represent Dubinin-Astakhov isotherm model fits.

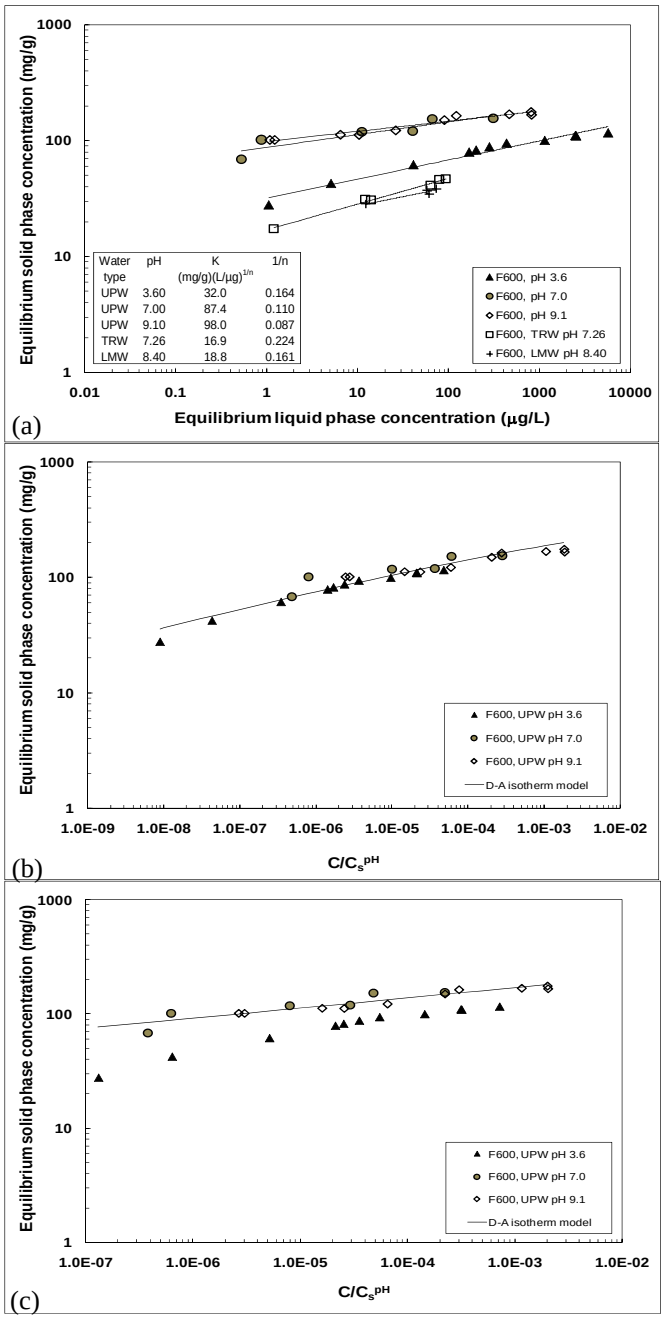

Figure 2. TMP adsorption isotherms on coal-based activated carbon F600 in UPW at different solution pHs, TRW, and LMW; (a) plotted against the equilibrium liquid phase concentration (table shows Freundlich isotherm parameters), (b) UPW data following normalization with theoretical C_s^{pH} values predicted with ACD/Labs software, and (c) UPW data following normalization with experimental C_s^{pH} values. Lines in panels (b) and (c) represent Dubinin-Astakhov isotherm model fits.

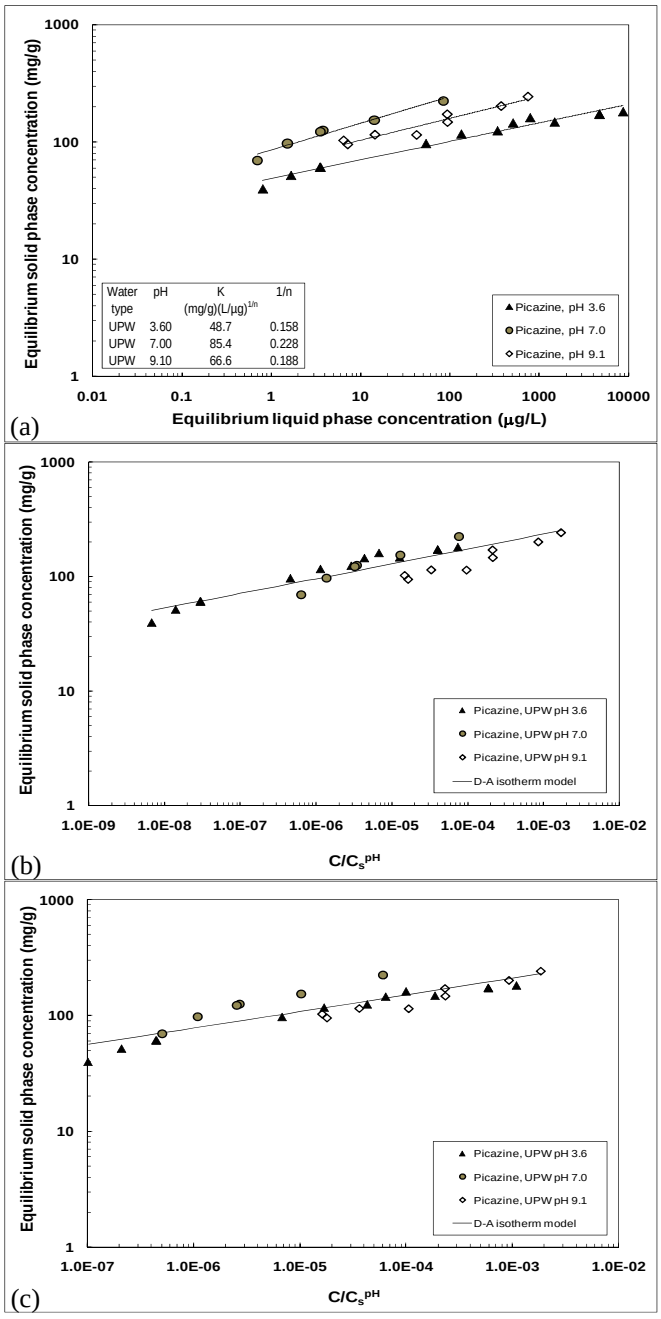

Figure 3. TMP adsorption isotherms on wood-based activated carbon Picazine in UPW at different solution pHs; (a) plotted against the equilibrium liquid phase concentration (table shows Freundlich isotherm parameters), (b) UPW data following normalization with theoretical C_s^{pH} values predicted with ACD/Labs software, and (c) UPW data following normalization with experimental C_s^{pH} values. Lines in panels (b) and (c) represent Dubinin-Astakhov isotherm model fits.

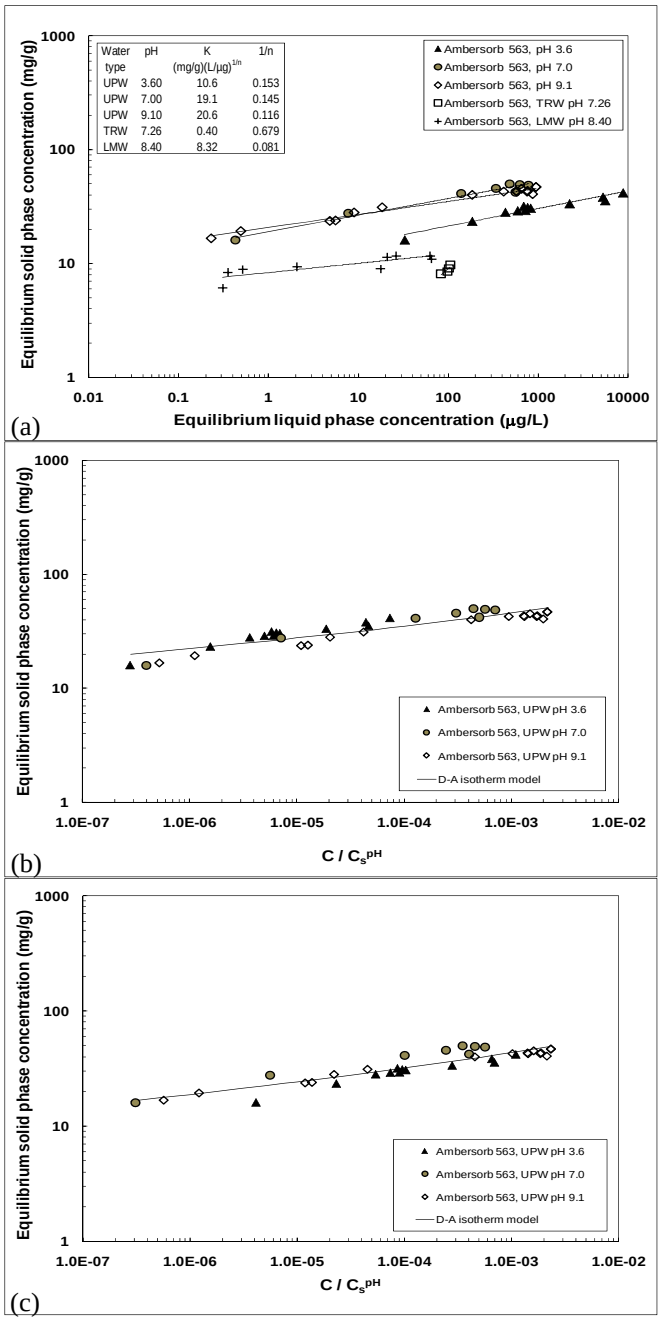

Figure 4. TMP adsorption isotherms on carbonaceous resin Ambersorb 563 in UPW at different solution pHs, TRW, and LMW; (a) plotted against the equilibrium liquid phase concentration (table shows Freundlich isotherm parameters), (b) UPW data following normalization with theoretical C_s^{pH} values predicted with ACD/Labs software, and (c) UPW data following normalization with experimental C_s^{pH} values. Lines in panels (b) and (c) represent Dubinin-Astakhov isotherm model fits.

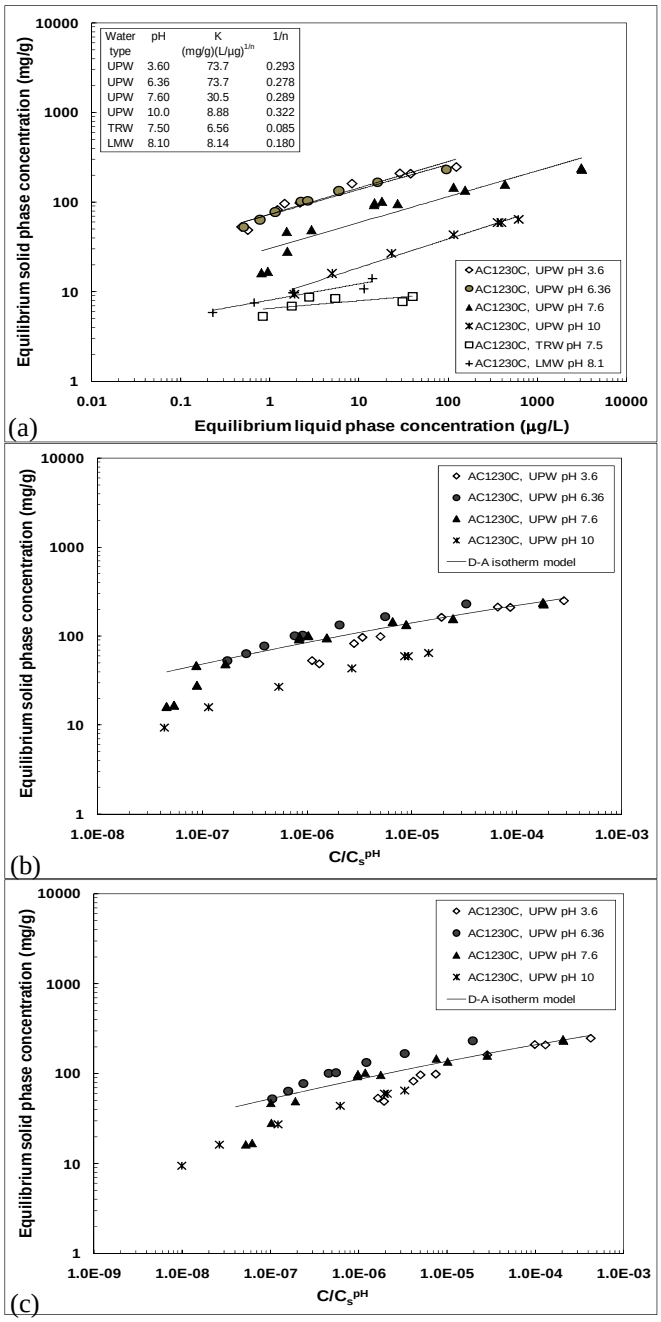

Figure 5. SMX adsorption isotherms on coconut shell-based activated carbon AC1230C in UPW at different solution pHs, TRW, and LMW; (a) plotted against the equilibrium liquid phase concentration (table shows Freundlich isotherm parameters), (b) UPW data following normalization with theoretical C_s^{pH} values predicted with ACD/Labs software, and (c) UPW data following normalization with experimental C_s^{pH} values. Lines in panels (b) and (c) represent Dubinin-Astakhov isotherm model fits.

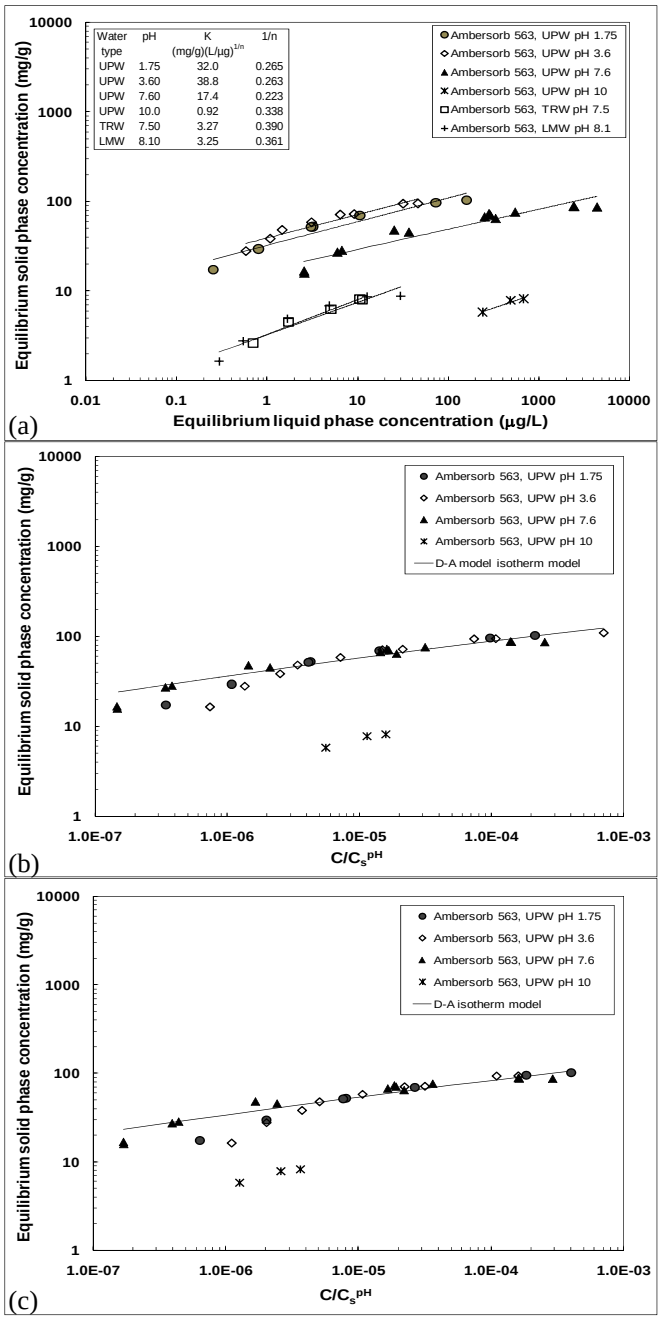

Figure 6. SMX adsorption isotherms on carbonaceous resin Ambersorb 563 in UPW at different solution pHs, TRW, and LMW; (a) plotted against the equilibrium liquid phase concentration (table shows Freundlich isotherm parameters), (b) UPW data following normalization with theoretical C_s^{pH} values predicted with ACD/Labs software, and (c) UPW data following normalization with experimental C_s^{pH} values. Lines in panels (b) and (c) represent Dubinin-Astakhov isotherm model fits.

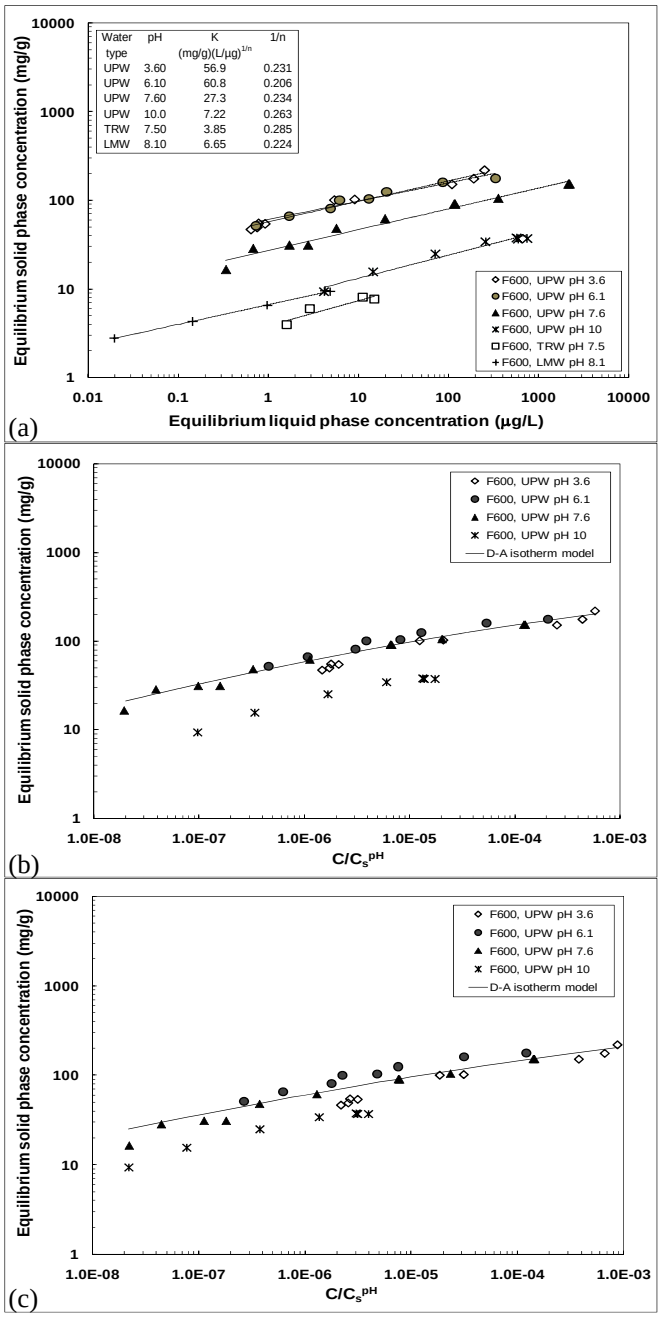

Figure 7. SMX adsorption isotherms on coal-based activated carbon F600 in UPW at different solution pHs, TRW, and LMW; (a) plotted against the equilibrium liquid phase concentration (table shows Freundlich isotherm parameters), (b) UPW data following normalization with theoretical C_s^{pH} values predicted with ACD/Labs software, and (c) UPW data following normalization with experimental C_s^{pH} values. Lines in panels (b) and (c) represent Dubinin-Astakhov isotherm model fits.

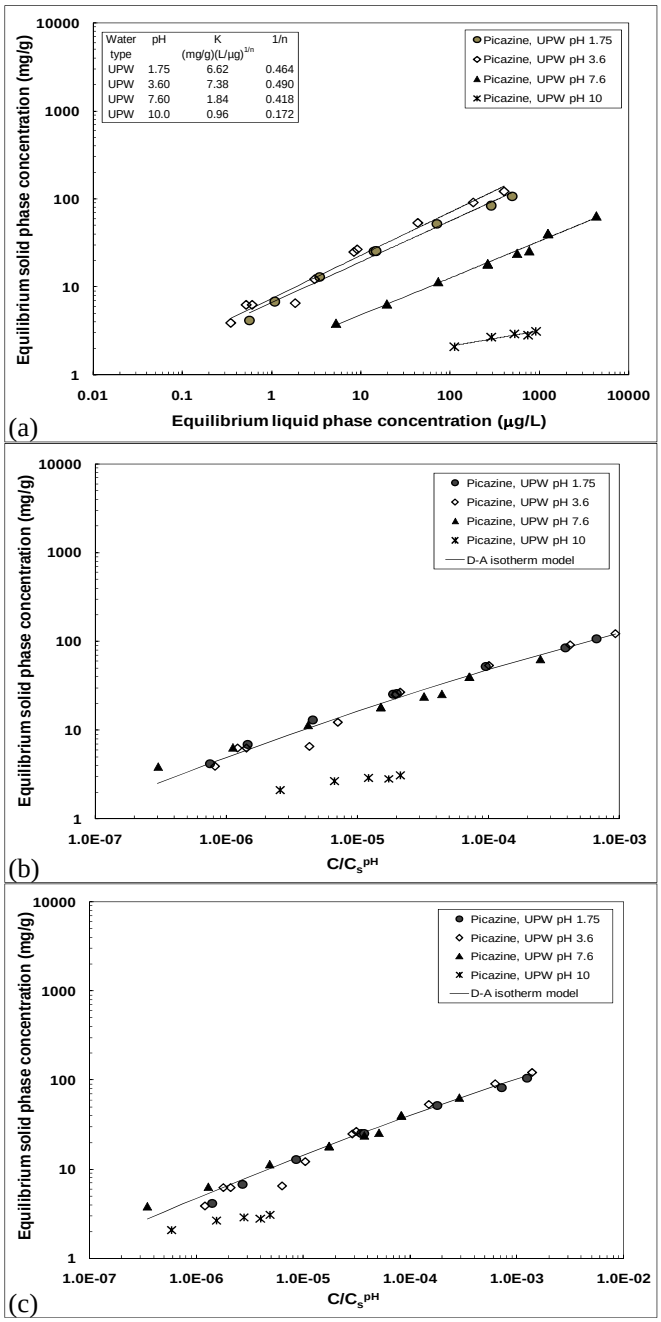

Figure 8. SMX adsorption isotherms on wood-based activated carbon Picazine in UPW at different solution pHs; (a) plotted against the equilibrium liquid phase concentration (table shows Freundlich isotherm parameters), (b) UPW data following normalization with theoretical C_s^{pH} values predicted with ACD/Labs software, and (c) UPW data following normalization with experimental C_s^{pH} values. Lines in panels (b) and (c) represent Dubinin-Astakhov isotherm model fits.